Methods[1]

Expedition 313 Scientists[2]

Chapter contents

Introduction

This chapter documents the primary procedures and methods employed by various operational and scientific groups during the offshore and onshore phases of Integrated Ocean Drilling Program (IODP) Expedition 313. This information concerns only shipboard and Onshore Science Party (OSP) methods as described in the site chapters. Methods for postexpedition research conducted on Expedition 313 samples and data will be described in individual scientific contributions to be published after the OSP. Detailed drilling and engineering operations are described in "Operations" in each site chapter.

Numbering of sites, holes, cores, and samples

Expedition numbers for IODP expeditions are sequential, starting with 301. Drilling sites are numbered consecutively, and for a European Consortium for Ocean Research Drilling (ECORD) Science Operator (ESO)–operated platform, numbering starts with Site M0001 (the "M" indicates the ESO-operated mission-specific platform [MSP]). For Expedition 313, the first site was Site M0027. Although not applicable to Expedition 313, multiple holes may be drilled at a single site. For all IODP drill sites, a letter suffix distinguishes each hole drilled at one site. The first hole drilled is assigned the site number with the suffix "A," the second hole takes the site number and the suffix "B," and so forth. For Expedition 313, only one hole was drilled at each site, so all holes take the suffix "A." The cored interval is measured by the drillers in meters below seafloor (mbsf). The depth below seafloor was determined by subtracting the initial drill pipe measurement to seafloor from the total drill pipe measurement. For Expedition 313, the cored interval normally consisted of the entire drilled section, but in some cases intervals were drilled without coring (e.g., the top of Hole M0028A and other intervals between spot cores). Recovered core is split into sections with a maximum length of 1.5 m and numbered sequentially from the top, starting at 1 (Fig. F1). By convention, material recovered from the core catcher of a sedimentary core is treated as a separate section labeled "CC" (core catcher) and placed below the last section recovered in the liner. The core catcher is assigned to the top of the cored interval if no other material is recovered. When recovered core is shorter than the cored interval, the top of the core, by convention, is equated

to the top of the cored interval to achieve consistency in reporting depth in core.

A soft to semisoft sediment core from less than a few hundred meters below seafloor, or a core of expanding clay, expands upon recovery (typically 10%–15%), so the recovered interval may not match the cored interval. In addition, a coring gap typically occurs between cores (i.e., some cored interval was lost during recovery or was never cut). Thus, a discrepancy exists between the drilling meters below seafloor and the curatorial meters below seafloor. For example, the curatorial depth of the base of a core can be deeper than the top of the subsequent core. Where appropriate, downhole logging data and core measurements were compared (e.g., total downhole natural gamma ray and core natural gamma ray) to correlate cores to the logging depth. This process is described in more detail in **"Stratigraphic correlation"** here and in each site chapter.

Any sample removed from a core is designated by distance measured in centimeters from the top of the section to the top and bottom of the sample removed. A full identification number for a sample consists of the following information: expedition, site, hole, core number, core type, section number, piece number (for hard rock), and interval in centimeters measured from the top of section. For example, a sample identification of "313-M0027A-3R-2, 35–40 cm," represents a sample removed from the interval 35–40 cm below the top of Section 2, Core 3R ("R" indicates core type; see below), from Hole M0027A during Expedition 313 (Fig. **F1**). All IODP core identifiers indicate core type. For Expedition 313, the following abbreviations are used:

H = hydraulic piston corer (HPC; equivalent to IODP's advanced piston corer [APC]),

X = extended nose corer (EXN; equivalent to IODP's extended core barrel [XCB]),

R = standard rotary corer (aka Alien Corer, or ALN; equivalent to IODP's rotary core barrel [RCB]).

Descriptions of these tools are given in **"Wireline coring."**

The meters below seafloor of a sample is calculated by adding the depth of the sample below the section top and the lengths of all higher sections in the core to the core-top datum measured with the drill string.

Site locations

At all Expedition 313 sites, Global Positioning System (GPS) coordinates from precruise site surveys were used to position the *L/B Kayd* on site. Once the *L/B Kayd* was positioned at a site, the legs were lowered and the vessel was allowed to settle onto the seabed. The final site position was the mean position calculated from GPS data collected from an antenna placed at the drill rig during a period of several hours while the *L/B Kayd* underwent its preload procedure.

Platform

The maximum required depth of the boreholes was 750 mbsf. The water depth at all three sites is shallow (35–40 m); thus, a lift boat equipped with a coring rig was selected to carry out the coring for Expedition 313. The drilling platform, chosen by Drilling, Observation and Sampling of the Earth's Continental Crust (DOSECC) and inspected by ESO, was the *L/B Kayd,* which is a three-legged, self-propelled 245 class liftboat (Fig. **F2**). The *L/B Kayd* had sufficient capacity by way of food and accommodation for 24 h operation but required weekly resupply by a contractor-arranged supply boat.

Coring rig

The coring rig was an Atlas Copco CS4002 mining rig, utilizing flush-jointed mining drill strings sized to allow the larger ones to act as casings when coring required it. The rig had a mast capable of handling 6 m string lengths, and coring was conducted using a top drive system installed in the mast (Fig. **F3**). Wireline operation of the core barrel was conducted through the top drive. The coring rig was cantilevered off the bow of the *L/B Kayd,* between the two forward jacking legs (Fig. **F2**).

Wireline coring

Three methods of wireline coring were employed in addition to open-hole drilling.

Hydraulic piston corer

The HPC is designed to operate primarily in soft muddy to clayey formations. The HPC operates by advancing the core barrel into the formation through pushing. The HPC is set up by fully retracting the core barrel into the core barrel housing, which is then held in place using shear pins. The core barrel housing is then locked into the bottom-hole assembly (BHA), which is at the base of the borehole at the end of the drill string. The BHA is then lowered to the base of the borehole and water/mud is applied at pressure, which produces a force that overcomes the shear pins. When the pins shear, the corer is released and fired/advanced into the sediment. The number of shear pins inserted dictate the pressure at which the core barrel is released and, consequently, the force at which the barrel is pushed into the formation.

During Expedition 313, the HPC was utilized in sandy formations with the aim of collecting undis-

turbed samples. After each sample was taken, the hole was advanced by drilling to the next sample point, adding time to the process. This was carried out either by "advance by recovery" or "advance by barrel stroke." When advancing by recovery, the depth of the next core run was dictated by the length of core recovered, which was not known until the core was back on deck. To reduce the cycle time, advance by barrel stroke was sometimes used, meaning the hole was advanced without knowing the true recovery of the last run.

In the interest of time, some HPC runs were taken every 3 m regardless of the core length recovered. Piston coring is slower than conventional drilling, as each section has to be cored with the HPC and then drilled out before the next sample can be taken.

Extended nose corer

The EXN is designed to cut through a clayey formation. It will not work with hard consolidated material.

The EXN barrel was locked into the BHA and advanced through rotation and flushing in a similar way to diamond rotary coring. The difference is that the end of the core barrel protrudes ahead (up to 12 cm) of the main cutting bit (which could be one of a series of bits: tungsten, surface set, impregnated diamond, or polycrystalline diamond [PCD]). This minimizes flushing at the point where the core enters the core barrel, reducing the undercutting and washing away that would occur when the flushing is at the same point as the core entering the barrel.

Standard rotary corer

The ALN is equivalent to a standard diamond rotary corer and is designed to core in hard formations.

The ALN was advanced by rotary coring, with flushing occurring at the point where the core entered the core barrel. When this corer is used in softer formations, with a basket-type catcher to hold in the material, undercutting of the core may result. Some undercutting also occurs with firmer material, as material can get caught in the tines of the basket, which has space to rotate around the core as it enters the barrel. The core cutting bit on the ALN is retrieved with each core run; thus, the cutting ability can be optimized for each formation encountered.

Coring methodology

A conductor pipe was run to the seabed to protect the first drill string from excessive movement and vibration and to aid hole reentry if the BHA had to be retrieved. Initially, the conductor pipe was not run into the seabed to allow core collection from the sea-

bed, but following this it was run to a suitable depth to maintain top-hole stability for the rest of the coring. The first coring string was a DOSECC lake drilling system (**dosecc.org/**) with a wireline core barrel and a PHD (mining pipe) or HWT (mining casing) flush-jointed drill string (114.3 mm outer diameter [OD]; 101.6 mm inner diameter [ID]). This system has interchangeable PQ-size inner core barrels; thus, the drill string was often referred to as the "PQ string." The outer core bit size is ~160 mm, and the core collected was ~62 mm in diameter. This is the "standard" IODP core size and was collected in IODP-standard liners.

The annulus between the hole and drill string was small, which was key to obtaining a stable borehole in delicate formations. The outer core barrel was able to accept a variety of inner core barrels (see **"Wireline coring"**), which helped to maximize core recovery in unconsolidated and consolidated formations. The inner core barrel bit or cutting shoe was interchangeable with the inner core barrel, allowing a good degree of flexibility to ensure that the best possible core recovery and quality were obtained.

The maximum core run length was 3 m. However, the length of a core run was chosen to maximize core recovery and maintain hole stability, even at the expense of overall penetration speed. In unconsolidated, sandy, or silty formations, these core runs were less than the 3 m maximum length.

In Hole M0028A, it was not possible to reach the required total depth (TD) with a single drill string (the PQ string). In this case, the PQ string was used as a casing for the completed part of the borehole. With the inner core barrel removed, sufficient clearance through the outer core barrel bit was available to allow a second string and core barrel to pass through and thus progress the borehole. This second drill string was also a flush-jointed mining system (HQ; 96.0 mm OD; 63.5 mm ID) and had a matched HQ-size mining core barrel. This drill string was often referred to as the "HQ string." The core was collected in a different plastic liner, and, because the hole diameter and annulus spacing were smaller, the core collected was essentially the same size (61 mm in diameter) as that cored by the PQ core barrel. The liner in the HQ core barrel is a standard mining type and is different from the IODP liner used in the PQ system. Both types of liner were provided to the curation and petrophysics teams for calibration prior to the expedition.

Drilling mud was used to condition the PQ and HQ portions of the borehole as dictated by the circumstances and the driller's requirements. Plastic bags containing fluorescent microspheres were attached to the core barrel, when required, to assist the evalu-

ation of contamination of samples for microbiology studies.

Appropriate instruments for gas monitoring, supplied by DOSECC and ESO, were used throughout the expedition. Note that although such instruments can detect and identify gas, they are empirical or semiquantitative and are not analytical instruments. The DOSECC-supplied instruments would sound an alarm in the presence of hydrogen sulfide (no reading). The ESO-supplied portable instruments were suitable for the measurement of hydrogen sulfide up to 50 ppm, methane up to 5% by volume, flammable gas (methane to pentane) up to 100% of the lower explosive limit (LEL), and oxygen up to 25% by volume. A record of gas detections was kept by ESO and was made available to the Expedition 313 scientists.

Downhole logging tools

Downhole logging services were contracted and managed by the European Petrophysics Consortium (EPC). Details and results of the expedition logging program are given in **"Downhole measurements"** here and in each site chapter.

Core handling and analysis

Offshore phase

As soon as a core was retrieved on deck, it was immediately curated by the ESO curators. This involved marking and cutting the core into sections (maximum 1.5 m length). Each section was sealed at the top and bottom by attaching color-coded plastic caps: blue to identify the top of a section and clear at the bottom. A yellow cap was placed on section ends where a whole-round sample was removed, and the sample code was written on the yellow cap. Caps were secured to liners used with the PQ coring system by coating the liner ends and inside rims of caps with acetone before attaching the caps. The smaller diameter liners used with the HQ coring system were sealed using plastic tape. Core section liners were permanently labeled with an engraving tool. The length of the core in each section and the core catcher sample were measured to the nearest centimeter; this information was logged into ESO's Offshore Drilling Information System (OffshoreDIS) and readily made available to the driller if the mode of "advance by recovery" for HPC operations was in effect. No core splitting took place during the offshore phase of Expedition 313.

After curation, the core proceeded through a sequence of processing steps. The geochemists and microbiologists were given access to the cores to sample for interstitial water and microbiology. This generally required 5 cm whole rounds to be taken, al-

though Rhizon syringes (Dickens et al., 2007) were employed at shallow depths if the core material was suitable. With the exception of interstitial water and microbiology, no sampling of the unsplit cores was undertaken during Expedition 313.

The core catcher, or a sample from the core catcher, was given to the sedimentologists for initial description. The shipboard sedimentologists also took the opportunity to describe the core sections through the clear plastic liners, although drilling fluid and mud cake often made this difficult or impossible. Samples of the core catcher were taken for initial Sr isotope analysis, initial quantification of sand/silt/clay ratios, initial marine palynology, and initial calcareous nannofossil analysis. These samples were periodically transported to shore, where volunteers from the Science Party carried out the analyses at their institutions and provided the results prior to the OSP as if they were "shipboard data."

The core sections were allowed to thermally equilibrate before they were run through the multisensor core logger (MSCL) (see **"Physical properties"**).

After MSCL measurements were complete, the core was moved to refrigerated storage.

Onshore Science Party

The OSP was held at the IODP Bremen Core Repository (BCR; Bremen, Germany) from 4 November to 4 December, 2009. Before splitting, all cores were measured for thermal conductivity and natural gamma radiation (NGR), and some sections were selected for computed tomography (CT) scanning.

After being taken out of refrigerated storage, cores were split lengthwise into working and archive halves. The splitting technique varied depending on the strength of the cores, which ranged from soupy to cemented. The core splitters had at their disposal horizontal and vertical wire cutters, steel plates to keep soupy material intact while the liner was cut, and a diamond cutting saw for indurated core. Wire-cut cores were split from bottom to top, so investigators should be aware that older material could have been dragged up the core on the split face of each section.

The sedimentologists described the archive halves visually, aided by thin sections and smear slides (see **"Lithostratigraphy"**). Digital images of archive halves were made with a digital imaging system followed by discrete color reflectance measurements (see **"Physical properties"**). Archive halves were then photographed using a color digital camera. Close-up color photographs were taken of particular features for illustrations in the summary of each site, as requested by individual scientists.

The working half of the core was sampled for both the OSP and postexpedition research. Each sample was logged into the Drilling Information System (DIS) by location and by the name of the investigator receiving the sample. The IODP curator and database maintain information about all samples taken. Samples were generally sealed in plastic bags, labeled, and stored as appropriate. Samples were routinely taken for OSP physical property studies, comprising X-ray diffraction (XRD) and total organic carbon (TOC) measurements; paleomagnetic studies; and micropaleontological analysis (see "Physical properties," "Paleomagnetism," and "Paleontology").

Following initial OSP measurements and sampling, both halves of the cores were cling-filmed and placed in labeled plastic D-tubes, sealed, and transferred to refrigerated storage at the BCR.

Data handling, database structure, and access

Data management during the offshore and onshore phases of Expedition 313 had two overlapping stages. The first stage was the capture of metadata and data during the expedition (offshore and onshore). Central to this was the Expedition Drilling Information System (ExpeditionDIS), which stored drilling information, core curation information, sample information, and primary measurement data. The second stage was the longer term postexpedition archiving of Expedition 313 data sets, core material, and samples. This function was performed by the World Data Center for Marine Environmental Sciences (PANGAEA/WDC-MARE) and the BCR.

The ExpeditionDIS is a flexible and scalable DIS, originally developed for the International Continental Drilling Program (ICDP). The underlying data model for the ExpeditionDIS is compatible with those of the other IODP implementing organizations and ICDP. For the specific expedition platform configuration and offshore and onshore workflow requirements of Expedition 313, the ExpeditionDIS data model, data import pumps, and user interfaces were adapted to form the New Jersey ExpeditionDIS. The ExpeditionDIS was implemented in SQLServer-2000 with Microsoft-based client PCs connecting to the system through a Microsoft Access–like user interface.

The expedition scientists and ESO staff also generated a variety of spreadsheet files, text documents, and graphics containing operations and scientific data, geological descriptions, and interpretations in different formats. Therefore, in addition to the structured metadata and data stored in the Expedition-

DIS, all data files were stored in a structured file system on a shared file server.

Incremental backups and full backups of the ExpeditionDIS and the file server were made regularly and archived.

Offshore, the ExpeditionDIS was used to capture metadata related to core and sample curation, store core photographs, and print section and sample labels. In addition, the database also stored primary measurements data. These were

- MSCL data,
- Visual core descriptions (VCDs) of core sections (through liner) and core catchers,
- Interstitial water analysis,
- Smear slide descriptions, and
- Microbiological data.

Onshore, additional data types were captured in the ExpeditionDIS, including microscopy images, core close-up images, line-scan images, color reflectance data, thin section data, NGR data, smear slide data, and VCD data. All other data were loaded to the shared file server.

In the second stage, all Expedition 313 data were transferred to the PANGAEA/WDC-MARE information system. WDC-MARE was founded in 2000 and is a member of the International Council of Scientific Unions WDC system. PANGAEA is the geoscience information system used by WDC-MARE. It has a flexible data model that reflects the information processing steps in earth science fields and can handle any related analytical data (Diepenbroek et al., 1999, 2002). It is used for processing, long-term storage, and publication of georeferenced data related to earth sciences. Essential services supplied by PANGAEA/WDC-MARE are project data management and the distribution of visualization and analysis software. Data management functions include quality checking, data publication, and metadata dissemination that follows international standards.

The data captured in the New Jersey ExpeditionDIS and the data stored in the shared file server were transferred to PANGAEA following initial validation procedures. The data transfer process was completed by the time of publication of the "Expedition reports" section of this *Proceedings* volume. Until the end of the moratorium period, data access was restricted to the expedition scientists. However, following the moratorium, all data except downhole wireline data were published on the Internet (www.PANGAEA.de/), and PANGAEA/WDC-MARE will continue to acquire, archive, and publish new results derived from Expedition 313 samples and data sets. Downhole wireline data were archived at

http://brg.ldeo.columbia.edu/logdb/ with a link from www.PANGAEA.de/.

The central portal for all IODP data, including Expedition 313 data, is the Scientific Earth Drilling Information Service (SEDIS; http://sedis.iodp.org/). IODP MSP data are also downloadable from iodp.wdc-mare.org/.

At the start of the onshore phase, an export function was developed to export data from the Expedition-DIS in formats compatible with loading into the Corewall Corelyzer application. New functionality was also added to the Corelyzer interface to make the import of expedition line-scan, MSCL, and downhole logging data more automated.

Throughout the onshore phase of the expedition, seismic correlation and interpretation was performed on the seismic data sets at and in the vicinity of the drill sites on a Landmark seismic interpretation system. At the end of the onshore phase, the Landmark project data were copied to the Co-Chief Scientists and a copy of the interpreted project data was archived by ESO.

Core, section, and sample curation using the New Jersey ExpeditionDIS

Expedition 313 followed IODP procedures and naming conventions in core, section, and sample handling (see "Core handling and analysis"). The ExpeditionDIS captured the curation metadata and printed the appropriate labels, also to IODP standards. The curation metadata comprise

- Expedition information,
- Site information (latitude, longitude, water depth, start date, and end date),
- Hole information (hole naming by letter, latitude, longitude, water depth, start date, and end date),
- Core data (core number, core type, top depth, bottom depth, number of sections, core catcher availability, curator, core on deck, date and time, and additional remarks),
- Section data (section number, section length, curated length, and curated top depth of section),
- Sample information (repository, request, request part, code observer, expedition, site, hole, core, section, half, sample top, sample bottom, and sample volume),
- Calculated core recovery percentage on the basis of the drilled or cored length and the curated recovery, and
- Calculated section recovery on the basis of the section length and the curated length.

No correction was made in cases where the recovery exceeded 100%. Top and bottom depths of the section (in meters below seafloor) were calculated on the basis of the core-top depth. The curation of subsections was also possible but not used during Expedition 313. Section and sample label formats follow the standard IODP convention. They include barcodes of the section/sample code and the complete section/sample code (Expedition-Site-Hole-Core-Core type-Section-Half-Interval and sample request code). This standardization guarantees data exchange between the repositories and enables the information flow between the Implementing Organizations.

Lithostratigraphy

This section outlines procedures followed to document the sedimentology of cores recovered during Expedition 313. The first part outlines the methodology of core description and sediment classification. The second part introduces the interpreted depositional environments, the nomenclature of clinoform physiography, and sequence stratigraphy. Information presented here concerns onshore operations and analyses described in the site chapters. Shipboard descriptions of core catcher samples and liner observations were consulted in making these descriptions, but offshore procedures are not described here.

Methodology of sediment description

Visual core description

Unsampled archive halves of split cores arrived in the sedimentology laboratory of the BCR along with paper copies of description forms (barrel sheets) that included the line-scan image of the accompanying core section on the left side of the sheet. The archive half was then examined, and visual observations were recorded manually on the barrel sheets. This information was then condensed and entered into the ExpeditionDIS to generate a simplified database of each core section unit described. Digital barrel sheets were generated from the information entered into the ExpeditionDIS and are presented in "Core descriptions."

Grain-size divisions for clay, silt, sand (very fine, fine, medium, coarse, and very coarse), granules, and pebbles follow Wentworth (1922) and were assessed using hand lenses and grain size cards. The lithology of each core section is represented on barrel sheets by graphic patterns in the column on the left side of the sheet and by drawing grain size out to the dominant grain size division (Fig. F4). Sediments recovered from the New Jersey continental shelf are gener-

ally siliciclastic but have a strong component of authigenic and detrital glauconite. Minor quantities of biogenic particles also occur. Diagenetic phases include pyrite and carbonate in dispersed and nodular form. Sediment composition is defined by the different proportions of clay, silt, and sand size classes as shown on the ternary diagram (Fig. F5).

A wide variety of features that characterize the sediment are indicated in the columns to the right of the graphic log on the digital barrel sheets and include items such as primary sedimentary structures, body and trace fossils, accessories, bioturbation intensity, core disturbance, sample locations, and general description. Where described, contacts between different sediment bedsets, beds, or laminasets are given in the Description column. Accessories (e.g., biogenic particles and macroscopically identified authigenic or diagenetic minerals) are minor components of the cores, and their relative abundance is assessed using the standard visual composition chart of Rothwell (1989). The symbols are schematic and are placed in the paper barrel sheets centered on the unit in which they were observed and do not necessarily indicate the precise stratigraphic position of the observation. Exact positions of sedimentary features are shown in the detailed section-by-section paper core description forms. Full sets of symbols used on the VCD sheets are keyed in Figure F4.

Ichnological analysis included evaluation of the intensity of bioturbation, as well as identification of trace-fossil types. To assess the degree of bioturbation semiquantitatively, a modified version of the Droser and Bottjer (1991) ichnofabric index (ii = 1 to 5) scheme was employed (e.g., 1 = barren or no bioturbation and 5 = abundant bioturbation or homogeneous) (Fig. F4). These indexes are illustrated using colored intervals in the Bioturbation column of the barrel sheets. For completely bioturbated sediments (ii = 5), ichnofabrics were assessed using a modified version of the scheme of Droser and Bottjer (1991) in an attempt to distinguish homogeneous or diffusely burrow-mottled backgrounds from discrete biogenic structures (e.g., ii5/4 refers to completely bioturbated background fabrics heavily overprinted by discrete ichnofossils). Finally, if the degree of bioturbation could not be determined, the ichnofabric index was assigned 0. The photographic atlas of Gerard and Bromley (2008) was used as a basis for trace fossil identification.

Hue and chroma attributes of sediment color were determined visually using Munsell Soil Color Charts (Munsell Color Company, Inc., 1988). Deformation and disturbance of sediment that clearly resulted from the coring process are illustrated in the Drilling Disturbance column, using symbols shown in Figure F4. Blank regions indicate an absence of apparent disturbance.

Sediment classification

The sediment classification scheme used during Expedition 313 is descriptive and is largely the same as the scheme previously used by the Ocean Drilling Program (ODP) (Figs. F4, F5), particularly during Leg 174A offshore New Jersey (Austin et al., 1998). Composition and texture are the only criteria used to define lithology. Genetic/interpretative terms such as pelagic, hemipelagic, turbidite, debrite, and so on, do not appear in this classification. The term "clay" is used for both clay minerals and other siliciclastic material <4 µm in size. The term "mud" as used herein describes a subequal mixture of silt and clay. If sand, silt, or clay is >50% of the sediment or rock, the principal name is determined by the relative proportions of sand, silt, and clay sizes when plotted on a modified Shepard (1954) classification diagram (Fig. F5). Examples of nonbiogenic principal names are clay, silty clay, silt, sandy silt, or sand. For lithified sediments, the suffix "-stone" is added to the principal names of sand, silt, clay, or mud. Where quartz is not the dominant mineral, a modifier (e.g., glauconite sand) is used to indicate the dominant mineral. A mineral that comprises >25% but <50% of the sediment is indicated with a modifier (e.g., glauconitic sand). Biogenic components are not described in textural terms. Thus, sediment with 55% sand-sized foraminifers and 45% siliciclastic clay is called foraminifer clay, not clayey foraminifer sand.

Smear slides

Smear slide observations are a complimentary technique in the identification of fine-grained sediments (clay, silt, and very fine sand). Grain-size estimates were made using polarizing and binocular microscopes with an ocular micrometer. The microscope (Olympus BH-2) was calibrated so that 8, 16, and 32 scale bars in the ocular micrometer under 100× magnification corresponded to the maximum size of silt, very fine sand, and fine sand. Sediments were classified using the scheme of Mazzullo et al. (1988). Percent composition of sand, silt, and clay were estimated semiquantitatively using the standard visual composition chart of Rothwell (1989), though clay-sized grains tend to be underestimated using this method.

Preliminary petrographic analysis of sediments was also performed using smear slides. Microfossil identification in smear slides during core descriptions can help steer sampling strategies. Major minerals, including quartz, orthoclase, plagioclase, mica, calcite, dolomite, pyrite, and glauconite, were identified.

Rock fragments, opaque heavy minerals, and black organic grains were also recognized, though positive identification requires thin sectioning or additional microscopic analysis. Identifiable whole microfossils and fragments include diatoms, silicoflagellates, sponge spicules, ostracodes, calcareous nannofossils, echinoid spines, and foraminifers. The percent abundance of bioclasts was also crudely estimated if their abundance was >1% of the sample.

Thin sections

Specific lithified intervals within cores were prepared as thin sections to allow material to be examined under a microscope using transmitted light as well as reflected light. This technique is particularly useful for examining microscopic details of clastic particles and their surrounding cement, as well as sedimentary textures. Attributes that can be determined include dominant grain types (mineralogy), presence or absence of inclusions, accessory minerals, and mineralogy of matrix or cement between sand grains.

Thin section mineralogy was also used as a check on descriptions provided using hand lenses by sedimentologists. For example, when cut by the rock saw, lithified cores are sometimes difficult to describe. In addition, fine-grained cements are difficult to identify except under higher magnification. Thin sections provided additional means to identify more accurately the lithified sedimentary deposits. Locations of thin sections are marked on the barrel sheets.

Following requests from sedimentologists, the location and orientation of samples for thin section preparation were flagged on the cores. After the thin section billets were cut with a diamond saw, they were dried in a furnace for 24 h at not more than 25°C. The billets then underwent stepwise impregnation with epoxy-resin in a vacuum desiccator for 48 h. After the sample was covered with resin, the base was ground until the sample surface was reached. This surface was lapped for ~45 min with 9 µm silicon carbide powder and water. The surface was then cleaned with water. The sample was glued onto the slide with the same resin used for impregnation. A pressure block was used to press the sample against the slide during the gluing process. The surface of the slide was cleaned and the sample identification scribed with a diamond pen. After trimming the sample to a thickness of ~250 µm, the thin section was lapped down to a thickness of 30 µm. A 150 µm thick glass cover was then glued to the thin section using cyanacrylate (ultraviolet resin). Finally, the thin section was cleaned with alcohol. For all lapping steps the automated system LP-50 auto from LOGITECH was used.

Computed tomography

A limited number of two-dimensional (2-D) and three-dimensional (3-D) X-ray CT scans were collected from unsplit cores prior to the OSP, using facilities in Bremen. CT is a useful technique for the investigation of the internal structures of 3-D objects. Measurements provide a digital data set of density variation. The CT scanner, originally developed for medical purposes, has several advantages: it is nondestructive, rapid, does not need slab preparation (cf. conventional geological X-ray analysis), and can be completed on full cores, giving 3-D images of undisturbed sediment prior to core splitting. The resolution of scans ranges between 1 mm and 1 cm.

Three types of scan were completed:

1. Exploratory scans (single radiographic plane/overview scan) limited to 50 cm length. This method required three scans on average to cover an entire 1.5 m section (Fig. F6A). These scans were made through the core axis longitudinally in two orthogonal sections (Fig. F6B) with a resolution of ~1 mm.
2. Transverse scans of 1 mm thickness (Fig. F7).
3. Transverse scans of 1 mm thickness every 1 mm through variable core lengths (up to 5 cm). Slices arranged this way allowed 3-D core views using the software visualization package, AMIRA (Fig. F7).

All scans were recorded in Digital Imaging and Communications in Medicine (DICOM) data format. The data files have a "tagged format" with a variable number of tags (DICOM data elements), which means that a core can be segmented into several small parts and later integrated into larger data sets. Each image is defined by a unique file name, referring to expedition, site, core number, core type, section, and depth in section.

CT scans provide useful sedimentological information that helps characterize sedimentary structures, including bioturbation, the arrangement of mollusk shells, mineral inclusions, heterogeneities such as fractures or erosion surfaces, structures in compact sandstones such as water transfer conduits, and successions of sedimentary laminae.

CT images are digital pictures, and all the current techniques designed for image processing such as smoothing or contrast enhancing can be easily used. Images are displayed as negatives, with high-density mineral components showing a lighter tone and

low-density material, such as organic matter, appearing much darker or black in the case of voids (Fig. F7).

Sedimentological interpretations and physiographic nomenclature

Clinoform nomenclature

The term "clinoform" is applied to both sigmoid sedimentary slopes and any accretionary feature with sigmoidal bounding surfaces (Mitchum et al., 1977). However, Rich (1951) used the term "clinothem" to describe the body of rock bounded by individual clinoform surfaces. Clinoforms and clinothems range in scale from bedform features of centimeter size to continental margin accumulations (shelf-slope-basin clinoforms) that are kilometers deep (Pirmez et al., 1998). Clinoform deposits are composed of three fundamental components: topsets, foresets, and bottomsets (Gilbert, 1885) (Fig. F8).

Intrashelf clinoforms are intermediate in scale and are located on the continental shelf seaward of clastic shorelines and/or major river mouths (shoreline clinoforms) and landward of shelf-slope-basin clinoforms (Fig. F8). Clinoform deposits are part of sedimentary successions that accrete and prograde in response to the interplay between sediment supply and local sea level change (Mitchum et al., 1977). This interplay drives progradation of clinoforms at all scales such that the shoreline clinoform slope can merge with the intrashelf clinoform slope and the intrashelf clinoform can merge with the shelf-slope-basin clinoform slope to form compound clinoforms (Fig. F8).

The topset deposits form the upper portion of the clinoform succession, whose depositional slopes dip gently seaward. Foreset deposits form from progradation of the steepest part of the clinoform sigmoid (typical dip is 1°–3° at the clinoform inflection point), which is referred to as the clinoform slope. The bottomset deposits dip gently seaward.

The upper clinoform break in slope (an area not a point) between the topset surface and the foreset surface is referred to as the (clinoform) rollover (Fig. F8). The lower clinoform break in slope, which defines the transition between foreset surface and bottomset surface, is referred to as the toe of (clinoform) slope (Fig. F8).

The New Jersey intrashelf clinoforms are typically 100–300 m in height (elevation between rollover and toe of slope), and the length of the foreset surface between these same upper and lower clinoform breaks in slope is 5–15 km.

Sedimentary facies and depositional environments

Assemblages of sedimentary structures, ichnofabric, sediment texture and composition, and fossil content were used to define individual sedimentary facies. These sedimentary facies form facies associations that can be interpreted in terms of depositional environments. The vertical succession of facies defines progressive trends interrupted by physical surfaces that can be correlated to changes of physical properties measured on core (MSCL logs) and downhole logs.

The association of sedimentary facies shows that some of the Expedition 313 depositional environments share characteristics of wave-dominated shoreline facies models (Reineck and Singh, 1972; Harms et al., 1975, 1982; McCubbin, 1982; Browning et al., 2006) and mixed river/wave delta facies models (Galloway, 1975; Bhattacharya and Walker, 1992). The team of Expedition 313 sedimentologists arrived at the OSP familiar with incompatible terms for the nearshore environments of linear clastic shorelines (Fig. F9). Early discussion resulted in a terminological framework based on one that has been used onshore New Jersey (Browning et al., 2006) and modified by integrating the multisource terminology found in, for example, Aigner (1982), Walker and James (1992), Guillocheau et al. (2009), Ando (1990), and Coe (2003), among many others. A generalized shoreface to offshore facies model has been adopted that includes key aspects of these settings (Fig. F10). It was agreed that environments above mean fair-weather wave base (MFWWB) would be termed shoreface and environments below mean storm wave base (MSWB) would be offshore (Figs. F9, F10). The depositional environment between MFWWB and MSWB (variously called lower shoreface, offshore transition zone, and upper offshore; see cited authors) would herein be the shoreface–offshore transition (SOT) zone. Where there are large amounts of allochthonous plant debris, micaceous sand, and current ripples (unidirectional flows), the presence of a mixed fluvial/wave-influenced system is inferred (Bhattacharya and Walker, 1992) (Fig. F10). In these instances, a river-influenced or river-dominated modifier was added to the environment of deposition (Fig. F10).

Coarse sediments deposited seaward of the clinoform rollover in the clinoform-slope (foreset) and toe-of-slope (bottomset) settings dominated by sediment gravity flow processes (debris flow and turbidity currents) were also identified (Fig. F11). Classification of clinoform-slope and toe-of-slope environments are based on facies models of Nelson et al.

(1983), Stow et al. (1984), Reading and Richards (1994), Pickering et al. (1989), Posamentier and Kolla (2003), and Posamentier and Walker (2006). The term "toe-of-clinoform-slope apron" is used to describe a line-source system that supplies coalesced submarine fans.

The facies association model used in this study is summarized in Figures F9, F10, and F11, and the following broad depositional environments are recognized:

- Fluvial: dominantly sand, including evidence of cut-and-fill channels, floored by gravels, mostly comprising clean sand with little clay or silt; sand commonly poorly sorted and subangular; commonly with plant debris.

- Estuarine: poorly sorted sand admixed with interlaminated and interbedded sand and clay, with steepening cross-laminae indicating migration of bedforms; commonly with plant debris.

- Proximal shoreface/foreshore: clean beach sand of fine to coarse grain size, with opaque heavy-mineral laminae highlighting cross-bedding and low-angle laminae with low-angle truncation, indicating migration of bedforms; mostly representing proximal shoreface, due to poor preservation of foreshore deposits.

- Shoreface: fine to medium sand, well sorted with rare to absent silt, and rare clay layers that may indicate lagoonal settings, rare low-angle cross-beds (swaley cross stratification [SCS] and hummocky cross stratification [HCS]), and rare symmetrical ripple laminae (oscillatory flow), but physical structures tend to be obscured by moderate to heavy bioturbation (mostly from *Skolithos* ichnofacies); thick-walled shell fragments. River-influenced and river-dominated shoreface deposits are interbedded fine and very fine sand with significant content of plant debris and micaceous sand.

- Shoreface–offshore transition (SOT): interbedded fine and very fine sand, commonly silty because of mixing and commonly rich in shelly material with whole shells preserved; deposited below fairweather wave base but above storm wave base. Commonly, the SOT contains discrete sharp-based normally graded sand beds (Aigner, 1982) with clean-sand bases, shell debris, convex-upward laminae (HCS), and symmetrical-ripple lamination, which show combined flow characteristics and little evidence of burrowing apart from at bed tops. By contrast, intercalated beds of silt and clay are intensely bioturbated. River-influenced and river-dominated SOT deposits are well bioturbated

to thinly laminated silt and clay with significant amounts of plant debris and micaceous sand. Intercalated sharp-based normally and/or inversely graded sand beds with cross-lamination, subparallel lamination, and occasional mud clasts are rich in plant debris and mica. These beds indicate episodic influx of coarse sediments that are evidence of river flood events. Soft-sediment deformation features indicate rapid deposition and dewatering processes.

- Offshore: dominantly clay and silty clay with thinly laminated silt beds, with common benthic foraminifers and thin-walled (articulated) shells deposited below the storm wave base. Discrete beds of intensely bioturbated sediment with common horizontal burrows alternating with unbioturbated and interlaminated beds. River-influenced and river-dominated offshore deposits are silty, contain visible plant debris and mica with rare graded very fine sand beds, and share characteristics with distal prodelta environments (Figs. F9, F10). "Deep" offshore is used for clay or silt successions deposited seaward of the lower clinoform break in slope.

- Coarse clastic deposits at clinoform rollover positions: poorly sorted, weakly graded, muddy sand and gravel with mud clasts, benthic foraminifers, and shell fragments interbedded with bioturbated mud, indicating an episodically high energy setting. These deposits may represent small deltas and/or gulleys filled with concentrated density currents. Subangular to angular gravels and pebbles with a range of lithologies indicate high-energy coarse-grained sediment supply with a short transport history.

- Toe-of-clinoform-slope apron: two broad types of coarse clastic deposits are located in toe-of-clinoform-slope positions: (1) normally graded, moderately sorted, and cross-stratified sand and granules in inclined meter-thick bedsets interpreted as deposits from turbidity currents and (2) ungraded, poorly sorted, poorly stratified bioturbated muddy sand with floating granules, articulated shells, and pristine benthic foraminifers, supported by a finer grained matrix, interpreted as deposits from cohesive debris flows. Rounded intraformational mud clasts indicate upslope erosion. Interbedded clay laminae record background conditions. Typically, quartz and lithic granules are subrounded to subangular, although the full range of well-rounded to angular granules is observed. Typically, toe-of-clinoform-slope deposits are either glauconitic or glauconite dominated in the expedition boreholes.

Lithostratigraphic unit definition

Lithostratigraphic units are defined as coherent assemblages of sedimentary facies bounded by surfaces of lithologic change that commonly equate to stratigraphic discontinuities; subunits are defined on the same basis but at a smaller scale. Although the primary objective was to place sediments into objectively defined units within the core, where practical, the boundaries between lithostratigraphic units were placed in order that sediments in a numbered unit at one site would correspond in age to those found at the other Expedition 313 sites. Lithostratigraphic units have thus been defined and numbered to indicate correlation between all three sites. Subunits were also defined to have correlative value, except in the case of Unit I, for which recovery was highly incomplete.

Sequence stratigraphy

A principal expedition goal is to evaluate the depositional sequence model as a product of eustatic sea level change. The depositional sequence (papers in Wilgus et al., 1988) comprises assemblages of sedimentary strata showing distinct transgressive or regressive vertical trends, bounded by key stratigraphic surfaces. These surfaces are stratigraphic discontinuities, or their correlative surfaces, and have a hypothesized relationship to relative sea level change. Comprehensive summaries and discussion of the sequence stratigraphic model and its variants can be found in compilations such as Coe (2003) and Catuneanu (2006). The sequence boundary is defined as an unconformity and its correlative conformity, formed broadly around the time of sea level fall and lowstand. A sequence boundary is characterized in distal sedimentary environments by a seaward shift in sedimentary facies. The maximum flooding surface (MFS) is characterized by distal sediment starvation formed broadly at the time of relative sea level rise and highstand. Theoretically, each surface can also have a distinct expression in a seismic reflection profile where relationships are defined by the geometric relationship between packages of acoustically reflecting surfaces (reflection terminations) and not necessarily by individual stratal surfaces.

The approach of the expedition has been to ask the question, "Can depositional sequences recognized from geometric relationships within seismic reflection profiles be used to predict relative sea level change and, because the setting is an old passive margin, eustatic sea level change?" Because independent observational evidence for variation in water depth can come only from analysis of core materials (sediments and fossils), one of the major tasks of the OSP was to identify the principal sequence stratigraphic surfaces in core and determine how they relate to the surfaces identified in petrophysical logs and on seismic reflection profiles.

Previous New Jersey onshore and offshore sequence stratigraphy

Onshore New Jersey sequences provide an interpretive framework for some facies successions in the Expedition 313 drill cores, although the sedimentary record offshore is more complete and shows a wider range of facies (cf. Browning et al., 2006). Onshore sequences follow a pattern of basal transgressive sand dominated by quartz in the Miocene and glauconite in the Paleogene and overlain by regressive silt and sand deposited in offshore to shoreface, delta front, and fluvial environments (Sugarman et al., 1993). Generally, lowstand deposits are absent in the modern coastal plain sites, and thus transgressive surfaces merge with sequence boundaries. In addition, onshore sequences provide little guidance for predicting the nature of MFSs in Expedition 313 drill cores. This is because onshore MFSs range from subtle surfaces separating transgressive from regressive facies in New Jersey to heavily bioturbated omission surfaces in Delaware that look similar to sequence boundaries (Browning et al., 2006). In general, MFSs are differentiated from sequence boundaries by the lack of an age break at an MFS, as well as by deepening-upward successions below an MFS in contrast to shallowing-upward successions below sequence boundaries. Characteristics of MFSs in distal offshore settings have been discussed in work from ODP Leg 174A, where distal toesets of middle to late Miocene clinoforms have been sampled. At those locations, MFSs have been identified as bioturbated surfaces eroded into underlying muds overlain by thin concentrations of quartz sand, presumably derived from the abandoned clinoform front, and a mixture of in situ and reworked glauconite (Savrda et al. 2001; Hesselbo and Huggett, 2001).

Identification of candidate sequence stratigraphic surfaces in cores

Candidate sequence stratigraphic surfaces were interpreted based on physical stratigraphy, facies changes, inferred paleobathymetric changes, facies stacking patterns, and, with estimated ties to seismic reflection characteristics, physical properties and age breaks. Criteria for recognizing key stratigraphic surfaces from sedimentology of the cores in topset positions include

- Irregular contacts, with as much as 5 cm of relief on a 6.2 cm diameter core;

- Reworking, including rip-up clasts found above the contact;

- Strong bioturbation, including burrows in firm substrate filled with overlying material;

- Major sedimentary facies shifts, typically upward from deepwater to shallow-water environments, or from fine to coarse; and

- Shell lags.

Seismic geometries in profiles crossing the Expedition 313 boreholes predicted significant lowstand deposits would be sampled seaward of the clinoform rollover position. Several factors hinder the simple translation of sequence stratigraphic terms and principles defined for shallow-water systems to the interpretation of deepwater (below MSWB) deposits:

- The direct evidence of relative sea level change is not preserved in deepwater sediments, unlike in shallow-water systems (e.g., shoreline position and ravinement surfaces).

- There is insufficient temporal resolution to correlate shallow- and deepwater deposits (Catuneanu, 2006).

- A physical disconnection exists between deepwater deposits with coeval shallow-water systems because of the position of the shoreline, the instability and remobilization of sediment at a shelf-break, and the bypass of sediment in steeper portions of the submarine slope (Catuneanu, et al. 2009).

- The position of deepwater deposits at the distal end of the sediment transport pathway means that a variety of factors influence the timing and location of delivery of sediment to deepwater environments (Posamentier and Allen, 1999).

- Inaccessibility and inactivity of modern analogs means that, in general, sediment gravity flow processes are less well understood than fluvial and shallow-water counterparts.

Despite these limitations, there is a general consensus on the hypothesized sequence stratigraphic framework for deepwater deposits that relates cyclic change in shelfal accommodation (due to relative sea level variations) to repeated changes in the character of the lithology and stacking of depositional elements (e.g., Posamentier and Kolla, 2003; Posamentier and Walker, 2006; Catuneanu et al., 2009). Typically, a cycle of deepwater sedimentation begins during low sea level stand when a subaerial unconformity forms on the shelf and the shoreline and river mouths are at their most distal (basinward) positions close to or beyond the shelf-edge break. The deepwater expression of this regressive phase is the

formation of a correlative conformity above which there is a marked increase in the supply of coarse-grained sediment via mass flow and density flow. In the core, a sequence boundary is evidenced by an abrupt increase in grain size and a basinward shift of facies. To prove such a surface is a sequence boundary rather than related to a local slide or slump or an autogenic process such as an avulsion, it has to be mappable regionally. A cycle of deepwater sedimentation commonly ends with a landward shift of facies during transgression, resulting in progressive deactivation of updip supply systems. During this transgressive phase, there is sufficient accommodation for much of the silt- and sand-grade material to be retained on the shelf and coastal plain. Ultimately, the delivery of sediment via turbidity currents to the deepwater environment becomes progressively more mud rich and infrequent as shelf accommodation becomes sufficient to store all coarse sediment. In core, the transgressive phase is marked by fining- and thinning-upward turbidite and debrite units. Identification of the deepwater equivalent of the MFS can be problematic, although a position within the interval with the lowest sedimentation rate and finest sediment is commonly used (Catuneanu et al., 2009).

Paleontology

Three microfossil groups were examined for biostratigraphic purposes: calcareous nannofossils, planktonic foraminifers, and dinoflagellate cysts (dinocysts). Pollen and other palynomorphs, together with palynofacies, provided information on paleoenvironments (both marine and terrestrial) and on sediment provenance and transport. Benthic foraminifers were used to estimate paleobathymetry and to establish preliminary paleoenvironment interpretations. Most planktonic foraminifer and dinocyst age assignments were made using core catcher samples collected during offshore operations; a select few foraminifer analyses were performed on samples from cores split at the OSP. By contrast, nearly all calcareous nannofossil determinations were made on samples taken from split cores during the OSP. Sample positions and the abundance, preservation, chronostratigraphic age or biozone, and/or paleoenvironments for these microfossil groups were entered into the ExpeditionDIS. Unless otherwise noted, biostratigraphic zonations and datums used in this work are tied to the Berggren et al. (1995) integrated magnetobiochronologic timescale (BKSA95), which is based on the geomagnetic polarity timescale (GPTS) of Cande and Kent (1995), and are summarized in Figure F12. References for these biostratigraphic age as-

signments are given in Tables **T1** and **T2.** Biostratigraphic and taxonomic references for each microfossil group are further discussed in the following sections and given in part for QA/QC purposes.

Despite some uncertainties in age control and correlations, the assumption is made that first and last appearance datums (FADs and LADs, respectively) are globally synchronous and accurately dated and that these can be correlated over large distances and across different environments. The absence of a fossil may indicate that the sediments were deposited prior to that organism's FAD or following its LAD, that the organism did not inhabit that environment, or that its fossil remains were not preserved. Geographic and ecological variations can result in regional differences among zonations of all taxa, and dinoflagellate cysts in particular. Calcareous nannofossil and planktonic foraminifer zonations erected in deep-sea environments are sometimes difficult to use in inner neritic environments such as the New Jersey shelf, as some marker taxa may be rare or absent in this setting. Problems can also arise when reworking occurs, as reworked specimens can look well preserved. This is particularly critical above sequence boundaries, and for this reason LADs should be applied with caution to sediments immediately overlying sequence boundaries.

Calcareous nannofossils

Calcareous nannofossil assemblages are primarily tied to the zonation scheme of Martini (1971) and secondarily to additional biohorizons within each zone. The zonal scheme and biohorizons are tied to the BKSA95 integrated magnetobiochronologic timescale and shown in Figure **F12.** Age estimates for these datums are taken from the literature and tied to the BKSA95 unless otherwise noted (Table **T1**). Taxonomic concepts are those given in Perch-Nielsen (1985) and Bown (1998).

Core catcher samples from all three holes were sent ashore during the offshore phase of Expedition 313 for preliminary nannofossil age assignments by Shijun Jiang (former Expedition 313 Science Party member who was unable to attend the OSP). Additional analyses performed on samples from core split during the OSP supersede those preliminary age assignments.

Preliminary age assessments were made during the OSP by examining one sample per every three cores (approximately one sample every 10 m). Additional samples were taken to refine age estimates as time permitted. All samples were prepared using standard smear slide techniques (e.g., Bown, 1998) and examined on an Olympus BX51 light microscope using cross-polarized and plane-transmitted light. Abun-

dance estimates were done at 1000×, with lower magnification used to scan for rare biostratigraphic marker taxa. Qualitative assessment of calcareous nannofossil preservation was recorded as follows:

P = poor (strong dissolution or crystal overgrowth, significant alteration of primary morphological features, and many specimens are unidentifiable at the species and/or generic level).
M = moderate (minor dissolution or crystal overgrowth observed, some alteration of primary morphological features, but most specimens are identifiable to the species level).
G = good (little or no evidence of dissolution and/or overgrowth, little or no alteration of primary morphological features, and specimens are identifiable to the species level).

A qualitative assessment of the total abundance of calcareous nannofossils for each sample was estimated as follows:

B = barren (no specimens encountered in 500 fields of view [FOVs]).
R = rare (1 specimen/≥51 FOVs).
F = few (1 specimen/11–50 FOVs).
Fr = frequent (1 specimen/2–10 FOVs).
C = common (1–10 specimens/FOV).
A = abundant (11–49 specimens/FOV).
V = very abundant (≥50 specimens/FOV).

The abundance of individual species for each sample was estimated as follows:

R = rare (1 specimen/≥51 FOVs).
F = few (1 specimen/11–50 FOVs).
Fr = frequent (1 specimen/2–10 FOVs).
C = common (1–10 specimens/FOV).
A = abundant (11–49 specimens/FOV).
V = very abundant (≥50 specimens/FOV).

Foraminifers

Approximately 300 samples were processed for Sr isotopes and foraminifers prior to the OSP. An additional ~20 core catcher samples were processed during the OSP. All samples (pre-OSP and OSP) that were examined for foraminifers were soaked in a sodium metaphosphate solution, washed through a 63 μm sieve, and oven dried. Planktonic and benthic foraminifers were examined from these coarse fractions (>63 μm).

For both the planktonic and the benthic foraminifers, preservation characteristics were divided into five categories:

P = poor (almost all specimens were dissolved or broken and fragments dominated).
M = moderate (30%–60% of specimens showed dissolved or broken chambers).

G   = good (60%–90% of specimens were well pre-
      served and unbroken).

VG = very good (>90% of specimens were well pre-
      served and unbroken).

E   = excellent (nearly all specimens were well pre-
      served and unbroken).

Planktonic foraminifers

The >150 µm fraction was examined for planktonic
foraminifers and the 63–125 µm fraction was studied
for zonal markers if they were absent in the larger
size fractions. The total number of planktonic fora-
minifers encountered in each sample was noted for
Hole M0027A. Presence/absence data were collected
for all species observed.

Species identification was made by reference to Blow
(1969), Bolli et al., (1985), and Kennett and Srini-
vasan (1983). The zonation schemes of Berggren et
al. (1995) for the Neogene and Berggren and Pearson
(2005) for the Paleogene were used to assign bio-
stratigraphic ages based on planktonic foraminifers.
In addition, the zonations of Blow (1969), Shackle-
ton et al. (1995), and Lourens et al. (2004) for the
Neogene and Berggren and Miller (1988) for the
Paleogene are also referred to in this study to enable
comparison of planktonic foraminifer data to results
from previous scientific ocean drilling legs. These zo-
nation schemes are tied to the BKSA95 integrated
magnetobiochronologic timescale and shown in Fig-
ure **F12.** Age estimates for important biohorizons are
given in Table **T2** and tied to the BKSA95 unless oth-
erwise noted. In cases where key marker species were
rare or absent, secondary markers were used whose
ranges were calibrated by Berggren et al. (1995), Bolli
et al. (1985), and Shackleton et al. (1999).

Benthic foraminifers

Benthic foraminifers were examined primarily from
the >150 µm size fraction. The >63 µm size fraction
was checked in barren samples and spot-checked
elsewhere. Paleobathymetric estimates were based on
qualitative assemblages, although in some samples
the total number of specimens encountered was re-
corded.

Bathymetric zones were defined as inner neritic (0–
50 m), middle neritic (50–100 m), and outer neritic
(100–200 m). Taxonomic concepts, paleobathymet-
ric estimates, and paleoenvironment interpretations
were based on multiple references (Culver and Gos-
horn, 1996; Cushman and Cahill, 1933; Gibson,
1983; Katz et al., 2003; Miller et al., 1997; Olsson et
al., 1987; Schnitker, 1970; Snyder et al., 1989), with
the general paleobathymetric model following Miller
et al. (1997) for coeval onshore New Jersey sections.
In general, *Elphidium*-dominated biofacies were in-

terpreted as upper inner neritic (<10 m), *Hanzawaia
concentrica*–dominated biofacies as middle inner ner-
itic (10–25 m), *Nonionella pizarrensis*–dominated bio-
facies as outer inner neritic (25–50 m), *Buliminella
gracilis*–dominated biofacies as upper middle neritic
(50–80 m), *Uvigerina juncea*–dominated biofacies as
lower middle neritic or deeper (>75 m), and high-di-
versity, low-dominance assemblages with key indica-
tor taxa (e.g., *Hanzawaia mantaensis* and *Oridorsalis*)
as outer neritic (>100 m). Paleobathymetric esti-
mates within this framework have a high degree of
confidence. Within a depth zone, a sample may be
noted to be, for example, "slightly deeper than the
previous sample" based on minor abundance
changes of key depth-indicator species, but this can-
not be quantified to the meter level.

In addition, assemblages dominated by infaunal taxa
such as *Uvigerina, Rectuvigerina,* and *Bulimina,* espe-
cially with diatom and radiolarian co-occurrences,
can indicate low-oxygen, high–organic carbon envi-
ronments typically associated with upwelling zones.
In contrast, assemblages dominated by epifaunal
taxa such as *Gyroidinoides, Cibicidoides,* and *Han-
zawaia* can indicate better oxygenated, low–organic
carbon oligotrophic environments.

Palynomorphs

Samples (mainly from core catchers collected off-
shore and prepared onshore before the OSP) of 5 mL
volume were processed for palynological analysis by
disaggregating samples in a warm, weak (0.02%) so-
dium metaphosphate solution prior to sieving using
15 µm Nitex mesh. Samples were centrifuged for 4
min at 3000 rpm, washed with distilled water, and
then treated with warm 10% HCl, dissolving a tablet
containing 10,500 ± 300 *Lycopodium* spores, which
allows for calculation of absolute abundances of pa-
lynomorphs in the sediment. Samples were centri-
fuged, rinsed with water, centrifuged again, and
treated with 48% HF. After a third centrifugation and
rinsing, the samples were sieved again prior to
mounting in glycerine jelly.

Dinocysts

Slides were examined at 400× and 1000× magnifica-
tion for dinoflagellate cysts. Dinocyst assemblages
were tied to the biostratigraphic zonations of de Ver-
teuil and Norris (1996), Van Simaeys et al. (2005),
and Eldrett et al. (2004) for the Miocene, Oligocene,
and Eocene sequences, respectively. These zonations
are correlated to the BKSA95 integrated magnetobio-
chronologic timescale. Reference was also made to
several other sources in the literature, such as Wil-
liams and Manum (1999), Louwye et al. (2000), Slu-
ijs et al. (2003), Munsterman and Brinkhuis (2004),

Dybkjær (2004), and Van Simaeys et al. (2004). Biostratigraphic zones were assigned to the Pleistocene sequence based on dinocyst assemblages and ranges following McCarthy and Gostlin (2000). The relative abundance of dinocysts versus pollen and plant spores was determined to facilitate sea level reconstructions, as described in McCarthy et al. (2003), together with an approximation of palynofacies following the criteria of Batten (1996). Dinocyst assemblages were used to make inferences regarding surface water conditions (temperature and salinity) to accompany paleoenvironmental interpretations based on the observation of terrestrial palynomorphs in the same slides.

Terrestrial palynomorphs

The slides used for the examination of dinoflagellate cysts were also used for the analysis of terrestrial palynomorphs. Slides were examined for terrestrial palynomorphs mainly under plane-transmitted light at 400× and 1000× magnification, with additional use of phase-contrast illumination. Slides were examined for pollen grains, plant spores, and fungal spores (morphotypes only). Pollen and plant spores were identified using McAndrews et al. (1973), Pazzaglia et al. (1997), Beug (2004), and Traverse (2007). In addition, foraminifer test linings, dinocysts, and other algal remains were counted to achieve a direct land-sea correlation and to compare with results from the analyses of marine palynomorphs.

Characteristics of different pollen types affect their transport and resistance to degradation, resulting in alteration of the original pollen assemblage during transport. For instance, bisaccate pollen is generally overrepresented in marine pollen assemblages because of its transport properties and high resistivity to oxidation (e.g., Traverse, 2007). It was therefore excluded from the sum used for calculation of pollen percentages. Additionally, the pollen production rates of different plant taxa were incorporated into the ecosystem reconstructions for the hinterland of the New Jersey shallow shelf. As an example, the overrepresentation of certain nonsaccate pollen types, such as oak/birch pollen (because of the high pollen production of these taxa) and hickory/linden pollen (mainly because of the extraordinary thickness of their exines), was taken into account for paleoenvironmental reconstruction.

When bisaccate pollen grains dominated the pollen assemblages, 75–150 nonsaccate pollen grains were counted per slide. When nonsaccate pollen grains dominated the pollen assemblages, 100–200 pollen grains (normally ~150) were counted per slide. Obviously degraded/reworked pollen grains were excluded from the pollen sums for percentage calculations. With this approach, statistical relevance could be guaranteed to a reasonable degree even with bisaccate pollen being excluded from the pollen reference sums. *Lycopodium* spores added to the samples during processing (see **"Palynomorphs"**) were counted to allow for calculation of pollen content per core catcher. Around 60 pollen types, 8 spore types, and 12 types of fungal remains were distinguished. Dinocysts were grouped into transparent chorate/proximate and brownish chorate/proximate dinocysts.

Geochemistry

Offshore interstitial water sampling and analysis

Cores were sampled for microbiology and pore water immediately on recovery. Pore water was sampled using Rhizon samplers as long as the sediment was soft enough to insert the plastic tip of the sampler. A Rhizon sampler (CSS-F 5 cm; Rhizosphere Research Products, Netherlands) is a narrow elongated cylindrical filter (0.2 µm pore size; 5 cm long; 130 µL volume) with a stiff plastic core (Seeberg-Elverfeldt et al., 2005). Before use it is soaked for several hours in pure water, which is ejected under pressure by syringe and discarded prior to sampling. A Rhizon sampler is inserted into the core through a 3.8 mm hole, the same diameter as the Rhizon sampler to facilitate sealing, and drilled through the plastic core liner using a spacer on the drill bit to prevent it from going into the core itself. Rhizon samplers draw water from sediment under negative pressure, which is applied by attaching the Rhizon sampler to a 20 mL all-plastic syringe, pulling the plunger back, and bracing it there with a small wooden stick. Pore water is collected in the syringe. Rhizon samplers were left in a core until the rate of water collection slowed greatly, typically within 1–10 h. For long extractions, we removed the Rhizon samplers so that the core could be logged and then reapplied fresh Rhizon samplers to the same holes afterward. Usually one or two but up to four Rhizon samplers were used per sample, spaced 10 or 20 cm apart downcore, to obtain sufficient pore water; water from the separate syringes would then be combined into a single sample in a 50 mL syringe for analysis. If the sediment was too stiff to penetrate with the plastic tip of the Rhizon sampler, we made a 2.5 mm hole first with a steel rod and then pushed the Rhizon sampler into it.

Within a depth range of 190–280 mbsf, the sediment became too hard and dry to extract water with Rhizon samplers. We then switched to squeezing of whole rounds 5 cm in length in the Bremen Teflon-

lined titanium squeezer of piston-cylinder design (described in detail at **www.marum.de/en/Pore_water_squeezer.html**). Whole rounds were nearly always cut from the bottom of the first section of core, as this material was most likely to be undisturbed; Rhizons were usually inserted into the first section well below its top for the same reason. Whole rounds were scraped clean on all surfaces to remove drilling mud and material from the outer surface that may have been smeared down the core liner. They were then shaved to <54 mm diameter to fit into the squeezer. Once in the squeezer, sediment was contained when under pressure (up to 15 tonnes, applied by a hydraulic press) by a circular titanium screen at the base of the cylinder overlain by nylon mesh and a paper filter (Whatman #1), through which the water was pushed to an online filter (0.45 µm; 25 mm; nylon) and through that into a 50 mL all-plastic syringe. All parts of the squeezer that touch sediment or pore water are either polytetra-fluoroethylene (PTFE), titanium (grade 2), or Polyamid plastic (Delrin). We measured the volume of pore water extracted, the downward distance the piston traveled during squeezing (Δh), and the height and weight of the final squeezed sediment sample, now compacted into a cylinder under the pressure of squeezing. We used these measurements to estimate the initial and final sediment densities before and after squeezing and thus the compressibility of the material, as well as the fraction of interstitial water that was squeezed out. Typically, sediment samples could be squeezed to a final dry density of 2.4–2.5 g/cm^3.

Drilling mud was used throughout Expedition 313 to remove cuttings from the hole. Various formulations were used, generally including bentonite clay with a biodegradable biopolymer (starch) as a suspension enhancer. Mud was mixed in tanks with seawater from the ship's firepump system. During drilling, mud pumped downhole flushes the outside of the core barrel and exits the drill pipe through a small gap between the barrel shoe and the inner side of the drill bit. Sufficiently porous or coarse sediment can thus become contaminated with drilling mud, especially if disturbed, and must be avoided in sampling for pore water analysis. This was readily done when cutting whole rounds for squeezing, as these could be inspected in detail and cleaned before putting them into the squeezer. It was more difficult when Rhizon samplers were used, as it was sometimes difficult to assess the condition of the sediment through the clear plastic core liner. We did not sample pore water from any depth interval unless the material penetrated by the Rhizon was at least moderately

stiff and therefore likely to be intact. We took samples of each of the seven mud formulations used during Expedition 313, separated the liquid from the solids using Rhizons, and analyzed this liquid along with pore water samples and ambient seawater to test for contamination. In filtering the drilling muds we found that they readily clogged the Rhizons, resulting in very slow flow rates. This rapid clogging effectively prevented us from inadvertently sampling drilling fluid instead of pore water, especially within the loose sands and disturbed sediment that were common within the upper 200 m of the sequence.

Once pore water was extracted from the sediment core into a syringe by Rhizon sampler or by squeezing, it was pushed through a 0.45 µm online filter (25 mm; nylon) into various containers for analysis. The water was analyzed immediately onboard for pH, alkalinity, ammonium, and salinity by refractive index. pH was measured by ion-specific electrode (±0.05 units; 1σ; based on 107 analyses of ambient seawater), alkalinity by single-point titration to pH < 3.9 with 0.01 N HCl using a 0.2–0.5 mL sample (±5.8%; 1σ; based on 109 analyses of ambient seawater), and ammonium by conductivity, after separation as NH_3 through a PTFE membrane in a flow-through system. In the latter technique, modified after Hall and Aller (1992), ammonia is stripped from a 100 µL sample by an alkaline carrier solution (0.2 M Na citrate in 10 mM NaOH), passed through a 200 mm × 5 mm PTFE membrane, and redissolved as NH_4^+ in an acidic solution (1 mM HCl). Ammonium ion is then measured as the resulting conductivity signal in the acidic carrier, in a micro flow-through cell.

We monitored the drilling operation and cores for H_2S and flammable gases using the ESO gas "sniffer," a handheld unit equipped with a small pump for pumping ambient gas past a sensor. We detected H_2S only twice and flammable gases four times, only in Holes M0027A and M0028A. No H_2S odor was ever detected in any pore water sample, so no analyses were done for this species.

A total of 179 samples of sediment were collected onboard for headspace analysis, usually from the base of Section 1 adjacent to the interstitial water sample. A plug of sediment weighing 8.5 ± 1.6 g (1σ) was injected into a 20 mL glass vial prefilled with 10 mL of a solution of 0.5 M NaCl and 0.1 M $HgCl_2$ and shaken vigorously to mix for postcruise determination of the concentration of dissolved methane and its stable C isotopic composition.

Aliquots of interstitial water for OSP and postcruise analyses included an acidified aliquot (10 µL concen-

trated HNO_3/mL) for inductively coupled plasma–atomic emission spectroscopy (ICP-AES) (Li, Na, K, Mg, Ca, Sr, Ba, Mn, Fe, B, Si, S, P, Al, and Ti), inductively coupled plasma–mass spectrometry (ICP-MS) (Rb, Cs, I, Cu, Ni, Zn, Co, Mo, V, Cr, and U), and Sr isotopic composition; an unacidified aliquot for chlorinity, chloride, bromide, sulfate, nitrate, and fluoride; untreated aliquots for the stable isotopes of O and H in water and S and O in dissolved sulfate; and a 2 mL aliquot treated with 20 µL saturated $HgCl_2$ for stable isotopes of C and O in total dissolved carbonate species. Aliquots analyzed onboard for alkalinity represent an additional acidified sample, as the amount of 0.01 N HCl added is known exactly, so we kept and stored these for additional analysis if needed.

Onshore chemical analyses in Bremen

Water samples

A total of 222 filtered (0.45 µm) and acidifed (10 µL concentrated HNO_3/mL) pore water samples were analyzed by ICP-AES for the 15 elements listed above. Two sets of dilutions were run, the first adjusted for each sample to bring its chlorinity into the range of 40–50 mmol/kg and the second at a constant dilution of 100-fold for Na, K, Mg, Ca, Sr, S, and Si. The first set was run twice, the first time with a cross-flow nebulizer and the second time with an ultrasonic nebulizer. Additional trace elements (Be, V, Cr, Co, Ni, Cu, Zn, As, Mo, Cd, and Pb) were sought in the second run. In all cases, standardization was done against multielement solutions prepared from commercial standards, adjusted to a similar NaCl concentration of the diluted samples. For those elements measured in more than one run, we found that the more concentrated dilution yielded less scattered results. Our ICP-AES data for sulfur average 2.9% higher than our ion chromatography data for sulfate but show similar profiles in all three holes. Given the near-complete absence of H_2S in these pore waters, these measurements suggest that our accuracy for major elements is about ±3%.

Unacidified aliquots of the same samples were analyzed for chlorinity at the University of Hawaii (USA) prior to the OSP by automated electrochemical titration with silver nitrate (±0.53%; 1σ; based on 114 duplicate analyses of samples) using International Association for the Physical Sciences of the Oceans (IAPSO) seawater as a standard and by ion chromatography during the OSP at the University of Bremen (Germany) for chloride (±0.57%; 1σ; based on 7 duplicates of samples and 93 replicates of IAPSO seawater), bromide (±3.5%; 1σ; based on 7 duplicates of samples and 89 replicates of IAPSO seawater), sulfate (±1.6%; 1σ; based on 14 duplicates of samples and 90

replicates of IAPSO seawater), and nitrate (less than the detection limit of 3.2 µM in all samples). For chloride and sulfate, we standardized against dilutions of IAPSO seawater, whereas for bromide and for sulfate at concentrations <5 mM, we used a series of artificial seawater standards with variable amounts of bromide and sulfate. Results for chlorinity by titration were higher than those for chloride plus bromide by ion chromatography by, on average, 0.42% (1σ). We preferred the chlorinity values because they yielded ratios of Br, Na, K, Mg, and Ca to chlorinity in our seawater samples that were closer to the accepted values for seawater. We preferred the ion chromatography sulfate data over the ICP-AES sulfur data for the same reason. For both chloride and sulfate, the two sets of data show identical depth profiles in all holes, and no interpretation was changed by using one set or the other.

We calculated Na concentrations from charge balance and used these values rather than those measured by ICP-AES. The measured values averaged 5.9% higher but were much more scattered, consistent with the precision of this technique of ~5% on 100-fold diluted samples. The calculated values have essentially the same precision as the chloride data, ~0.6%. The two data sets for Na yielded similar depth profiles in each hole.

Sediment samples

About 150 samples of sediment (5 cm^3) were freeze-dried and finely ground by hand in an agate mortar. Sediment samples were analyzed for contents of organic carbon, carbonate, and sulfur using a LECO CS-125 carbon-sulfur analyzer at the University of Bremen. Approximately 50 mg of dried, ground sample was weighed in a ceramic cup and heated in a furnace. The evolved CO_2 and SO_2 were then measured with a nondispersive infrared detector. A second aliquot of ~90 mg was weighed in a ceramic cup, reacted with 12.5% HCl twice, washed with deionized water twice, and reanalyzed as above. The CO_2 measured in the second run was assumed to come from organic carbon. The analytical precision is about ±0.02% absolute.

X-ray diffraction

A subset of the same freeze-dried and ground samples was analyzed for mineral content by XRD. XRD measurements were performed at the Crystallography Department of Geosciences, University of Bremen, on a Philips X'Pert Pro X-ray diffractometer equipped with a Cu tube (Kα λ 1.541), a fixed divergence slit (¼°2θ), a 15 sample changer, a secondary monochromator, and the X'Celerator detector system. Measurements were made from 3° to 85°2θ with

a calculated step size of 0.016°2θ (see also Vogt, 2009, and Expedition 302 Scientists, 2006, for IODP Expedition 302). The calculated time per step was 100 s. Peak identification was done graphically using the Macintosh program MacDiff (version 4.5), available at **http://servermac.geologie.uni-frankfurt.de/ Staff/Homepages/Petschick/Petschick.html** (Petschick et al., 1996).

For mineral identification, integrated intensities for the investigated mineral peaks were calculated by MacDiff. Ratios of these intensities to the total intensity for a given scan were then used to estimate the proportions of the various minerals present. The fraction of the total intensity represented by the 35 peaks quantified for 29 different minerals or mineral groups varied from 90% to 93%. To provide an easy comparison to published data on surface samples from the potential source regions (Andersen et al., 1996; Vogt, 1997; Vogt et al., 2001), the fixed divergence was changed to automatic divergence using an algorithm integrated in MacDiff.

Quality assurance and quality control

Care was taken throughout to obtain uncontaminated sediment and interstitial water for analysis, as documented above. Sampling and analytical procedures that have long been standard practice within ODP and IODP were used throughout.

Physical properties

The primary objective of the petrophysical program was to collect high-resolution petrophysical property data that would

- Enable characterization of lithologic units and formation properties,

- Facilitate hole-to-hole correlation and the retrieval and construction of complete composite stratigraphic sections together with lithologic and sedimentological descriptions for each hole, and

- Provide data for post-OSP construction of synthetic seismograms and investigation of the characteristics of major seismic reflectors.

Offshore, the petrophysics program involved collecting high-resolution, nondestructive measurements on whole cores using a Geotek MSCL. The MSCL was outfitted with four sensor types in order to measure gamma density, transverse compressional wave (*P*-wave) velocity, noncontact electrical resistivity (NCR), and magnetic susceptibility. Note that "gamma density" refers to the bulk density of the core as derived from the collimation of gamma rays across the core (see **"Gamma density"**).

Onshore, petrophysical measurements included NGR (measured on whole-round cores prior to the OSP), digital line scan images, and color reflectance (split cores during the OSP). Lower resolution measurements of thermal conductivity on unsplit cores using a full-space needle probe prior to the OSP and on samples extracted from cores split and measured during the OSP for discrete *P*-wave velocities and moisture and density (MAD) were routinely performed manually. Discrete *P*-wave velocities were mostly measured at the same depth as MAD determinations at an approximate resolution of one per core section from the working half of split cores. A helium gas pycnometer was used to measure the volume (for density determinations) of discrete samples at an approximate resolution of one per core section from the working half of split cores. This allowed independent determination of bulk density, dry density, grain density, water content, porosity, and void ratio, all of which were used to calibrate the high-resolution, nondestructive measurements made offshore on whole cores with the MSCL.

Offshore petrophysical measurements

The MSCL has four primary measurement sensors mounted on an automated track that sequentially measure gamma density, *P*-wave velocity, NCR, and magnetic susceptibility. Two secondary measurement sensors are also present that allow these primary measurements to be corrected for core diameter and temperature. Whole-round core sections were measured with the MSCL set up in horizontal mode. Standard mode measurements were taken on all core sections except for cores below Core 313-M0029A-173R (see **"P-wave velocity"**) after they were equilibrated to ambient temperature. Core catcher pieces were not included in the logging process.

Data quality is a function of both core quality and sensor precision. Optimal measurements for all sensors require a completely filled core liner and fully water-saturated cores for *P*-wave velocity and gamma density measurements. In sections where the core liner is not filled or the core is insufficiently saturated, the measurement quality is compromised. In terms of sensor precision, gamma density and magnetic susceptibility sensors are affected by the duration of each point measurement. *P*-wave velocity, resistivity, and magnetic susceptibility measurements are affected by room and core temperature. The influence of room temperature is corrected for in postprocessing. To provide high-resolution data during Expedition 313, a downcore measurement sampling interval of 1 cm for all sensors was chosen on the ba-

sis of the amount of core and time, coupled with attaining optimal resolution of data.

A full calibration of the MSCL sensors was conducted at the start of the expedition, every time the system was rebooted (for example, after power failure or after transit), and when calibration checks revealed unacceptable departures from the full calibration values (see below) (Table T3). Checks on the full calibration were then performed approximately once every five to six cores. The calibration check involved logging three calibration reference pieces (magnetic susceptibility piece, standard core liner saturated with distilled water, and standard core liner saturated with 3.5 g/L salinity fluid) and comparison with the values derived during the full calibration. This allows the performance of the four primary sensors to be assessed quickly for gamma density, *P*-wave velocity, electrical resistivity, and magnetic susceptibility. Only if the values departed from the acceptable range was a repeat full calibration performed (Table T3).

Measurement principles

Gamma density

Gamma density is measured by determining the attenuation of gamma rays (mainly by Compton scattering) that pass through the cores. Gamma density is used to estimate bulk density. The degree of attenuation is proportional to the electron density in the gamma path (Rider, 2006; see 2008GEO.PDF in PHYSPROP in "Supplementary material"). Gamma attenuation coefficients vary as a function of atomic number, but as most rock-forming minerals have similar and low atomic numbers, the correlation between gamma density and bulk density is generally very good. A small (370 MBq) ^{137}Cs source (half life = 30.2 y) was used to produce a gamma beam with primary photon energies of 662 keV. Two collimators are available (2.5 and 5 mm). Measurement intervals were set at 1 cm with count time set at 10 s (the same as the magnetic susceptibility sensor) and the 5 mm collimator position selected in order to maximize gamma counts. The resolution with this setup is 0.5 cm.

Calibration of the system for Expedition 313 was completed using stepped water/aluminium density standards (provided by Geotek). Initial full calibration was performed using a standard core liner (~0.3 m length) containing a stepped aluminium calibration piece centered inside the liner, which was filled with water. Gamma counts were taken for 30 s through each of the five aluminium steps of known thicknesses (6, 5, 4, 3, and 2 cm). In addition, the

gamma counts of a liner filled with only distilled water was recorded. Regular (every five to six cores) calibration checks were conducted during logging, using the distilled water calibration piece (used for *P*-wave velocity in the main calibration).

P-*wave velocity*

Transverse *P*-wave velocity was measured using two *P*-wave transducers aligned perpendicular to the core axis with *P*-waves passing through the core horizontally (in whole core set up). A compressional wave pulse centered on a frequency of 320 kHz was transmitted through the core. A pair of displacement transducers monitored the separation between the *P*-wave transducers so that small variations of the distance (liner diameter) over which the traveltime was measured could be corrected for. As for the other sensors, measurement spacing was set at 1 cm.

Initial calibration was performed using a distilled water–saturated standard core liner piece (~0.3 m length) at known temperature. This was repeated as necessary following checks by logging the calibration piece at regular intervals during the logging process (one calibration check every five to six cores).

This measurement is critically affected by the quality of the core. Poor data results occur where undersized core causes a separation between the core material and core liner and where the core is insufficiently water saturated to allow for optimal propagation of *P*-waves. During Expedition 313, whenever the core was clearly insufficiently water saturated and/or contact with the liner was poor, the quality of the *P*-wave data was considered to be unreliable and the data were either deleted from the final processed data set or a note was appended to the comments column in the MSCL spreadsheet. In some cores, the poor quality of core/lack of fluid in the liner resulted in "cycle skipping," where the automatic picker in the software cannot pick the first arrival of the signal and chooses a later waveform. This results in a constant offset in the data, some of which was corrected prior to the OSP (Fig. F13B).

A change in procedure was decided upon during measurements of Hole M0029A cores because of poor or no signal through the sediment. This was attributed to small bubbles in the fluid in the liner, which were thought to impede the passage of the signal through the sediment (see "Physical properties" in the "Site M0029" chapter). Tests indicated that results improved when measurements were made on cores cooled to ~4°C so that gases partially dissolved in the fluid. Cores below Core 313-M0029A-173R were measured in this manner.

Noncontact electrical resistivity

Electrical resistivity of sediment cores was measured using the noncontact resistivity sensor. The sensor operates by inducing a high-frequency magnetic field in the core from a transmitter coil, which in turn induces electrical currents in the core. These currents are inversely proportional to resistivity (Jackson et al., 2006). The small magnetic fields regenerated by these electrical currents are measured by a receiver coil and normalized with a separate set of identical coils operating in air. The spatial resolution of measurement is ~2 cm. The measurement interval selected was 1 cm, as for the other sensors.

Initial calibration was performed using six standard core liner sections (~0.3 m in length) containing water of varying but known salinity. The five standards were made up to concentrations of 35 (35,000 ppmw), 17.5, 8.75, 3.5, 1.75, and 0.35 g/L. This calibration procedure was repeated as necessary following regular checks by logging a piece of core liner filled with saline fluid from the middle of the anticipated salinity range (3.5 g/L) of the logged core.

Resistivity measurements indicate the amount and kind of pore fluid in the core sediment. Because these values are integrated over a depth of several centimeters, measurements taken near the ends of a core section are not included. Furthermore, any trends in values toward these deleted values should be used with caution.

Magnetic susceptibility

Whole-core magnetic susceptibility was measured on the MSCL using a Bartington MS2 meter coupled to a MS2C sensor coil. The loop sensor has an internal diameter of 80 mm, corresponding to a coil diameter of 88 mm. The loop used for Expedition 313 is a nonstandard loop operating at a frequency of 513 Hz, which necessitates a correction factor ($\times$ 0.908) to be applied to the data. The MS2 system operates on two fixed sensitivity levels—$\times$0.1 and $\times$1—corresponding to 10 and 1 s sampling integration periods, respectively. The mode used was adjusted according to the signal response from the cores in order to optimize the data quality. For all cores except a small interval in Hole M0027A, the $\times$0.1 setting was most appropriate. Measurements were made at a spacing of 1 cm. The sensor automatically zeroes and takes a free air reading at the start and end of each run in order to account for instrument drift by subtraction of a linear interpolation between readings. Magnetic susceptibility data were recorded as corrected volume specific units ($\times 10^{-5}$ SI).

The accuracy of the magnetic susceptibility sensor was checked using a calibration standard (made of impregnated resin) with a bulk susceptibility of 213 $\times 10^{-6}$ cgs. This calibration piece was centered within a core liner, and calibration checks were carried out approximately every five to six cores to check reliability of the sensor.

Because of a sensor problem in Hole M0029A, the 80 mm loop was changed to a 120 mm loop with a standard operating frequency of 565 Hz for all cores deeper than Section 313-M0029A-120R-1. Caution should be taken with data in cores measured from some depths above the change because of occasional skips in the data resulting from the sensor malfunctioning. Extra care should also be used in analyzing magnetic susceptibility data from Hole M0029A subsequent to the change in procedure (see **"P-wave velocity"**) because of variable unknown effects of colder temperatures on the electronics of the magnetic susceptibility loop.

Quality assurance and quality control

A quality assurance/quality control (QA/QC) check was carried out in three stages: during the offshore phase of the expedition, before the OSP, and during the OSP. During the offshore phase, QA/QC involved core quality description, use of hard copy and electronic MSCL log sheets and calibration sheets, and repeat MSCL logging of selected cores as described below. Postoffshore systematic cross-checks of electronic calibration, data files, and processed data were made. A considerable number of core sections were relogged for QA/QC and will enable more comprehensive postexpedition analysis than has been carried out to date, especially relating to corrections using core liner fill estimations and the effect of measuring cores "cold." The final data set was made available during the onshore phase as raw, processed, and filtered data.

Repeat logging for QA/QC

The reproducibility of the MSCL data was assessed by repeat logging a selection of core sections from each hole while offshore (Fig. **F13;** Table **T4**). Attempts were made to log core sections from roughly every 50 m in depth to avoid any bias. Typically sections with good liner-filling were selected to ensure measurements could be obtained from all sensors. A few cores were selected for QA/QC to document the influence of core thickness and drilling mud filling the core liner. When procedural or method changes occurred, such as changing to a larger magnetic susceptibility loop size and measuring cores at a colder temperature, additional cores were relogged to enable evaluation of the effect of the change and to test for consistency of the measurements.

In general, reproducibility is good. Gamma density is very consistent, with deviations <3% (Fig. F13A; Table T4). *P*-wave velocity, resistivity, and magnetic susceptibility have deviations between 10% and 40% (Fig. F13B, F13C, F13D; Table T4).

MSCL logsheets

Throughout the expedition, information was recorded on both hard copy and electronic MSCL logsheets in an attempt to ensure all information that affects the quality of the result was retained. QA/QC included

- Observation of core liner fill, fluid content, and cracks in the core;
- Top depths cross-checked with final DIS depths;
- Notes for sections where there were apparently sensor issues;
- Notes for those sections measured at a 2 cm sampling interval (instead of the standard 1 cm);
- A column for mud type used (cross-checked with Operations Log);
- Notes on the presence of metal in any section noted and cross-checked with the DIS;
- Notes where cores were measured cold; and
- Notes as to which magnetic susceptibility loop was used.

Core quality and liner fluid fill

In an attempt to allow improvement of the MSCL data set in the future, the percentage of liner fill and the percentage of drill fluid in the liner were estimated and noted on the MSCL logsheets. In particular, electrical resistivity is affected by core liner saturation with drill fluid. Most short sections have low core liner saturation. In general, all Section 3s (generally short sections) are removed from the plotted results in the site chapters.

For gamma density data, it is clear that the tops of cores and ends of cores often have greatly reduced densities. From core inspection, this problem is a result of fractured/disturbed core top and bottom. In case of short Section 2s or 3s, the problem seems persistent, especially if short sections contain hard cemented sediments. The most obvious of these data were removed during the logging process offshore. Other than this, no attempt was made to correct for this, except through numerical high pass filtering (in the results). Future analyses could choose to filter out any sections shorter than a certain length (~20 cm) or to check whether the values of a short section are lower than the average of the core.

Deletion of values around core end-caps

Offshore, operators deleted from the processed files all data around end-caps that were clearly affected by these caps, although the decision was to be conservative if any operator was unsure. As the amount of data affected varies for each sensor and the effect is gradational away from the end of the core, different analyzers may choose to delete various amounts of data. For this reason, a column was included in the final spreadsheet listing all values within 10 cm of an endcap.

QA/QC before OSP

MSCL calibration sheets were checked for errors and consistency before the OSP and compiled into a summary file that is accessed for data processing of all raw data files.

MSCL calibration summary file

A MSCL Calibration Summary File was created that included

- A compilation of all the processing parameters for each of the calibrations and
- A calculation of all processing parameters cross-checked between electronic and hard copies.

Reprocessing of raw MSCL data

After correction of calibration files and the calibration summary file, all raw MSCL data files and raw QA/QC data from the offshore part were reprocessed. This involved *P*-wave velocity and resistivity in the merged MSCL excel sheet. The final data set was made available for the OSP as raw, processed, and filtered data.

Onshore petrophysical measurements

Onshore petrophysical methods are described in the order in which they were done. NGR and thermal conductivity required measurement on whole cores, and measurements were therefore taken in advance of the OSP. Line scanning and color reflectance measurements were conducted on split-core sections, and it was necessary to do these measurements as soon after splitting as possible to record accurate colors before the core dried. The remaining measurements (discrete *P*-wave and MAD) were conducted on discrete samples taken from the split cores and were done last.

Natural gamma radiation

NGR emissions of sediments are a function of the random and discrete decay of radioactive isotopes, predominantly those of ^{238}U, ^{232}Th, and ^{40}K and their

radioactive daughter products (for example, [208]Tl, [228]Ac, and [214]Bi). These decays are measured through scintillation detectors housed in a shielded collector (see 2008GEO.PDF in PHYSPROP in "Supplementary material"). Total counts per second were measured by integration of all emission counts over the gamma ray energy range between 0 and 3 MeV. Measuring total counts gives a reasonable precision with relatively low counting times (minutes per sample) and is well suited for correlation with core and downhole wireline log measurements used for core depth corrections. No corrections were made to NGR data from Expedition 313 to account for volume effects related to sediment incompletely filling the core liner.

NGR measurements began 6 weeks prior to the start of the OSP and continued into the second week of the OSP. A Geotek XYZ frame system was employed that allowed up to six core sections to be logged during a single run. The gamma ray detector has a measurement window of 7.5 cm, and the sampling interval was set at 9 cm to maximize the resolution of measurements in the time available while minimizing resampling of intervals. For the shortest sections, measuring points were individually selected. The count time at each sampling point was set at 3 min. This sampling interval and count time provided the highest resolution and best data quality possible within the time available to complete core logging. Where appropriate, sampling intervals on short cores were manually set so that a greater density of data points could be acquired.

Measurements were carried out at ~5°C in the refrigerated core repository at the Center for Marine Environmental Sciences (MARUM) at the University of Bremen to ensure there was no drift in measurement over time. After the equipment became temperature equilibrated, a source of [133]Ba and a source of ^{60}Co were used for energy calibration of the spectrum. A zero reading of background NGR counts was taken before measurement began, followed by measurement of the background when a core of similar density in a liner was in the machine. This allowed for the correction of data at ambient levels of gamma radiation. These measurements were repeated at the completion of logging. The Geotek XYZ software was used for measuring background NGR and calibration and for standard measurements.

Fourteen core sections across the three holes were relogged with the NGR to assess the repeatability of the results. Generally speaking, the trends observed in the two data sets were very similar. However, original values were usually greater than their QA/QC counterparts (9% higher, on average). There is no correlation between the number of counts and the difference in values between the original and repeated values.

Thermal conductivity

Thermal conductivity was measured with the TeKa TK04 system using the needle-probe method in full-space configuration for soft sediments (Von Herzen and Maxwell, 1959). The needle probe contains a heater wire and calibrated thermistor. It is assumed to be a perfect conductor because it is significantly more conductive than the sediments measured. Cores were measured at 4°–6°C.

Thermal conductivity of unsplit cores from Expedition 313 was measured by inserting the needle probe into the sediment through a small hole drilled into the core liner parallel to the working half/archive half surface (splitting surface) to ensure minimum disturbance to either split-core section. Generally, thermal conductivity (k) is calculated from the following:

$$k(t) = (q/4\pi) \times \{[\ln(t_2) - \ln(t_1)]/[T(t_2) - T(t_1)]\},$$

where

T = temperature (K),
q = heating power (W/m), and
t_1, t_2 = time interval (normally 80 s duration) along the heating curve(s).

The optimal choice of t_1 and t_2 is difficult to determine; commonly, thermal conductivity is calculated from the maximum interval (t_1 and t_2) along the heating curve where $k(t)$ is constant. In the early stages of heating, the source temperature is affected by the contact resistance between the source and the full space and in later stages is affected by the finite length of the heating source (assumed infinite in theory). The special approximation method (SAM) employed by the TK04 software is used to develop a best fit to the heating curve for all of the time intervals where

$$20 \le t_1 \le 40,$$

$$45 \le t_2 \le 80,$$

and

$$t_2 - t_1 > 25.$$

A good measurement results in a match of several hundred time intervals along the heating curve. The best solution (output thermal conductivity) is that which most closely corresponds to the theoretical curve. Numerous measuring cycles were automatically performed at each sampling location.

Thermal conductivity measurements were taken at one location within a core (all cores from Expedition 313 were <3 m), and core sections were sampled at a frequency of one per every five cores within Section 1 where available. If core quality was not appropriate for measurements in the fifth core, the nearest section to it was selected. Measurements were taken primarily in soft sediments, into which the TK04 needles could be inserted without risk of damage. However, if sediments were partially or completely lithified, a small hole was drilled into the core prior to inserting the TK04 needle. Twelve additional measurements were taken at the request of an expedition geochemist.

The quality of thermal conductivity measurements was monitored as measurements were taken. Multiple measurements (up to 99 per thermal conductivity run) were taken at the selected depth within each core. Data quality was evaluated by the operator, with spurious or poor data owing to boundary effects and reflections (especially where there was not good contact between the core and the probe [due to cracking]) being removed prior to calculation of a mean thermal conductivity and standard deviation.

Digital imaging

Digital line scan images of the split cores were obtained during the OSP using the Avaatech Superslit X-ray fluorescence (XRF) core scanner in operation at MARUM. The linescanner is supported by the DFG-Leibniz Center for Surface Process and Climate Studies at the University of Potsdam (Germany). The XRF scanner has an option for line scan camera and linear light source. The line scanner produces high-resolution color images and also outputs accurate color data in red-green-blue (RGB) and Commission Internationale d'Eclairage (CIE) Lab (lightness) a (green to red chromacity) b (blue to yellow chromacity) units (L*a*b*) because of individual charge-coupled device (CCD) pixel calibration. The Line Scan program uses the Stemmer Common Vision Blox (CVB) platform to acquire and process color images.

The camera system contains a CCD camera using 3×2048 pixels with beam-splitter and a manually controlled Pentax 50 mm lens. The image resolution is ~150 pixels/cm in crosscore and downcore directions. With an exposure time of 5 ms, a scan speed of 125 mm/s was achieved. Added to this is initialization time and camera repositioning after a scan. The image coverage is ~13.5 cm crosscore and a maximum of 153 cm downcore.

After every split core was imaged, a color/gray chart was measured with the same settings as those used for the core. Three output files were generated for each core section: a high-resolution bitmap file (.BMP), a compressed image file (.JPEG), and a numeric text file (.TXT). Numeric data are in RGB units. The line scan system was calibrated every 24 h with black and white calibration. All split cores were measured using aperture setting f/5.6+ (a fixed value between 5.6 and 8) and white calibration level f/11+ (a fixed value between 11 and 16). Consistency of equipment settings was chosen over custom settings in order to ensure uniformity of the data set. Software features necessitated the length of line scan images at a couple of centimeters longer than the curated core length. For Expedition 313, bitmap picture files were modified to match the length of the cores after the image was taken. Where a whole-round sample had been removed from the core, a foam placer was inserted in its place. Numeric data files were corrected to the same length as the modified .BMP picture files. Sections longer than ~154 cm extend beyond the length of the scanner and thus were scanned twice (opposite ends at the top of the scanner). The images were carefully merged in Adobe Photoshop. Both original and corrected files were uploaded to the database. All images were checked by the operator to ensure that the full core section had been captured by the scan before the data was accepted.

Diffuse color reflectance spectrophotometry

Archive halves of all split cores were measured during the OSP at a 2.5 cm sampling interval using a Minolta spectrophotometer (model CM-2600d) installed on the MSCL system. Where the split cores were exceptionally underfilled or disturbed, the measurement interval was changed to 10 cm. In certain instances where core sections contained a lot of fluid, the sections were not measured because of the risk that fluid might come into direct contact with the sensor. On this integrated system, the spectrophotometer moves vertically up and down, interlocked with the *P*-wave equipment. For Expedition 313, color reflectance measurements were carried out separately with all other sensors switched off. White calibration of the spectrophotometer was carried out twice per day, and a calibration for zero was performed once per day on starting up the machine. Vertical adjustment of spectrophotometer and pusher adjustment to the reference point were performed before every run. The split calibration piece (stepped aluminium) for gamma density was used as the reference height of the spectrophotometer. Prior to measurement, the core surface was covered with

clear plastic wrap to maintain a clean spectrometer window.

Spectrophotometric analysis produced three types of data:

- L*, a*, and b* values, where L* is a total reflectance index ranging from 0% to 100%, a* is green (–) to red (+) chromaticity, and b* is blue (–) to yellow (+) chromaticity;

- Munsell color values; and

- Intensity values for 31 contiguous 10 nm wide bands across the 400–700 nm interval of the visible light spectrum.

Measurement quality is affected by the degree and uniformity of sediment fill in the split liner, by cracks or core disturbance, and by the smoothness of the clear plastic wrap over the core surface. Comments for every section were uploaded to the database along with the data to allow for better retrospective evaluation of data quality. When utilizing the spectrophotometric measurements, it is recommended that detailed examination of core photos/images and disturbance descriptions/tables be undertaken in order to filter out unreliable or spurious data.

P-wave velocity from discrete samples

P-wave velocity in material removed from a split core can be derived from the traveltime of seismic waves passing through a sample of known thickness. *P*-wave velocity varies with the lithology, porosity, and bulk density of the material; the state of stress, such as lithostatic pressure; and the fabric or degree of fracturing. In marine sediments and rocks, velocity values are also controlled by the degree of consolidation and lithification, by fracturing, and by occurrence and abundance of free gas and gas hydrates. *P*-wave velocity is used together with density measurements to calculate acoustic impedance or reflection coefficients, which can be used to estimate the depth of reflectors observed in seismic profiles and to construct synthetic seismic profiles.

P-wave velocity was measured during the Expedition 313 OSP using a Geotek *P*-wave logger for discrete samples (PWL-D). The equipment consists of a mechanical section containing the transducers (between which the sample to be measured is placed), a set of electronics, and a PC. The two transducers also contain receivers. Acoustic coupling is through solid neoprene surfaces (pads on the transducers) and is improved by applying downward pressure on the sample between transducers and by wetting the neoprene with distilled water. A laser distance transducer measures the thickness of the sample. The PWL-D system can measure velocities on cubic or cylindri-

cal, consolidated or lithified core specimens. Unconsolidated samples are not suitable for measurement with the PWL-D because they tend to crumble when placed between the transducers. The system allows measurement on split cores in the direction perpendicular to the split core surface.

The basic velocity equation is

$$v = d/t,$$

where

> d = distance traveled through the material (m) and
> t = traveltime (s).

The PWL-D was calibrated at the start of each set of samples measured. Calibration involved the measurement of a sample of known length and *P*-wave velocity, and a measurement was also taken with the transducers touching (zero distance). In order to monitor drift of the measurements, the velocity of the calibration piece was also noted at the end of each measuring session.

Time delays subtracted to correct traveltime are (1) delays related to the transducers and electronics (t_{delay}) and (2) delays related to the peak detection procedure (t_{pulse}). Delays were determined during calibration with zero distance. For routine measurements on discrete samples with the PWL-D system, the equation for the velocity is

$$v_{sample} = (10000 \times d_{sample})/(TOT - PTO),$$

where

> v_{sample} = velocity through sample (m/s),
> d_{sample} = measured thickness of the sample (mm),
> TOT = measured total travel time (µs), and
> PTO = delay correction (µs).

A pulse is sent to the transmitter sensor, which generates an ultrasonic compressional pulse at ~230 kHz that propagates through the sample and is received by the receiver sensor. The received signal is processed through an analog to digital converter before appearing in the software display. The signal is digitized at a sampling frequency of 12.5 MHz.

In the software, a threshold detector determines the first positive or negative excursion on the received pulse; this determination can be adjusted by the operator. Pulse timing is achieved by measuring the time to the first zero crossing after the threshold has been exceeded. In this way, the traveltime measured is approximately one-half of the wavelength after the start of the pulse but is measured without any errors caused by signal amplitude. This value represents a delay that can be used to define the point at which the software should start its threshold detec-

tion. The delay should be set before the start of the signal.

Sample quality strongly affects the ability to acquire *P*-wave velocity data. It was important during Expedition 313 to prepare the sample correctly in order to get good contact between the transducers. Preparation involved cutting the sample to ensure there were two flat, parallel surfaces to aid in good acoustic coupling with the transducers; surfaces were wetted, and downward pressure was applied. *P*-wave velocity is also sensitive to temperature (Leroy, 1969) and increases with increasing temperature. Temperature was recorded during every measurement and was so uniform that no temperature corrections needed to be applied. The *P*-wave system was calibrated before every measuring session.

P-wave measurements were made on discrete samples taken one per section on average, in most cases at the same depth or near the MAD sample. It was not possible to measure all samples. This was because some samples were not well consolidated and crumbled when placed between the transducers. *P*-wave measurement was performed three times for each sample to check for consistency. No averaging was made. The data files are in comma-separated value (CSV) format, containing a header with the core and sample ID followed by measured data and calculated velocity. The waveform is recorded in two columns containing the time base and voltage changes.

A batch of samples was remeasured on different days in order to check the repeatability of the data and ascertain the validity of the calibration. Discrete *P*-wave results were shown to be consistent when measuring these same samples at different times.

Moisture and density

MAD measurements (bulk density, dry density, grain density, water content, porosity, and void ratio) were determined from measurements of the wet and dry masses of core plugs and dry volumes. Together with sonic velocity, density measurements are used to calculate acoustic impedance or reflection coefficients, which can be used to estimate the depth of reflectors observed in seismic profiles and to construct synthetic seismic profiles. Density measurements also reflect lithologic variations.

Discrete samples of <10 cm³ were taken from working-half sections and transferred into previously weighed 10 mL glass beakers. Samples were taken at an interval of one sample per section where core quality allowed. An additional 3 to 15 cm³ sample was collected as close as possible to the MAD sampling point for discrete transverse *P*-wave velocity measurements.

Wet samples were weighed to a precision of 0.001 g using an electronic balance (M_{wet}). Samples were dried in a convection oven at 60° ± 5°C for a period of 48 h followed by cooling to room temperature in a desiccator. Dry sediments were successively weighed (M_{dry}) and measured using a Quantachrome pentapycnometer (helium-displacement pycnometer) with a precision of 0.02 cm³. This equipment allowed the simultaneous analysis of four different samples and one standard (calibration spheres). Volume measurements were repeated a maximum of five times or until the last three measurements exhibited <0.02% standard deviation, with a purge time of 1 min. Volume measurements were averaged per sample (V_{dry}). Calibration spheres were cycled from cell to cell of the pycnometer during each run to check for accuracy, instrument drift, and systematic error.

The mass of the evaporated water (M_{water}) is given by

$$M_{water} = M_{wet} - M_{dry}.$$

The volume of pore water (V_{pw}) is given by

$$V_{pw} = M_{pw}/pw,$$

where

M_{pw} = mass of the pore water and
pw = pore water density (1.024 g/cm³).

Salt precipitated in sample pores during the drying process is included in M_{dry} and V_{dry} values, resulting in the following approximations:

- The mass of pore water (M_{pw}) is given by the mass of the evaporated water ($M_{water} = M_{pw}$);
- The mass of solids, including salt (M_{solid}), is given by the dried mass of the sample ($M_{dry} = M_{solid}$); and
- The volume of solids, including salt (V_{solid}), is given by the measured dry volume from the pycnometer ($V_{dry} = V_{solid}$).

The wet volume (V_{wet}) is given by

$$V_{wet} = V_{solid} + V_{pw}.$$

For all sediment samples, water content (*w*) is expressed as the ratio of the mass of pore water to the wet sediment (total) mass:

$$w = M_{pw}/M_{wet}.$$

Wet bulk density (*w*), dry bulk density (*d*), sediment grain density (*g*), and porosity (ϕ) are calculated from the previous equations (density is given in g/cm³):

$$w = M_{wet}/V_{wet},$$

$$d = M_{solid}/V_{wet},$$

$$g = M_{solid}/V_{solid},$$

and

$$\phi = V_{pw}/V_{wet}.$$

Expedition 313 samples were selected from undisturbed intervals. However, it was not possible to ensure that all were completely uncontaminated by fluid introduced during the core splitting and sampling process. QA/QC assessment included measuring samples taken at the same depth ("different sample, same day") and remeasuring selected samples at different times ("same sample, different day"). The repeated measurements differed by ±2% to ±8% (Table **T5**). Despite any uncertainties, there is reasonable correspondence between gamma density (MSCL) and wet bulk density (see **"Physical properties"** in the "Site M0027" chapter).

Porosity values derived from MAD measurements may be underestimated—in particular, sand units by ~10% and perhaps up to 19%, based on measurements after resaturation of dried samples. This is as a result of the high permeability of these sediments, which allow the cores to drain off fluid. Finer grained cores are less permeable and less susceptible to such draining, and as such, the porosity estimates are more accurate.

Paleomagnetism

The main objective of the shore-based paleomagnetic study was to produce a polarity magnetostratigraphy in as much detail as possible. At selected depth intervals in all three holes, attempts were also made to characterize the remanence carrier and to make preliminary estimates of relative paleointensity. These objectives were achieved through measurements of natural remanent magnetization (NRM) and alternating-field (AF) demagnetization of discrete samples (one from each section) taken from the working half. In addition, specific intervals selected on the basis of their high clay content and relatively high susceptibility were sampled at denser intervals ranging from one sample every 50 cm to one sample every 10 cm. No U-channels were measured at the OSP, as explained in **"Samples."**

Taking discrete samples in this case meant lower overall sample resolution than can be achieved with access to a long-core (pass-through) magnetometer. However, the discrete sample approach has the ad-

vantage of better measurement precision and allows more extensive demagnetizations of each sample compared to the 15 mT standard shipboard half-core measurements. Using this method, we were able to separate different components of the magnetic signal and, when possible, isolate the characteristic remanent magnetization (ChRM) using principal component analysis (PCA) (Kirschvink, 1980), yielding short successions of high resolution.

The conventional right-handed ODP coordinate system was used throughout (+z = downcore; +x = perpendicular downward from the split surface of the working half). The cores were recovered without the use of a Tensor tool and therefore were not oriented with respect to horizontal. However, because of the relatively high latitude (~40°N) of the sites, the lack of horizontal orientation did not present a problem for the purpose of constructing a polarity timescale.

Samples

Lithologic conditions that frequently alternated between soupy and hard cemented layers prevented the systematic collection of U-channel samples, although a cryogenic super-conducting quantum interference device (SQUID) rock magnetometer (755–4000, horizontal pass-through type) is available at the University of Bremen. Three U-channels were taken in Hole M0027A for postexpedition research (Sections 313-M0027A-222R-1, 68–147 cm; 223R-1, 0–150 cm; and 223R-2, 92–150 cm). These U-channels will be used to investigate in detail the paleomagnetic behavior/transition across the Eocene–Oligocene glacial maximum. At the OSP, oriented cube samples (6.2 cm^3) were carefully collected from working-half cores. For clear characteristic magnetization, NRM was measured after detailed stepwise demagnetization on each axis of the sample up to 100 mT soon after a discrete cube sample was collected. All Expedition 313 paleomagnetic results are provided in SI units.

Instrumentation

All paleomagnetic measurements were carried out in the paleomagnetic laboratory at the University of Bremen. Discrete sample NRM measurements were made using a 2G Enterprises pass-through direct-current (DC) SQUID cryogenic magnetometer (model 755–4000; horizontal orientation) equipped with an automated AF demagnetizer and an automated sample handler capable of processing 96 discrete samples (8 each × 12 sets) in one batch (Fig. **F14**). All measurements were made in a ferromagnetically shielded

space to prevent samples from being exposed to the ambient laboratory magnetic field.

Measurements and procedures

Measurements of remanent magnetization were carried out on all discrete samples. In addition, all samples were also AF demagnetized at 5 mT increments up to 60 mT to isolate the ChRM. A few samples were then further AF demagnetized at 10 mT up to a maximum field of 100 mT.

During the first batch (96 samples) of AF demagnetization and measurements of core from Hole M0027A, we discovered that many samples were acquiring a magnetization, typically at AF fields higher than 40 mT. We interpreted this to be a gyroremanent magnetization (GRM), which is AF demagnetization–induced magnetic remanence acquired perpendicular to the applied alternating field in strongly anisotropic magnetic material (Stephenson, 1980). In light of this finding, we changed the demagnetization procedure for the other samples following the technique proposed by Dankers and Zijderveld (1981), where the remanence in each axis is measured directly after AF demagnetization of the same axis. The theory is that any remanence acquired in one axis during AF demagnetizations of another axis will be removed when the axis is AF demagnetized by the same field strength.

ChRM was determined using PCA on a sequence of demagnetization steps determined individually for each lithology. For the first batch of samples, which were demagnetized without the technique proposed by Dankers and Zijderveld (1981), the interference of the GRM forced us to use a different approach. Because the z-axis was always demagnetized last, the intensity information in this axis was not affected by the acquisition of a GRM. In these cases, we settled on establishing the direction of the samples using demagnetization steps at fields below 40 mT.

Data quality

The quality of the paleomagnetic data varied markedly for different lithologies. The best results were obtained in clay-rich intervals, whereas in most sandy parts of the cores, data were too noisy to determine a prevailing remanence direction. A few samples were not fully demagnetized even with alternating field strengths of 100 mT, suggesting the presence of a high-coercivity component.

Magnetostratigraphy

Polarity histories were reconstructed for a few of the clay-rich stratigraphic intervals based on the ChRM inclination data. Polarity zones were tentatively cor-

related to the GPTS of Cande and Kent (1995) using age control provided primarily by Sr isotope stratigraphy and limited biostratigraphic constraints. The resulting age assignments for the reversals must be considered uncertain because of fairly large errors in age control (~1 m.y.) and fairly rapid polarity changes in the GPTS for the stratigraphic intervals with polarity history.

Data from the sandy sequences often proved to be too noisy for magnetostratigraphic interpretations. The poor data quality is attributed to unstable or weak NRM in the sediments.

Downhole measurements

Borehole geophysical instruments

Offshore downhole logging operations for Expedition 313 were provided by the University of Montpellier (Laboratoire de Géosciences-Montpellier; France), part of the EPC under ESO. The EPC is primarily responsible for the planning, acquisition, QA/QC, science support, and education outreach related to petrophysical measurements on MSPs. Petrophysics in relation to this consortium includes downhole measurements (i.e., borehole logging) and physical properties (continuous and discrete; see **"Physical properties"**) measured on cores (e.g., magnetic susceptibility, acoustic properties, and density and porosity).

The set of downhole geophysical instruments utilized during Expedition 313 was constrained by the scientific objectives, the coring technique (PQ and HQ diameter boreholes), and the hole conditions at the three sites.

Slimline logging tools of several manufactures were used (Table **T6**). The suite of downhole geophysical methods was chosen to obtain high-resolution images of the borehole wall, to measure borehole size, and to measure or derive petrophysical or geochemical properties of the formation such as porosity, electrical resistivity, acoustic velocities, and natural gamma radioactivity. Deployment of nuclear tools was not allowed during Expedition 313.

The slimline suite comprised the following tools:

- Spectral natural gamma probe (ASGR): allows identification of individual elements that emit gamma rays (e.g., potassium, uranium, and thorium).

- Induction conductivity probe (DIL45): measures electrical conductivity of the geological formation. The output of the tool comprises two logs: induction electrical conductivity of medium investigation depth (ILM; 0.57 m) and induction

electrical conductivity of deeper investigation depth (ILD; 0.83 m).

- Magnetic susceptibility probe (EM51): measures magnetic susceptibility in a wide range of formations.

- Acoustic borehole televiewer (ABI40): produces millimeter-scale, high-resolution (72 parts per thousand [ppt]) images of the borehole surface using acoustic pulse and echo techniques.

- Full waveform sonic probe (2PSA-1000): measures compressional wave velocities of the formation.

Vertical seismic profiles (VSPs) were acquired by the University of Alberta (Department of Physics; Canada) in Holes M0027A, M0028A, and M0029A for two primary purposes: (1) to calibrate time to depth correlations of the seismic reflection profile and, upon additional processing, (2) to construct seismic traces from the upgoing wavefield that may be directly compared to the reflection profile.

Operations

The logging team consisted of two engineers supervised and assisted by the Petrophysics Staff Scientists. A total of three boreholes (Holes M0027A, M00028A, and M0029A) were prepared for downhole geophysical measurements. Where possible, measurements were performed in open borehole conditions (no casing). The majority of spectral gamma ray logs and VSP measurements were done through the casing. Despite difficult borehole conditions (nonconsolidated formations, risk of collapse, etc.), the recovery and overall quality of the downhole logging data are very good.

In each hole, spectral gamma logs were acquired as the first measurements through the steel drill string. After completion, the pipe was pulled up in steps because of difficult borehole conditions, the development of bridges, and difficulties in pulling the pipe up (e.g., in sandy sections in the upper 200 m of each hole and in other sand-prone intervals in Holes M0027A and M0028A). After conditioning the hole with drill mud, open-hole measurements were logged at each step. When logged in sections, each slimline tool run was identified as (1) lower, (2) middle, and (3) upper. In each section, if some tools were logged in several runs, runs are numbered 1 (deepest) upward. Because of borehole conditions and time constraints it was not possible to log with all tools in every borehole section (Table T7).

Logging procedure and data recording

Each slimline tool was logged on an individual string. A logging run commenced with zeroing the tool to a fixed point (drillers zero) corresponding to the top of the drill pipe (Fig. F15). The zeroing point was measured for each run because of depth discrepancies that may arise when moving from one open interval to another. Zeroing the tool in this way is important for achieving the most accurate postprocessing depth integration between tools for each borehole.

Each logging run was recorded and stored digitally. During acquisition, data flow was monitored for quality and security in real time using tool-specific acquisition boxes (Advanced Logging Technology Ltd. [ALT] and Mount Sopris Instrument Company, Inc. [MSI] loggers) and software (ALTlogger and MSlog). Table T6 summarizes the acquisition system for each tool. Tools were raised at speeds that ranged from a minimum of 2 m/min for ABI40 image logs to a maximum of 10 m/min for induction conductivity logging. Recordings were taken both downhole and uphole. Because of the real-time data display, it was possible to stop uphole recovery once the casing/drill pipe was entered. At the end of each log run, the instrument was rezeroed at the top of the drill pipe. After each run, the WellCAD software package (Advanced Logic Technology) was used for visualization, QA/QC, processing, interpretation, and plotting the data. Except in specific cases, only uphole logs were used to process data.

VSP setup for measurements is shown in Figure F16. The seismic source consisted of two air guns (20 in³ and 40 in³) (supplied by DWS International, Corpus Christi, Texas [USA]) linked to a high-pressure air reservoir of four bottles that were recharged by a high-pressure air compressor. The air gun was hung from the ship starboard crane at a depth of ~2 m below the sea surface. Compressed air (~1500 psi) and electrical firing signals were provided to the air gun via an umbilical that hung from the ship deck.

A number of recording sensors were employed in the measurements, including

- The wall-locking borehole geophone,

- A seismic hydrophone placed 10 to 15 m above the seafloor, and

- A 4C seafloor detector system that includes three geophones in a gimballed arrangement that ensures the "vertical" component is always properly aligned with a hydrophone.

This last detector is now commonly used in deep-sea seismic exploration studies. The borehole geophone was lowered on a four-conductor armored wireline; unfortunately, only the vertical component could be measured, as the wireline carried insufficient conductors. Note that geophones detect particle velocities and hydrophones detect wave pressure.

Each VSP shot was recorded and stored digitally. The signal received by the geophone was digitized using a Geometrics "Geode" and recorded using Geometrics Seismodule Controller software. Raw data were saved in SEG2 format. Table **T8** provides details of the surveys carried out in terms of date, interval spacing, and the segments obtained with the downhole geophone in open hole or within the steel drill string.

Logging tool description and acquisition parameters

Technical schemes on individual tools are shown in Figure **F17.** Additional information can be found on the manufacturers' Web sites (**www.antares-geo.de/, www.mountsopris.com/, www.geovista.co.uk/,** and **www.alt.lu/**). Detailed information on their geological applications can also found in Schlumberger (1989) and Serra (1984, 1986).

Spectral natural gamma probe

Unlike other slimline instruments that record total gamma ray emissions, the ASGR (ANTARES Datensysteme GmbH) allows identification of individual elements that emit gamma rays. Naturally occurring radioactive elements such as K, U, and Th emit gamma rays with a characteristic energy. K decays into two stable isotopes (Ar and Ca), and a characteristic energy of 1.46 MeV is released. U and Th decay into unstable daughter elements that produce characteristic energy at 1.76 and 2.62 MeV, respectively. The most prominent gamma rays in the U series originate from decay of ^{214}Bi and in the Th series from decay of ^{208}Tl. It is thus possible to compute the quantity (concentration) of parent ^{238}U and ^{232}Th in the decay series by counting gamma rays from ^{214}Bi and ^{208}Tl, respectively.

The ASGR detector for gamma rays is a bismuth germanate (BGO) scintillation crystal optically coupled to a photomultiplier. The BGO detector has an absorption potential eight times greater than the more classic NaI crystal. As most of the spectral discrimination is performed in the high-energy range, only instruments equipped with BGO detectors prove to be reliable in the slimline tool domain. The instrument was master-calibrated by the manufacturer. On site, the stability of the sensor was checked using a volume of pure potassium.

As the probe moves up the borehole, gamma rays are sorted according to their emitted energy spectrum (the tool has 512 reference spectra in memory) and the number of counts in each of three preselected energy intervals are recorded. These intervals are centered on the peak values of ^{40}K, ^{214}Bi, and ^{208}Tl. Tool output comprises K, U, and Th in Becquerel per kilogram and total gamma ray counts in counts per second (cps). The vertical resolution of the tool is ~15 cm. The downhole measurement interval was 0.1 m.

Induction resistivity probe

The ALT DIL45 measures electrical conductivity of the geological formation. Variations in electrical conductivity correspond primarily to variations in lithology (composition and texture), formation porosity and saturation, and interstitial fluid properties (salinity).

An oscillator sends an alternating current of constant amplitude and frequency through an emitting coil. This current generates an alternating electromagnetic field that induces Foucault currents in the formation. These Foucault currents are proportional to the formation conductivity and generate their own electromagnetic fields. When passing through a receiving coil (solenoid), these secondary magnetic fields induce electromotive forces that are proportional to the flow running through the coil. The output of the DIL45 tool comprises two conductivity logs: ILM (0.57 m) and ILD (0.83 m). Measured conductivity can be converted into electrical resistivity. The instrument was calibrated against a Wenner array in a reference hole. The measurement window ranges from 5 to 5000 mmho, with a resolution of 0.5 mmho. The downhole measurement interval was 0.05 m.

Magnetic susceptibility

The Geovista EM51 probe measures formation electrical conductivity and formation magnetic susceptibility using electromagnetic induction. This measurement relies on a principle similar to the DIL45 induction probe, whereby a current is induced by an oscillating magnetic field in the probe within a toroidal zone of formation at some radial distance from the probe coils. The oscillating current produces a secondary field that is detected by the receiver coils. The "in-phase" signal is a measure of susceptibility in formations with magnetic properties. The probe is most effective in high-conductivity geological formations and low-conductivity borehole fluid, including air.

The instrument was calibrated using a set of two coils for conductivity measurements and another set of two coils for magnetic susceptibility measurements. The measurement window ranges from 10^{-5} to 2 SI. The downhole measurement spacing interval selected was 0.05 m. Expedition 313 was the first

time this specific slimline probe was used during IODP.

Acoustic borehole televiewer

The ALT ABI40 produces millimeter scale, high-resolution images of the borehole surface and can be directly used for sedimentological and structural interpretation.

A voltage is applied in a piezoelectric ceramic to produce acoustic waves (1.2 MHz) at regular intervals. On hitting a focalizing mirror, these waves are deflected perpendicularly to the wave source and toward the borehole wall. The focal point corresponds to the point of maximum energy, giving an ~4 mm diameter footprint on the wall in a 100 mm diameter borehole. To obtain a 360° image, the mirror pivots on a central axis. The resolution is user defined and depends on the number of measurements made in one rotation and the rate at which the tool is raised up the borehole while measurements are made. The highest quality images are obtained with a vertical sampling of 2 mm and a radial sampling with 288 shots per circumference. During Expedition 313, ABI40 acoustic images were acquired with various resolutions ranging from 72 samples × 4 mm to 288 samples × 2 mm, which results in a pixel size of <5 (horizontal) × 4 (vertical) mm to <4 (horizontal) × 2 (vertical) mm.

The ABI40 produces two distinct images of the borehole wall. First, an acoustic impedance image (from the contrast between the borehole fluid and wall) is derived from the reflected wave amplitude obtained around the hole. The amplitude ratio between the emitted wave and the reflected wave provides information on the formation's capacity of absorption (low returned amplitude corresponds to a high capacity of absorption [i.e., soft formation]). Second, a traveltime image is derived from the reflected wave traveltime from the ceramic transducer to the borehole wall and back. The traveltime is directly proportional to the distance between the borehole wall and the probe. The tool is equipped with magnetometers and accelerometers for tool orientation with respect to north. The precision of the measured inclination is 0.5°, and the precision of the measured azimuth is 1.5°. For each of the two images, a set of false colors is assigned. From the measurements, a virtual image of the borehole wall depth is produced. This image is displayed as an unfolded representation of the 360° view. If mudcake is present, the images of those intervals would be expected to have a homogeneous appearance. As core features can be correlated to the images in many places, it is assumed that mudcake is absent over these intervals.

Full waveform sonic probe

The Mount Sopris 2PSA-1000 sonic probe was used to measure compressional wave velocities of the formation. When bulk density is known (from core), elastic properties (bulk and shear moduli) and an estimate of porosity can be derived from sonic measurements.

This downhole instrument is composed of an acoustic transmitter and two receivers. The transmitter transmits an acoustic signal that propagates through the borehole fluid to the rock interface, where some of the energy is critically refracted along the borehole wall. As a result of wavefront spreading (Huygens principle), some of the refracted energy is transmitted back into the borehole adjacent to a receiver. Each receiver picks up the signal, amplifies it, and digitizes it. Recorded waveforms are then examined, and wave arrival times are manually or automatically selected (picked). Arrival times are the transit times of the acoustic energy. By measuring the acoustic transit time and knowing the distance between the two receivers (1 ft), the velocity in the fluid, and the borehole diameter, the sonic velocity of the rock is calculated. Consequently, the interval velocity value is calculated at each sampling point. In the specific configuration used, *P*-waves (15 kHz monopole survey) were recorded.

Calibration of the tool was performed either in water (1500 m/s for *P*-wave; freshwater at 28°C) or in a steel pipe (5440 m/s) while running downhole. The downhole measurement interval was 0.1 m.

Vertical seismic profiling

A VSP test consists of sending a seismic signal from a surface source down to a geophone at depth in the borehole. The downhole geophone converts wave particle motions into an electrical signal that is transferred to the surface via the wireline to be digitally recorded. The wave field is recorded at a number of positions along the borehole. The one-way traveltime from surface to depth is obtained by picking the times of arrival on the observed records; these are often called check shot times. Check shot times are used to assign true depths to the events seen in a seismic reflection profile. VSP profile times can be erroneous for a variety of reasons, including error-prone velocity analysis that may be contaminated by noise and seismic multiples, as well as seismic anisotropy that normally results in any layered sedimentary environment. Further processing of the reflection profile allows for the construction of a zero-offset seismic trace that may be further compared to the seismic reflection profile to assist in assigning depths to the reflectors and to allow for the

removal of multiple reverberations that can some-times appear as events within the surface seismic profile.

During VSP operations, each VSP shot was recorded on seven channels (Table T9) to measure the vertical component on the downhole geophone, the vertical and two horizontal components on a seafloor geophone, a seafloor hydrophone (within the housing of the seafloor geophone), a suspended hydrophone, and the electrical signal caused by the movement of the air gun shuttle. Of the two air guns (20 and 40 in^3), only the 20 in^3 was fired during each shot. The record lengths were 2.5 s, covering the time period from –0.5 to 2 s. The sampling rate was 250 µs. The vertical measurement spacing in Holes M0027A, M0028A, and M0029A was, respectively, 0.91, 1.83, and 3.05 m. Depending on noise conditions (primarily weather dependent) and signal strength, up to five individual records were obtained at each depth.

Data processing

Slimline logging data were processed using the Well-CAD software package. The processing procedure is described below for the logs: natural gamma radioactivity (ASGR), induction (DIL45), and magnetic susceptibility (EM51); image data (ABI40); and sonic data (2PSA).

Depth adjustments

One main processing task involved evaluating the depth of each log run and referencing the data to the rig floor and seafloor. While deploying all the tools separately in the same section, a fixed zero depth position (loggers zero) was maintained at the top of the drill pipe. Typical reasons for depth corrections include ship heave and tides, but as the logging for Expedition 313 was performed from a platform resting directly on the seafloor, no such corrections were necessary.

Using WellCAD, the original logs were depth adjusted to the rig floor (in meters wireline log depth below rig floor [m WRF]). This adjustment included several corrections:

- Difference in zero tool depths (discrepancies in depths between initial zeroing and zeroing on removal of the tool were generally <1 m),
- Difference between loggers and drillers zero points (Fig. F15),
- Corrections specific to certain tools (2PSA measurement point), and
- Correction because of winch coupling to an external encoder in Hole M0029A.

Logs were subsequently shifted to the seafloor (in meters wireline log depth below seafloor [m WSF]) using the drillers depth to seafloor. Slight discrepancies (<0.5 m) may exist between the seafloor depths determined from the downhole logs (ASGR) and those determined by the drillers ("bottom felt" depth).

When necessary, logs have been matched manually by the log analyst to a reference log using distinctive peaks. In such cases, gamma ray logs through pipe (or occasionally induction logs) are taken as reference logs (continuous). Generally, depth discrepancies between logs are <1.5 m. Matched log depths are referenced to seafloor and are referred to as meters wireline log matched depth below seafloor (m WMSF). The EM51 log from Hole M0028A and the EM51 and 2PSA logs from Hole M0029A have been depth matched.

Invalid data

Invalid log values have been replaced by a null value of –999.25. Invalid log values removed can include the following:

- Log data in pipe (DIL45, EM51, ABI40, and 2PSA),
- The effect when approaching the metallic pipe (DIL45, EM51, and some channels of ABI40) in open-hole condition,
- Negative values in the ASGR logs related to sedimentary intervals where gamma ray emission is too low for accurate statistical calculation,
- The lowermost data points affected by the cessation of measurement, and
- Data just above or below depths where acquisition halted during measurement.

Environmental corrections

Environmental corrections are designed to remove any effect from the borehole (size, roughness, temperature, and tool standoff) or the drilling fluids that may partially mask or disrupt the log response from the formation. Here, no postacquisition corrections of this type were applied.

Log merges

Where applicable for the processed logs, overlapping log runs have been merged to give one continuous log. In the overlapping regions, data have been checked by the log analyst to make sure distinctive peaks and troughs correlate. For all except three logs (EM51 log from Hole M0028A and EM51 and 2PSA logs from Holes M0029A), no match adjustments were required before merging.

Quality control

Data quality is assessed in terms of reasonable values for the logged formation, repeatability between different passes of the same tool, and correspondence between logs affected by the same formation property (e.g., the conductivity log should show inverse response features to the gamma log). Repeatability between data acquired on down and up acquisition of logs was checked by the log analyst. Considering the challenging borehole conditions, the overall quality of the downhole logging data is very good.

The quality of the ASGR data is good even when logging through pipe. Negative values indicative of incorrect statistics were <12% of the total record. Gamma ray logs recorded through drill pipe should, however, be used only qualitatively because of attenuation of the incoming signal. Sections were acquired in open-hole conditions in two intervals of Hole M0027A and a small interval in Hole M0029A for through-pipe data calibration. ASGR data clearly correlate/anticorrelate with magnetic susceptibility and conductivity. ASGR data also correlate very well with NGR measurements on the unsplit cores (see **"Physical properties"**), allowing, when necessary, precise core depth positioning with respect to log depth.

The quality of EM51 data is good. Magnetic susceptibility logs compare well with MSCL magnetic susceptibility data acquired on core sections. High values of magnetic susceptibility tie with levels where either glauconite or other possible magnetic minerals have been described by the sedimentologists.

The quality of DIL45 data is good. Induction conductivity is a deep-investigation measurement and is least sensitive to borehole conditions. Conductivity log values are within the expected range. Logs correlate well with the EM51 logs and anticorrelate with the MSCL resistivity data acquired on core sections.

The quality of ABI40 data varies from one hole to another. The resolution selected during image acquisition also varied between 72 and 288 shots per circumference. As the distance to the borehole wall also affects the quality of this imaging log, the probe should be run with centralizers. However, for technical reasons related to the size of the coring bit diameter relative to the diameter of the open hole below (larger), centralization was not possible in most cases, resulting in medium quality images containing dark lines oriented at 180°. For this reason, image data in these sections should be treated with great care. Only in the middle section of Hole M0028A were acoustic images acquired at high resolution and with centralizers, resulting in high-quality and high-resolution images. The presence of mudcake in some places in the hole possibly affects image quality by partly or totally masking borehole geology.

The quality of the 2PSA data is good. Measurements of compressional wave velocity are highly dependent on borehole conditions. Larger cavities cause the induced wave to scatter, and acoustic energy is lost more rapidly. The picked *P*-wave arrivals show features very similar to the EM51 logs and the MSCL density signal from core sections.

ABI40 image data processing

Several corrections have been applied to the ABI40 data using the WellCAD software.

Bad trace interpolation

"No Data" or "NULL" traces in the images have been removed using an algorithm that replaces bad traces with the closest trace containing valid data points.

Image centralization

Where possible, traveltime images have been corrected for decentralization effects of the probe within the borehole. Assuming that the decentralization effect on the data can be approximately described through a sinusoid, the "Centralize Process" in the WellCAD software was used to remove this trend and correct the input data according to a best-fitted sinusoid.

Caliper calculation

ABI40 images of the borehole wall were apparently unaffected by borehole fluid quality. Acoustic caliper values were obtained by assuming an acoustic wave velocity of 1530 m/s through borehole fluid. The calculation was checked using known internal pipe diameter.

Oriented presentation

Images available in any format have been oriented with respect to magnetic north. In some borehole intervals, several passes have been oriented and merged on the same presentation.

Images provided in PDF format have been depth corrected to the seafloor (m WSF). Images are displayed as an unwrapped borehole cylinder. A dipping plane in the borehole appears as a sinusoid on the image, with the amplitude of this sinusoid proportional to the dip of the plane. Using the image module of WellCAD, a "static" normalization of the images has also been applied to enhance structure visualization. In the static normalizations, the amplitude and traveltime ranges of the entire interval of data have been computed and partitioned into 256 color levels. Because of the decentralization tool effect, a change in

image color is observed at the contact between successive logged sections.

Data delivery

ABI40 image files in PDF format (⅕ and ¹⁄₂₀₀ scales) are available online in the U.S. Implementing Organization (USIO) log database. ABI40 raw and processed data are also available in ASCII format. ASCII-processed data are depth corrected to the seafloor (m WSF); bad traces have been interpolated, and images have been centralized. Images have not been normalized.

ASCII raw data have been oriented with respect to magnetic north and have been depth corrected to the rig floor (m WRF). In some cases, several passes have been oriented and merged together on the same presentation.

2PSA acoustic data

The 2PSA tool was run at a frequency of 15 kHz, and resultant logs can be used to calculate compressional wave velocities. Data were processed in the WellCAD logging package. For processing purposes, data were filtered (frequency filter) in such a way that only the energy around the induced frequency was analyzed. Waveform picking was done manually in the Well-CAD logging package to ensure good quality data. Where no clear arrivals in the waveform were present in two receivers, a null value was entered in the database. Time picks were saved, and acoustic velocities were calculated. The precision of acoustic travel-time measurements is ~5%.

Vertical seismic profiling

Data flow was monitored for quality in real time, and data quality was recorded on paper to be entered into an Excel spreadsheet postsurvey, along with shot and receiver coordinates (datum WGS84). Where available, borehole tilt and azimuth measured by borehole logging are used to calculate the horizontal location of the downhole receiver. Where this information is not available, the borehole is assumed to be vertical. The Excel quality and coordinate measurements were entered into the VSP data files using Mathworks MATLAB and Seismic Imaging Software VISTA software. Data were then processed using MATLAB and VISTA.

Processing involved removing poor-quality shots and stacking the remaining shots at a given depth to improve the signal to noise ratio. 3-D offset information (Fig. F16) was calculated and entered. Where possible, first break arrival times were picked for the downhole data, the vertical seafloor geophone, the suspended hydrophone, and the air gun shuttle signal. Based on a combination of data from the vertical seafloor geophone, suspended hydrophone, and air gun shuttle signal, static corrections were calculated and applied to account for any time shift caused by the air gun firing past time zero. The wave form and arrival times of these data were assessed for each survey to determine the best technique of calculating static corrections.

In most cases, obtaining records in open hole was preferred, as this eliminated any noise induced by the drill string. Indeed, "ringing" of the drill string as the seismic waves passed reduced data quality substantially unless the drill string was in good contact (i.e., stuck) with the borehole. This problem was particularly severe for Hole M0029A, where borehole stability conditions did not allow for any open-hole measurements and drill string reverberations were strong.

For Holes M0027A and M0028A, no processing was conducted prior to first break picking of the seismic arrival through the sediment. For Hole M0029A, it was necessary to apply F-K and bandpass filters prior to picking seismic arrivals through the sediment for survey "a." An F-K filter and automatic gain control was applied prior to picking sediment arrival times on survey "b." The F-K filters were designed to remove all upgoing waves and downgoing waves traveling with velocities over ~3000 m/s. These filters were not saved in order to preserve the information within the data for further research. Interference from seismic arrivals through steel meant that, despite processing, the only consistent first break from survey "a" was a peak, whereas in survey "b" from Hole M0029A and on all surveys from Holes M0027A and M0028A, where this interference did not exist, the first break picked was a trough. Times derived from survey "a" are therefore likely to be time shifted by a half-wavelength.

For Hole M0027A, the seafloor geophone in conjunction with the air gun shuttle signal was used to determine traveltime from the source to the seafloor. The seafloor geophone peak was picked, and the times the air gun shuttle signal amplitude began to be clipped were used. Variations in air gun elevation and firing time differences between the two air guns are accounted for using this time, and data are time shifted within the stacked data to reflect the source firing at time zero and at a constant elevation. The time shift reflects the source firing at time zero. The stacked data files are all time shifted, with the static shift used saved within the stacked data files. Because of the nature of SEG-Y formatting, the time used for the static shift has been truncated to be an

integer; however, static shifts used reflected the 250 µs sampling rate and were calculated and applied with this 250 µs accuracy.

For Hole M0028A, the seafloor geophone was used in conjunction with the air gun firing time data from Hole M0029A measurements to correct for variations in air gun firing times, and the stacked downhole data are shifted to reflect the air gun firing at time zero. For Hole M0028A uniquely, the seafloor geophone first arrival did not have a clear peak. Here, the first breaks for the seafloor geophone were picked when the signal came up from zero amplitude. The first breaks (peaks) of the hydrophone suspended 20 m above the seafloor geophone are assessed in conjunction with the seafloor arrivals to confirm a relatively vertical ray path for the seismic wave between the source and the seafloor receiver. The static shifts are applied and saved within the stacked data file, as above.

For Hole M0029A, the suspended hydrophone and its known distance from the air gun source were used to determine the firing time of the air gun, and from this the stacked data were shifted to reflect the air gun firing at time zero. Peaks observed on the hydrophone records were picked for this purpose. First breaks (peaks) were also picked for the seafloor geophone and used to determine the traveltime through the water column. The remotely operated vehicle (ROV) was dispatched for both surveys on this hole to assess the location of the seafloor hydro-/geophone. In both cases, there was estimated to be a maximum 5 m horizontal offset between the top of the cable where it came onto the ship and the bottom of the cable where it connects to the seafloor hydro-/geophone.

Despite the considerable effort and time devoted to the collection and processing of VSP data, their reliability as check shot information was limited in the time available. Further analysis may determine that these provide time-depth conversions superior to those derived from stacking velocities (see discussion in "Stratigraphic correlation"), but for this volume we have chosen the latter. Particular issues of concern regarding VSP data forcing this decision include the following:

- VSP data could not be collected continuously from seafloor to TD in Hole M0027A.

- Offsets due to separate geophone deployments within each hole need to be addressed and corrected.

- Difficulties in picking first breaks in a noisy environment and ringing drill pipe degraded check shots in several instances.

- Although the slope of check shot arrivals is similar to that of time-depth pairs derived from stacking data, indicating similar interval velocities (Fig. **F18A, F18B, F18C**), unreasonable interval velocities in the upper few tens of meters of burial depth are required for this trend of VSP data to intersect 0 m at 0 ms, suggesting a timing delay or that an acquisition geometry correction may be needed.

Data delivery

Processed and raw data are available in the USIO online log database. Processed standard data are available in ASCII format. Processed depths are referred to as either WSF and/or WMSF scales. ABI40 image files are also available in PDF format ($\frac{1}{5}$ and $\frac{1}{200}$ scales). Raw data are provided in ASCII format with depths in m WRF.

Stratigraphic correlation

Stratigraphic correlation consisted of synthesizing the following: (1) seismic sequence and facies analysis, (2) seismic-core (sedimentary facies) correlation, and (3) incorporation of lithostratigraphy with other data sets (paleontology, Sr isotope). Correlation between seismic profiles and cores used a velocity-depth function tested by comparison with major core surfaces, downhole logs (particularly total gamma ray, spectral K as a proxy for glauconite, spectral U for organic-rich sediments, sparse velocity logs, and magnetic susceptibility), and MSCL logs (density and magnetic susceptibility). This procedure required the distillation of information based on lithology, interpreted sedimentary facies and paleoenvironments, paleodepths inferred by benthic foraminifer distribution, chronostratigraphic ages, seismic facies, and comparisons with physical property boundaries. Chronostratigraphic correlations were also an important part of the correlation loop; these are discussed in **"Chronology."**

Sequences in seismic profiles

Holes M0027A, M0028A, and M0029A are located on seismic profiles that embed several generations of seismic data (Fig. **F1** in the "Expedition summary" chapter). Greenlee et al. (1988) first identified reflectors of mid-Cenozoic age in proprietary Exxon profiles that crossed the outer Baltimore Canyon Trough (middle to outer continental shelf off the mid-Atlantic United States). An informal workshop to correlate features on many of these proprietary data, attended by researchers from Exxon, Lamont-Doherty Earth Observatory, and Rutgers in 1990, resulted in the recognition of 17 surfaces as probable sequence bound-

aries based solely on their seismic character (Table T10). Eight of these were traced to a new grid of improved vertical resolution (~15 m) public data (Ew9009) and tied to drill sites with their ages estimated by Greenlee et al. (1992) (Table T10). From oldest to youngest these were green, pink-2, blue, yellow-2, tuscan, red-1, yellow-1, and pink-1. Drilling on the continental slope during ODP Leg 150 (Mountain, Miller, Blum, et al., 1994) sampled all but one of the original 17 candidate sequence boundaries previously identified, and each was renamed to an alphanumeric system with an age assigned (Table T10). Higher resolution (~5 m vertical) site survey Oc270 reflection data were collected in 1995 mainly on the outer shelf and slope but included line 529 (Fig. F5 in the "Expedition summary" chapter), which duplicated the lower resolution line 1003 of the earlier Ew9009 data set and extended to within 15 km of the shoreline. A reconnaissance grid of similar quality data (~5 m resolution) was collected during Cruise CH0698; this grid focused on the middle to inner shelf along New Jersey and included three grids of variably spaced lines (150–600 m; each roughly 6 km in length) that met safety assessment criteria across proposed drill sites MAT-1, MAT-2, and MAT-3 (Proposal 564), which were subsequently drilled as Expedition 313 Holes M0027A, M0028A, and M0029A, respectively (Fig. F7 in the "Expedition summary" chapter).

Seismic sequence boundaries were transferred from the older data sets to site survey CH0698 and loop correlated throughout this new seismic grid (Monteverde et al., 2008; Monteverde, 2008). Several additional lower Miocene sequence boundaries were identified in the process and, in keeping with the alphanumeric labeling scheme, were inserted into the hierarchy based on stratigraphic position. These new boundaries include, from oldest to youngest, m5.8, m5.7, m5.5, m5.47, m5.45, and m5.3 (Monteverde et al., 2008; Monteverde, 2008) (Table T10). Seismic sequences have since been named according to their basal reflector boundary, such that Sequence m5.5 lies on Reflector m5.5, for example.

Coreholes were drilled in the New Jersey coastal plain as part of ODP Legs 150X and 174AX (Miller et al., 1994; Miller, Sugarman, Browning, et al., 1998), and despite the obvious lack of seismic profiles tying these sites, correlations have been made (Table T10). Miller et al. (1997) bases ties on chronostratigraphy; Monteverde (2008) bases ties on synthetic seismograms of well data both offshore and onshore to profiles of the CH0698 grid. These latter onshore ties between onshore and offshore sequences do not agree in all cases (Table T10). One source of error is the uncertainty of ties from the outer shelf and slope (where Greenlee et al., 1992, and Miller et al., 1996, 1997, dated sequence boundaries) to the inner shelf, where sequence boundaries m5 to m6 are best expressed.

Prior to Expedition 313, seismic reflections were correlated for age control to industry wells on the outer continental shelf (Greenlee et al., 1992) and to coreholes onshore and on the continental slope (Browning et al., 2006; Monteverde et al., 2008; Monteverde, 2008) (Fig. F1 in the "Expedition summary" chapter). Ties for sequence boundaries m1–m4 between Holes M0027A, M0028A, and M0029A and drill sites on the slope provide relatively uncertain ages because of ambiguities resulting from long-distance seismic correlations (75 km and more). Correlations to onshore sequences are more reliable because seismic profiles were collected close to shore and pass within 1–3 km of onshore Leg 150X coreholes at Island Beach; Atlantic City, NJ (USA); and Cape May. In addition, synthetic seismograms provide a close match between those profiles and the coreholes (Monteverde, 2008).

Seismic profiles in two-way traveltime have been correlated to Expedition 313 cores using a velocity-depth function that provided approximate depths below seafloor to features of interest in the upper 1000 ms of reflection time (Fig. F18A, F18B, F18C). The velocity to depth conversion was developed as follows. Stacking velocities (Vrms) were examined at 22 common depth point (CDP) gathers along Oc270 MCS line 229. This profile is the seaward continuation of MCS line 529, which crosses the Expedition 313 drill sites (Fig. F1 in the "Expedition summary" chapter). The distance between adjacent CDP gathers was roughly 500 m, and all crossed a nearly level seabed (two-way traveltime = 77–80 ms) chosen because of the uniformity of the underlying acoustic structure down to 1000 ms; Vrms values at greater traveltimes showed increased scatter and were not included further. No meaningful along-profile variation in Vrms was observed, and each of the five to eight velocity-traveltime pairs at every gather was graphed and a third-order polynomial was fit to the entire set of data pairs above 1000 ms. This provided a single Vrms versus traveltime relationship to which the Dix (1955) equation was applied to derive interval velocities in 10 ms increments from 0 to 800 ms. The seafloor was within a few milliseconds of 80 ms in all of the Vrms-traveltime pairs used in this preparation. Accordingly, pairs above 80 ms were then discarded, leaving only those data corresponding to Vrms versus traveltime below the seafloor. This provided a means to calculate depths in mbsf versus traveltime in 10 ms increments, and to this was fit another third-order polynomial.

The polynomial used during the OSP was unconstrained; a later effort followed this identical procedure but forced this time-depth regression to pass through 0 ms and 0 mbsf. The resulting two polynomials differ by only a small amount (e.g., a travel-time of 500 ms predicts a depth of 433 mbsf for the former, 443 mbsf for the latter) (Fig. F18A, F18B, F18C). For simplicity we have used the former (unconstrained) function in the site chapter discussions, but in some figures in "Stratigraphic correlation" in each site chapter we show depth predictions using both. This technique provided a relationship of two-way traveltime below seafloor versus traveltime below seafloor that could be applied to a sediment column in any water depth, providing the pattern of velocity versus burial depth was sufficiently close to that along line 229. Initially, this was viewed as a means to simply estimate depths of reflectors at Expedition 313 sites. However, the match of these predicted depths to physical features in the cores and/or wireline logs thought to cause reflections proved to be remarkably accurate, with errors generally <3% of the predicted depth. Comparison to depths predicted by the independently measured VSP showed close agreement in most of the intervals with some exceptions that are discussed in "Stratigraphic correlation" in each site chapter. Because of various aspects of the VSP acquisition (see "Downhole measurements") there were gaps or modest/severe data degradation in some intervals (Fig. F18B). Despite the uncertainty of relying on a single time-depth relationship at three sites along line 529 that have such obvious subseafloor differences in stratigraphy, we chose to continue using the predictions derived from the stacking velocities. The correlations provide a model testable with data sets collected during Expedition 313.

Seismic facies interpretation through the CH0698 and Oc270 seismic grids was instrumental in predicting sedimentary facies for Expedition 313 (all data from CH698 and Oc270 were collected in opposite phase, i.e., a positive pulse in one is a negative pulse in the other, meaning that black in one data set is white in the other). High-amplitude, continuous horizontal reflectors that become sigmoidal at their corresponding clinoform rollovers and display downlapping reflector terminations along their relatively level topsets and onlapping terminations along their dipping foresets have been identified as sequence boundaries (Mitchum et al., 1977). Each was loop correlated through the CH0698 grid and to Oc270 line 529. Packages of discontinuous, low-amplitude reflectors that onlap the seaward front of clinoform rollovers have been interpreted as lowstand facies. Reflectors within the same packages terminate with downlap onto underlying sequence boundaries at their distal locations. Retrograde stacking of reflectors above and landward of the clinoform rollover comprises packages that are typically too thin to resolve with clarity with available seismic data. Where detected, these packages are marked by limited reflector onlap landward of the preceding rollover and by discontinuous, moderate amplitude, generally parallel reflectors. Transgressive surfaces within these packages are generally so close to the underlying sequence boundary as to be undetectable with existing seismic data. Downlap terminations are more clearly imaged seaward of the rollover where the flooding surfaces generally steepen and merge with the underlying sequence boundary. Reflectors within aggradational to progradational highstand facies are generally parallel to the underlying horizontal flooding surface with limited evidence of downlapping terminations.

Mapping surfaces throughout the CH0698 seismic grid showed shoreline-parallel changes in the thickness of the lower to middle Miocene sequences due largely to changing locations of sediment supply (Browning et al., 2006; Monteverde et al., 2008). In addition, postdepositional failure and erosion appear to have contributed to these along-strike thickness variations. Several seismic surfaces displaying all the necessary reflector terminations to be defined as sequence boundaries on several lines flatten out along strike, no longer display typical clinoform geometry, and merge with overlying surfaces. Such variations can be seen on Oc270 line 529 where sequence boundaries m5.5 and m5.47 merge to form a single, nearly planar surface. This merged surface locally truncates part of the m5.6 sequence boundary between Holes M0027A and M0028A (see Fig. F15 in the "Expedition 313 summary" chapter). Sequence boundary m5.45, elsewhere associated with a clinoform buildup, correlates to a nearly planar surface across the Expedition 313 drill sites, apparently due to postdeposition erosion.

Late Miocene boundaries m1–m4, which track near Hole M0029A, are continuous, moderate-amplitude planar reflectors that become broadly discontinuous, lower amplitude, and subparallel in the landward direction across Holes M0027A and M0028A. Seismic facies shallower than 250 ms in the vicinity of Expedition 313 drill sites are less clear than those below. These shallower reflectors are discontinuous, low to

moderate amplitude, dominantly subparallel to locally chaotic, and difficult to trace. Isolated incised channels are clearly imaged in the upper 100 ms.

Sequences in cores

The preliminary velocity function provided predictions for the depth of each seismic sequence boundary in the cores (see tables in "Stratigraphic correlation" in each site chapter), but the sequences in cores were defined on the basis of physical stratigraphy (see "Lithostratigraphy"), age breaks (see "Chronology"), and downhole and core log data (see "Downhole measurements" and "Physical properties").

In general, predicted depths of seismic sequence boundaries closely matched surfaces noted in cores (within ±5 m). In some cases, multiple lithostratigraphic surfaces were encountered within a 10 m interval, and the correlation to any of several nearby seismic sequence boundaries was uncertain. The possible placement of these and all seismic sequence boundaries was made on the basis of significant variations in sediment physical properties, lithologic changes, or the combination of the two parameters. The choice of placement of any single surface was preserved in tables and figures (e.g., Fig. F83 and Table T14 in the "Site M0027" chapter). Moreover, in some cases, a disagreement of as much as 10 m can be observed in the position of predicted seismic boundaries and corresponding surfaces picked in the core. No single explanation can be generally applied to decipher all mismatches; individual cases are discussed in each site chapter.

Sequence boundaries and MFSs are often associated with downhole and MSCL gamma peaks. In addition, density and velocity core logs are occasionally useful in picking out surfaces in the cores (see "Core-seismic sequence boundary integration" in each site chapter). All MSCL data provided useful indicators of lithologic variations. Physical properties of sediments depend to a large extent on lithology, grain size, and the proportion of the different components of the sediment (e.g., Austin et al., 1998). Bulk density in water-saturated sediments is related to porosity and partially controlled by grain size. Acoustic velocity is controlled by porosity, and magnetic susceptibility may reflect changes in lithology, particularly the proportion of biogenic components (carbonate and silica) to lithogenic components. Log data have been visually examined to detect trends and tentatively grouped according to their physical properties and corresponding stratigraphy.

In most cases, the changing patterns of physical properties are in good agreement with the boundaries and the nature of the major stratigraphic units.

Sequence boundaries typically correspond to low total gamma ray values, but this is not always reliable because their definition is based on stratal geometry and not on lithic composition. In particular, downhole logging data proved useful in filling core gaps due to poor recovery in unconsolidated sandy intervals or where a spot coring strategy was adopted.

An acoustic impedance log was computed for Expedition 313 holes to aid in core-seismic integration. For Holes M0027A and M0029A, the impedance (velocity × density) log was constructed using MSCL bulk densities and velocities from both MSCL velocity logs and downhole sonic logs. For Hole M0028A, only MSCL data were available, as a sonic log was not obtained. MSCL density quality is generally good, though MSCL velocity suffers from artifacts (e.g., cores not filling liners and uneven distribution of drilling fluids in liner). The downhole sonic velocities are more reliable, though they also suffer in some intervals (e.g., washout zones); however, velocity logs were only obtained on about ⅓ of the Expedition 313 section.

Tables and stratigraphic synthesis figures in each site chapter provide a distillation of information used to identify fundamental stratigraphic surfaces, particularly sequence bounding unconformities. There is general agreement among methods used to identify surfaces, with predictions from seismic sequence-core correlations, lithostratigraphic discontinuities, changes in stacking patterns, and abrupt changes in physical and log properties converging on the identification and placement of major stratal surfaces (e.g., Fig. F66 in the "Site M0027" chapter and Figs. F55 and F57 in the "Site M0029" chapter). However, there are a few cases where differences in interpretation and placement of surfaces differ amongst techniques:

- Some unconformities recognized on seismic profiles have subtle or little lithostratigraphic signature (e.g., seismic sequence m5.6 in Hole M0029A; Fig. F63 in the "Site M0029" chapter).

- A few lithostratigraphic breaks that appear as candidate sequence boundaries occur within seismic sequences (Fig. F56 in the "Site M0028" chapter; ~290 mbsf).

- There are cases where correlation of multiple stratal surfaces noted by their lithologic character cannot be unequivocally matched to seismic predictions (e.g., Fig. F66 in the "Site M0028" chapter; 500–530 mbsf).

Chronology

Chronology ages (in Ma) for stratigraphic surfaces identified first on seismic profiles and tied to cores

(see **"Stratigraphic correlation"**) were obtained by constructing an age-depth plot for each hole. Plots were constructed through correlation of biostratigraphic zonations to the GPTS of Cande and Kent (1995) as given in the BKSA95 timescale (Fig. **F12**). Details for the biostratigraphic zonation are provided in **"Paleontology."** The Martini (1971) calcareous nannofossil zonation was tied to the GPTS by the BKSA95; when available, more recent and additional age estimates were used and tied to the BKSA95 unless otherwise noted (Table **T1**). Planktonic foraminifer zonations tied to the BKSA95 are defined in the BKSA95 (Neogene) and Berggren and Pearson (2005) (Paleogene). Miocene dinocyst zones are correlated to the BKSA95 and defined in de Verteuil and Norris (1996). The Oligocene dinocyst zonation is that of Van Simaeys et al. (2005), who provided correlations to the GPTS, though correlations to the U.S. Atlantic margin must be considered tentative. Error bars (e.g., Fig. **F34** in the "Site M0027" chapter) for the entire zone assigned in each site report are given following the BKSA95. In cases where a portion of the zone is preferred (e.g., upper Zone DN5), a dashed line is used for the less preferred portion of the zone. Methods and errors for strontium (Sr) ages and semiquantitative lithology are discussed below.

A total of 229 samples were obtained from core catchers on the *L/B Kayd* during drilling and processed onshore at Rutgers University (USA) prior to the OSP for Sr isotope stratigraphy and semiquantitative lithology. Samples were disaggregated in a sodium hexametaphosphate solution (5.5 g/L) and washed through a 63 µm sieve, discarding the mud fraction. Mollusk shells and foraminifer tests were picked from this coarse fraction for Sr isotopic analysis. Many barren intervals, limited availability of shipboard samples in certain zones, and time constraints limited Sr isotopes to 98 analyses (Table **T11**). For each measurement, ~4–6 mg of carbonate was cleaned in an ultrasonic bath and dipped in dilute HCl; carbonate was then dissolved in 1.5 N HCl. Sr was separated using standard ion exchange techniques (Hart and Brooks, 1974). Samples were analyzed on an Isoprobe T Multicollector thermal ionization mass spectrometer (TIMS) at Rutgers University supervised by M. Feigenson. Internal (instrument) precision on the Isoprobe for the OSP data set averaged 0.000006; external precision (approximate sample reproducibility) on the TIMS is approximately ±0.000008 based on replicate analyses of standards. The mean value of the NBS 987 standard is measured for these analyses at 0.710241 normalized to $^{86}Sr/^{87}Sr$ of 0.1194.

We assigned ages using the BKSA95 timescale (Fig. **F12**); calibrations to the Geological Time Scale 2008 (Ogg et al., 2008) were made using the tsConvert utility previously available at www.chronos.org. We used the Oligocene Sr isotope/age regressions of Reilly et al. (2002) and the Miocene regressions of Oslick et al. (1994). The Oslick et al. (1994) regression is only for sections older than 9.9 Ma (Sr isotopic values = <0.708930), but this includes all Miocene analyses completed for the OSP. We also computed ages for all analyses using the "look-up" tables of McArthur et al. (2001).

For the Pleistocene analysis, we derived a linear regression using the data of Farrell et al. (1995), correcting their data to a mean value of NBS987 of 0.710255 and fitting a linear segment to the data between 0 and 2.5 Ma:

$$Age = 15235.08636 - 21482.27712 \times (^{86}Sr/^{87}Sr).$$

Miller et al. (1991) and Oslick et al. (1994) estimated age errors derived from linear regressions of Sr isotopic records. Age errors for 22.8–15.5 Ma are ±0.61 m.y. and for 15.5–9.7 Ma are ±1.17 m.y. at the 95% confidence interval for a single analysis. Increasing the number of analyses at a given level improves the age estimate (±0.40 and ±0.76 Ma for three analyses each in the two intervals; Oslick et al., 1994). The regression for the late Pliocene–Pleistocene (2.5–0 Ma) has an age error of ±0.35 m.y. for one analysis at the 95% confidence interval or ±0.2 m.y. for three analyses at the 95% confidence interval (K.G. Miller, unpubl. analysis of data; Farrell et al., 1995). The regression for the late Oligocene to earliest Miocene (27.5–22.8 Ma) and latest Eocene to Oligocene (34.4–27.5 Ma) have age errors of ±1 and 1.2 m.y., respectively, for one analysis at the 95% confidence interval (Reilly et al., 2002). These errors are applied to the Sr isotope values for the age-depth plots.

A primary goal of Expedition 313 is to provide the ages of surfaces and hiatuses; hence, an additional aspect of chronologic assessment is to attempt to correlate the age-depth patterns of each hole to regional surfaces revealed by seismic profiles. Seismic sequence boundaries (identified by onlap, downlap, erosional trunction, and toplap), as well as other prominent reflectors (Monteverde, 2008; Monteverde et al., 2008), were initially correlated to each hole using a traveltime-depth relationship developed from seismic stacking velocities (see **"Stratigraphic correlation"**). When necessary, small adjustments (typically <10 m) were made to match the depths of reflectors predicted by this procedure to surfaces observed in cores and/or to MSCL and downhole mea-

surements (see "Stratigraphic correlation" in each site chapter). In all cases, the original depths predicted by seismic interpretation are preserved in the tables given in each site chapter. An approximate average sedimentation rate (ignoring compaction) for each sequence was obtained by a visual best fit between core thickness and ages obtained by combined biostratigraphic and Sr isotopic analysis. Age-depth plots are preliminary in that micropaleontological and Sr isotopic studies are ongoing. In general, age errors for most surfaces are less than ±0.5 m.y., as shown on figures and tables in the site chapters.

Samples analyzed for Sr isotopes also provided coarse fraction semiquantitative lithology data presented on age-depth plots (e.g., Fig. F34 in the "Site M0027" chapter). The cumulative percent of lithologic components of core sediments was computed from shipboard samples. Each sample was dried and weighed before washing, and the dry weight was used to compute the percentage of sand versus silt and clay. The coarse (sand) fraction was dry sieved through a 250 μm sieve, and the fractions were weighed to obtain a quantitative measure of the percent of very fine and fine versus medium and coarser sand. Sand fractions were examined using a microscope, and a visual semiquantitative estimate was made of the relative percentages of quartz, glauconite, carbonate (foraminifers and other shells), mica, and other materials contained in the sample.

References

Aigner, T., 1982. Calcareous tempesties: storm-dominated stratification in upper Muschelkalk limestones (Middle Trias, SW-Germany). *In* Einsele, G., and Seilacher, A. (Eds.), *Cyclic and Event Stratification:* Berlin (Springer-Verlag), 180–198.

Andersen, E.S., Dokken, T.M., Elverhøi, A., Solheim, A., and Fossen, I., 1996. Late Quaternary sedimentation and glacial history of the western Svalbard continental margin. *Mar. Geol.,* 133(3–4):123–156. doi:10.1016/0025-3227(96)00022-9

Ando, H., 1990. Stratigraphy and shallow marine sedimentary facies of the Mikasa Formation, Middle Yezo Group (Upper Cretaceous). *Chishitsugaku Zasshi,* 96:279–295.

Austin, J.A., Jr., Christie-Blick, N., Malone, M., Mountain, G.S., and the Leg 174A Shipboard Party, 1998. Miocene to Pleistocene sand-rich sequences and sea-level changes at the New Jersey outer shelf: results from Leg 174A. *JOIDES J.,* 24(1):4–6, 19. http://www-odp.tamu.edu/publications/citations/joides_j/joides_j_24_1.pdf

Backman, J., and Raffi, I., 1997. Calibration of Miocene nannofossil events to orbitally tuned cyclostratigraphies from Ceara Rise. *In* Shackleton, N.J., Curry, W.B., Richter, C., and Bralower, T.J. (Eds.), *Proc. ODP, Sci.*

Results, 154: College Station, TX (Ocean Drilling Program), 83–99. doi:10.2973/odp.proc.sr.154.101.1997

Batten, D.J., 1996. Palynofacies and petroleum potential. *In* Jansonius, J., and McGregor, D.C. (Eds.), *Palynology: Principles and Applications* (Vol. 3): College Station, TX (Am. Assoc. Stratigraphic Palynol. Found), 1065–1084.

Berggren, W.A., Kent, D.V., Swisher, C.C., III, and Aubry, M.-P., 1995. A revised Cenozoic geochronology and chronostratigraphy. *In* Berggren, W.A., Kent, D.V., Aubry, M.-P., and Hardenbol, J. (Eds.), *Geochronology, Time Scales and Global Stratigraphic Correlation.* Spec. Publ.—SEPM (Soc. Sediment. Geol.), 54:129–212.

Berggren, W.A., and Miller, K.G., 1988. Paleogene tropical planktonic foraminiferal biostratigraphy and magnetobiochronology. *Micropaleontology,* 34(4):362–380. doi:10.2307/1485604

Berggren, W.A., and Pearson, P.N., 2005. A revised tropical to subtropical Paleogene planktonic foraminiferal zonation. *J. Foraminiferal Res.,* 35(4):279–298. doi:10.2113/35.4.279

Beug, H.-J., 2004. *Leitfaden der Pollenbestimmung für Mitteleuropa und Angrenzende Gebiete:* München (Verlag Friedrich Pfeil).

Bhattacharya, J.P., and Walker, R.G., 1992. Deltas. *In* Walker, R.G., and James, N.P. (Eds.), *Facies Models*: *Response to Sea Level Change:* St. John's, Newfoundland (Geol. Assoc. Can.), 157–177.

Blow, W.H., 1969. Late middle Eocene to Recent planktonic foraminiferal biostratigraphy. *Proc. Int. Conf. Planktonic Microfossils,* 1:199–422.

Bolli, H.M., Saunders, J.B., and Perch-Nielsen, K. (Eds.), 1985. *Plankton Stratigraphy:* Cambridge (Cambridge Univ. Press).

Bown, P.R. (Ed.), 1998. *Calcareous Nannofossil Biostratigraphy:* Dordrecht, The Netherlands (Kluwer Academic Publ.).

Browning, J.V., Miller, K.G., McLaughlin, P.P., Kominz, M.A., Sugarman, P.J., Monteverde, D., Feigenson, M.D., and Hernández, J.C., 2006. Quantification of the effects of eustasy, subsidence, and sediment supply on Miocene sequences, mid-Atlantic margin of the United States. *Geol. Soc. Am. Bull.,* 118(5):567–588. doi:10.1130/B25551.1

Cande, S.C., and Kent, D.V., 1995. Revised calibration of the geomagnetic polarity timescale for the Late Cretaceous and Cenozoic. *J. Geophys. Res., [Solid Earth],* 100(B4):6093–6095. doi:10.1029/94JB03098

Catuneanu, O., 2006. *Principles of Sequence Stratigraphy:* Amsterdam (Elsevier).

Catuneanu, O., Abreu, V., Bhattacharya, J.P., Blum, M.D., Dalrymple, R.W., Eriksson, P.G., Fielding, C.R., Fisher, W.L., Galloway, W.E., Gibling, M.R., Giles, K.A., Holbrook, J.M., Jordan, R., Kendall, C.G.St.C., Macurda, B., Martinsen, O.J., Miall, A.D., Neal, J.E., Nummedal, D., Pomar, L., Posamentier, H.W., Pratt, B.R., Sarg, J.F., Shanley, K.W., Steel, R.J., Strasser, A., Tucker, M.E., and Winker, C., 2009. Towards the standardization of sequence stratigraphy. *Earth-Sci. Rev.,* 92(1–2):1–33. doi:10.1016/j.earscirev.2008.10.003

Coe, A.L. (Ed.), 2003. *The Sedimentary Record of Sea-Level Change:* Cambridge (Cambridge Univ. Press).

Culver, S.J., and Goshorn, J.H., 1996. Foraminifera and paleoenvironments of the Eastover Formation (upper Miocene, Virginia, U.S.A). *J. Foraminiferal Res.,* 26(4):300–323. doi:10.2113/gsjfr.26.4.300

Cushman, J.A., and Cahill, E.D., 1933. Foraminifera of the coastal plain of the Eastern U.S. *U.S. Geol. Surv. Prof. Pap.,* 175A.

Dankers, P.H.M., and Zijderveld, J.D.A., 1981. Alternating field demagnetization of rocks, and the problem of gyromagnetic remanence. *Earth Planet. Sci. Lett.,* 53(1):89–92. doi:10.1016/0012-821X(81)90029-7

de Verteuil, L., and Norris, G., 1996. Miocene dinoflagellate stratigraphy and systematics of Maryland and Virginia. *Micropaleontology,* 42(Suppl.). doi:10.2307/1485926

Dickens, G.R., Koelling, M., Smith, D.C., Schneiders, L., and the IODP Expedition 302 Scientists, 2007. Rhizon sampling of pore waters on scientific drilling expeditions: an example from the IODP Expedition 302, Arctic Coring Expedition (ACEX). *Sci. Drill.,* 4: 22–25. doi:10.2204/iodp.sd.4.08.2007

Diepenbroek, M., Grobe, H., Reinke, M., Schindler, U., Schlitzer, R., Sieger, R., and Wefer, G., 2002. PANGAEA—an information system for environmental sciences. *Comp. Geosci.,* 28(10):1201–1210. doi:10.1016/S0098-3004(02)00039-0

Diepenbroek, M., Grobe, H., Reinke, M., Schlitzer, R., and Sieger, R., 1999. Data management of proxy parameters with PANGAEA. *In* Fischer, G., and Wefer, G. (Eds.), *Use of Proxies in Paleoceanography—Examples from the South Atlantic:* Heidelberg (Springer), 715–727.

Dix, C.H., 1955. Seismic velocities from surface measurements. *Geophysics,* 20(1):68–86. doi:10.1190/1.1438126

Droser, M.L., and Bottjer, D.J., 1991. Trace fossils and ichnofabric in Leg 119 cores. *In* Barron, J., Larsen, B., et al., *Proc. ODP, Sci. Results,* 119: College Station, TX (Ocean Drilling Program), 635–641. doi:10.2973/odp.proc.sr.119.206.1991

Dybkjær, K., 2004. Morphological and abundance variations in *Homotryblium*-cyst assemblages related to depositional environments: uppermost Oligocene–lower Miocene, Jylland, Denmark. *Palaeogeogr., Palaeoclimatol., Palaeoecol.,* 206(1–2):41– 58. doi:10.1016/j.palaeo.2003.12.021

Einsele, G., 2000. *Sedimentary Basins—Evolution, Facies, and Sediment Budget* (2nd ed.): Berlin (Springer).

Eldrett, J.S., Harding, I.C., Firth, J.V., and Roberts, A.P., 2004. Magnetostratigraphic calibration of Eocene–Oligocene dinoflagellate cyst biostratigraphy from the Norwegian–Greenland Sea. *Mar. Geol.,* 204(1–2):91–127. doi:10.1016/S0025-3227(03)00357-8

Expedition 302 Scientists, 2006. Methods. *In* Backman, J., Moran, K., McInroy, D.B., Mayer, L.A., and the Expedition 302 Scientists, *Proc. IODP,* 302: Edinburgh (Integrated Ocean Drilling Program Management International, Inc.). doi:10.2204/iodp.proc.302.103.2006

Farrell, J.W., Clemens, S.C., and Gromet, L.P., 1995. Improved chronostratigraphic reference curve of late Neogene seawater $^{87}Sr/^{86}Sr$. *Geology,* 23(5):403–406. doi:10.1130/0091-7613(1995)023<0403:ICR-COL>2.3.CO;2

Galloway, W.E., 1975. Process framework for describing the morphologic and stratigraphic evolution of deltaic depositional systems. *In* Broussard, M.L. (Ed.), *Deltas: Models for Exploration:* Houston (Houston Geol. Soc.), 87–98.

Gerard, J.R.F., and Bromley, R.G., 2008. *Ichnofabrics in Clastic Sediments—Application to Sedimentological Core Studies: A Practical Guide:* Madrid (J. Gerard).

Gibson, T.G., 1983. Key foraminifera from upper Oligocene to lower Pleistocene strata of the central Atlantic coastal plain. *Smithson. Contrib. Paleobiol.,* 53:354–453. http://www.sil.si.edu/smithsoniancontributions/Paleobiology/pdf_hi/SCtP-0053.pdf

Gilbert, G.K., 1885. The topographic features of lake shores. *U.S. Geol. Surv. Annu. Rep.,* 5:75–123.

Greenlee, S.M., Devlin, W.J., Miller, K.G., Mountain, G.S., and Flemings, P.B., 1992. Integrated sequence stratigraphy of Neogene deposits, New Jersey continental shelf and slope: comparison with the Exxon model. *Geol. Soc. Am. Bull.,* 104(11):1403–1411. doi:10.1130/0016-7606(1992)104<1403:ISSOND>2.3.CO;2

Greenlee, S.M., Schroeder, F.W., and Vail, P.R., 1988. Seismic stratigraphic and geohistory analysis of Tertiary strata from the continental shelf off New Jersey; calculation of eustatic fluctuations from stratigraphic data. *In* Sheridan, R.E., and Grow, J.A. (Eds.), *The Geology of North America,* Vol. I-2: *The Atlantic Continental Margin:* Boulder (Geol. Soc. Am.), 437–444.

Guillocheau, R., Dabard, M.-P., Loi, A., and Robin, C., 2009. Les depots de tempetes des domaines marins ouverts aux milieux restreints. *Cr. Fr. Sedimentol.,* 65:3–52

Hall, P.O.J., and Aller, R.C., 1992. Rapid, small-volume, flow injection analysis for ΣCO_2 and NH_4^+ in marine and freshwaters. *Limnol. Oceanogr.,* 37(5):1113–1119. doi:10.4319/lo.1992.37.5.1113

Harms, J.C., Southard, J.B., Spearing, D.R., and Walker, R.G., 1975. Depositional environments as interpreted from primary sedimentary and stratigraphic sequences. *SEPM Short Course,* 2.

Harms, J.C., Southard, J.B., and Walker, R.G., 1982. Structures and sequences in clastic rocks. *SEPM Short Course,* 9.

Hart, S.R., and Brooks, C., 1974. Clinopyroxene-matrix partitioning of K, Rb, Cs, and Ba. *Geochim. Cosmochim. Acta,* 38(12):1799–1806. doi:10.1016/0016-7037(74)90163-X

Helland-Hansen, W., and Hampson, G.J., 2009. Trajectory analysis: concepts and applications. *Basin Res.,* 21(5):454–483. doi:10.1111/j.1365-2117.2009.00425.x

Hesselbo, S.P., and Huggett, J.M., 2001. Glaucony in ocean-margin sequence stratigraphy (Oligocene–Pliocene, offshore New Jersey, U.S.A.; ODP Leg 174A). *J. Sediment. Res.,* 71(4):599–607. doi:10.1306/112800710599

Howell, J.A., and Flint, S.S., 2003. Tectonic setting, stratigraphy and sedimentology of the Book Cliffs. *In* Coe, A.L., Bosence, D.W.J., Church, K.D., Flint, S.S., Howell, J.A., and Wilson, R.C.L. (Eds.), *The Sedimentary Record of Sea-Level Change:* Cambridge (Cambridge Univ. Press), 135–157.

Jackson, P.D., Lovell, M.A., Roberts, J.A., Schultheiss, P.J., Gunn, D., Flint, R.C., Wood, A., Holmes, R., and Frederichs, T., 2006. Rapid non-contacting resistivity logging of core. *Geol. Soc. Spec. Publ.,* 267(1):209–217. **doi:10.1144/GSL.SP.2006.267.01.15**

Katz, M.E., Wright, J.D., Miller, K.G., Cramer, B.S., Fennel, K., and Falkowski, P.G., 2005. Biological overprint of the geological carbon cycle. *Mar. Geol.,* 217(3–4)323–338. **doi:10.1016/j.margeo.2004.08.005**

Kennett, J.P., and Srinivasan, M.S., 1983. *Neogene Planktonic Foraminifera: A Phylogenetic Atlas:* Stroudsburg, PA (Hutchinson Ross).

Kirschvink, J.L., 1980. The least-squares line and plane and the analysis of palaeomagnetic data. *Geophys. J. R. Astron. Soc.,* 62(3):699–718. **doi:10.1111/j.1365-246X.1980.tb02601.x**

Leroy, C.C., 1969. Development of simple equations for accurate and more realistic calculation of the speed of sound in seawater. *J. Acoust. Soc. Am.,* 46(1B):216–226. **doi:10.1121/1.1911673**

Lourens, L.J., Hilg, F.J., Shackleton, N.J., Laskar, J., and Wilson, D., 2004. The Neogene period. *In* Gradstein, F.M., Ogg, J.G., and Smith, A.G. (Eds.), *A Geological Time Scale 2004.* Cambridge (Cambridge Univ. Press), 409–440.

Louwye, S., De Coninck, J., and Verniers, J., 2000. Shallow marine lower and middle Miocene deposits at the southern margin of the North Sea Basin (northern Belgium): dinoflagellate cyst biostratigraphy and depositional history. *Geol. Mag.,* 137(4):381–394. **doi:10.1017/S0016756800004258**

Martini, E., 1971. Standard Tertiary and Quaternary calcareous nannoplankton zonation. *Proc. Int. Conf. Planktonic Microfossils,* 2:739–785.

Mazzullo, J.M., Meyer, A., and Kidd, R.B., 1988. New sediment classification scheme for the Ocean Drilling Program. *In* Mazzullo, J.M., and Graham, A.G. (Eds.), *Handbook for shipboard sedimentologists.* ODP Tech. Note, 8:45–67. **doi:10.2973/odp.tn.8.1988**

McAndrews, J.H., Berti, A.A., and Norris, G., 1973. *Royal Ontario Museum Life Sciences Miscellaneous Publication: Key to the Quaternary Pollen and Spores of the Great Lakes Region:* Ontario (Royal Ontario Museum).

McArthur, J.M., Howarth, R.J., and Bailey, T.R., 2001. Strontium isotope stratigraphy: LOWESS version 3: best fit to the marine Sr-isotope curve for 0–509 Ma and accompanying look-up table for deriving numerical age. *J. Geol.,* 109(2):155–170. **doi:10.1086/319243**

McCarthy, F.M.G., and Gostlin, K.E., 2000. Correlating Pleistocene sequences across the New Jersey margin. *Sediment. Geol.,* 134(1–2):181–196. **doi:10.1016/S0037-0738(00)00019-1**

McCarthy, F.M.G., Gostlin, K.E., Mudie, P.J., and Hopkins, J.A., 2003. Terrestrial and marine palynomorphs as sea-level proxies: an example from Quaternary sediments on the New Jersey margin, U.S.A. *In* Olson, H.C., and Leckie, R.M. (Eds.), *Micropaleontologic Proxies for Sea-Level Change and Stratigraphic Discontinuities.* Spec. Publ.—Soc. Sediment. Geol., 75:119–129.

McCubbin, D.G., 1982. Barrier-island and strand-plain facies. *In* Scholle, P.A., and Spearing, D. (Eds.), *Sandstone Depositional Environments:* AAPG Mem., 31:247–279.

Miller, K.G., et al., 1994. *Proc. ODP, Init. Repts.,* 150X: College Station, TX (Ocean Drilling Program). **doi:10.2973/odp.proc.ir.150X.1994**

Miller, K.G., Feigenson, M.D., Wright, J.D., and Clement, B.M., 1991. Miocene isotope reference section, Deep Sea Drilling Project Site 608: an evaluation of isotope and biostratigraphic resolution. *Paleoceanography,* 6(1):33–52. **doi:10.1029/90PA01941**

Miller, K.G., Mountain, G.S., the Leg 150 Shipboard Party, and Members of the New Jersey Coastal Plain Drilling Project, 1996. Drilling and dating New Jersey Oligocene–Miocene sequences: ice volume, global sea level, and Exxon records. *Science,* 271(5252):1092–1095. **doi:10.1126/science.271.5252.1092**

Miller, K.G., Rufolo, S., Sugarman, P.J., Pekar, S.F., Browning, J.V., and Gwynn, D.W., 1997. Early to middle Miocene sequences, systems tracts, and benthic foraminiferal biofacies, New Jersey coastal plain. *In* Miller, K.G., and Snyder, S.W. (Eds.), *Proc. ODP, Sci. Results,* 150X: College Station, TX (Ocean Drilling Program), 169–186. **doi:10.2973/odp.proc.sr.150X.313.1997**

Miller, K.G., Sugarman, P.J., Browning, J.V., et al., 1998. *Proc. ODP, Init. Repts.,* 174AX: College Station, TX (Ocean Drilling Program). **doi:10.2973/odp.proc.ir.174AX.1998**

Mitchum, R.M., Jr., Vail, P.R., and Thompson, S., III, 1977. Seismic stratigraphy and global changes of sea level, Part 2. The depositional sequence as a basic unit for stratigraphic analysis. *In* Payton, C.E. (Ed.), *Seismic Stratigraphy: Applications to Hydrocarbon Exploration.* AAPG Mem., 26:53–62.

Monteverde, D.H., 2008. Sequence stratigraphic analysis of early and middle Miocene shelf progradation along the New Jersey margin [Ph.D. dissert.]. Rutgers Univ.

Monteverde, D.H., Mountain, G.S., and Miller, K.G., 2008. Early Miocene sequence development across the New Jersey margin. *Basin Res.,* 20(2):249–267. **doi:10.1111/j.1365-2117.2008.00351.x**

Mountain, G.S., Miller, K.G., Blum, P., et al., 1994. *Proc. ODP, Init. Repts.,* 150: College Station, TX (Ocean Drilling Program). **doi:10.2973/odp.proc.ir.150.1994**

Munsell Color Company, Inc., 1988. *Munsell Soil Color Charts:* Baltimore, MD (Munsell).

Munsterman, D.K., and Brinkhuis, H., 2004. A southern North Sea Miocene dinoflagellate cyst zonation. *Geol. Mijnbouw,* 83(4):267–285. **http://www.njgonline.nl/publish/articles/000060/article.pdf**

Nelson, C.H., 1983. Modern submarine fans and debris aprons: an update of the first half century. *In* Boardman, S.J. (Ed.), *Revolution in the Earth Sciences: Advances in the Past Half-Century:* Dubuque, IA (Kendall Hunt), 148–166.

Ogg, J.G., Ogg, G., and Gradstein, F.M., 2008. *The Concise Geologic Time Scale*: Cambridge (Cambridge Univ. Press). http://www.cambridge.org/catalogue/catalogue.asp?isbn=9780521898492

Olafsson, G., and Villa, G., 1992. Reliability of sphenoliths as zonal markers in Oligocene sediments from the Atlantic and Indian Oceans. *In* Proto Decima, F., Monechi, S., and Rio, D. (Eds.), *Proc. Int. Nannoplankton Assoc. Conf., Firenze 1989.* Mem. Sci. Geol., 43:261–275.

Olsson, R.K., Melillo, A.J., and Schreiber, B.L., 1987. Miocene sea level events in the Maryland coastal plain and the offshore Baltimore Canyon Trough. *In* Ross, C.A., and Haman, D. (Eds.), *Timing and Depositional History of Eustatic Sequences: Constraints on Seismic Stratigraphy.* Spec. Publ.—Cushman. Found. Foraminiferal Res., 24:85–97.

Oslick, J.S., Miller, K.G., Feigenson, M.D., and Wright, J.D., 1994. Oligocene–Miocene strontium isotopes: stratigraphic revisions and correlations to an inferred glacio-eustatic record. *Paleoceanography,* 9(3):427–443. doi:10.1029/94PA00249

Pazzaglia, F.J., Robinson, R.A.J., and Traverse, A., 1997. Palynology of the Bryn Mawr Formation (Miocene): insights of the age and genesis of middle Atlantic margin fluvial deposits. *Sediment. Geol.,* 108(1–2):19–44. doi:10.1016/S0037-0738(96)00047-4

Perch-Nielsen, K., 1985. Cenozoic calcareous nannofossils. *In* Bolli, H.M., Saunders, J.B., and Perch-Nielsen, K. (Eds.), *Plankton Stratigraphy:* Cambridge (Cambridge Univ. Press), 427–554.

Petschick, R., Kuhn, G., and Gingele, F., 1996. Clay mineral distribution in surface sediments of the South Atlantic: sources, transport, and relation to oceanography. *Mar. Geol.,* 130(3–4):203–229. doi:10.1016/0025-3227(95)00148-4

Pickering, K.T., Hiscott, R.N., and Hein, F.J., 1989. *Deep-Marine Environments: Clastic Sedimentation and Tectonics:* London (Unwin Hyman).

Pirmez, C., Pratson, L.F., and Steckler, M.S., 1998. Clinoform development by advection—diffusion of suspended sediment: modelling and comparison to natural systems. *J. Geophys. Res., [Solid Earth],* 103(b10):24141–24157. doi:10.1029/98JB01516

Posamentier, H.W., and Allen, G.P., 1999. *Siliciclastic Sequence Stratigraphy—Concepts and Applications.* SEPM Concepts Sedimentol. Paleontol., 7.

Posamentier, H.W., and Kolla, V., 2003. Seismic geomorphology and stratigraphy of depositional elements in deep-water settings. *J. Sediment. Res.,* 73(3):367–388. doi:10.1306/111302730367

Posamentier, H.W., and Walker, R.G., 2006. Deep-water turbidites and submarine fans. *In* Posamentier, H.W., and Walker, R.G. (Eds.), *Facies Models Revisited.* Spec. Publ.—SEPM (Soc. Sediment. Geol.), 84:399–520.

Raffi, I., Backman, J., Fornaciari, E., Pälike, H., Rio, D., Lourens, L., and Hilgen, F., 2006. A review of calcareous nannofossil astrobiochronology encompassing the past 25 million years. *Quat. Sci. Rev.,* 25(23–24):3113–3137. doi:10.1016/j.quascirev.2006.07.007

Raffi, I., and Flores, J.-A., 1995. Pleistocene through Miocene calcareous nannofossils from eastern equatorial Pacific Ocean (Leg 138). *In* Pisias, N.G., Mayer, L.A., Janecek, T.R., Palmer-Julson, A., and van Andel, T.H. (Eds.), *Proc. ODP, Sci. Results,* 138: College Station, TX (Ocean Drilling Program), 233–286. doi:10.2973/odp.proc.sr.138.112.1995

Reading, H.G., and Richards, M., 1994. Turbidite systems in deep-water basin margins classified by grain size and feeder system. *AAPG Bull.,* 78(5):792–822. http://aapg-bull.geoscienceworld.org/cgi/content/abstract/78/5/792

Reilly, T.J., Miller, K.G., and Feigenson, M.D., 2002. Latest Eocene–earliest Miocene Sr isotopic reference section, Site 522, eastern South Atlantic. *Paleoceanography,* 17(3):1046–1054. doi:10.1029/2001PA000745

Reineck, H.E, and Singh, I.B., 1972. Genesis of laminated sand and graded rhythmites in storm-sand layers of shelf mud. *Sedimentology,* 18(1–2):123–128. doi:10.1111/j.1365-3091.1972.tb00007.x

Rich, J.L., 1951. Three critical environments of deposition, and criteria for recognition of rocks deposited in each of them. *Geol. Soc. Am. Bull.,* 62(1):1–20. doi:10.1130/0016-7606(1951)62[1:TCEODA]2.0.CO;2

Rider, M., 2006. *The Geological Interpretation of Well Logs* (2nd ed.): Sutherland, Scotland (Whittles).

Rothwell, R.G., 1989. *Minerals and Mineraloids in Marine Sediments: An Optical Identification Guide:* London (Elsevier).

Sato, T., Kameo, K., and Mita, I., 1999. Validity of the latest Cenozoic calcareous nannofossil datums and its application to the tephrochronology. *Earth Sci.,* 53(4):265–274. [in Japanese]

Savrda, C.E., Browning, J.V., Krawinkel, H., and Hesselbo, S.P., 2001. Firmground ichnofabrics in deep-water sequence stratigraphy, Tertiary clinoform-toe deposits, New Jersey slope. *Palaios,* 16(3):294–305. doi:10.2307/3515606

Schlumberger, 1989. *Log Interpretation Principles/Applications:* Houston (Schlumberger Educ. Services), SMP–7017.

Schnitker, D., 1970. *Upper Miocene Foraminifera from Near Grimeland, Pitt County, North Carolina.* Spec. Publ.—N. C., Div. Miner. Resour., 3.

Seeberg-Elverfeldt, J., Schlüter, M., Feseker, T., and Kölling, M., 2005. Rhizone sampling of porewaters near the sediment-water interface of aquatic systems. *Limnol. Oceanogr.: Methods,* 3(8):361–371.

Serra, O., 1984. *Fundamentals of Well-Log Interpretation* (Vol. 1): *The Acquisition of Logging Data:* Amsterdam (Elsevier).

Serra, O., 1986. *Fundamentals of Well-Log Interpretation* (Vol. 2): *The Interpretation of Logging Data:* Amsterdam (Elsevier).

Shackleton, N.J., Crowhurst, S., Hagelberg, T., Pisias, N.G., and Schneider, D.A., 1995. A new late Neogene time scale: application to Leg 138 sites. *In* Pisias, N.G., Mayer, L.A., Janecek, T.R., Palmer-Julson, A., and van Andel, T.H. (Eds.), *Proc. ODP, Sci. Results,* 138: College Station,

TX (Ocean Drilling Program), 73–101. doi:10.2973/odp.proc.sr.138.106.1995

Shackleton, N.J., Crowhurst, S.J., Weedon, G.P., and Laskar, J., 1999. Astronomical calibration of Oligocene–Miocene time. *In* Shackleton N.J., McCave, I.N., and Graham, P.W. (Eds.), *Astronomical (Milankovitch) Calibration of the Geological Time-Scale.* Philos. Trans. R. Soc., Ser. A., 357(1757):1907–1929. doi:10.1098/rsta.1999.0407

Shepard, F.P., 1954. Nomenclature based on sand-silt-clay ratios. *J. Sediment. Res.,* 24(3):151–158.

Sluijs, A., Brinkhuis, H., Stickley, C.E., Warnaar, J., Williams, G.L., and Fuller, M., 2003. Dinoflagellate cysts from the Eocene–Oligocene transition in the Southern Ocean: results from ODP Leg 189. *In* Exon, N.F., Kennett, J.P., and Malone, M.J. (Eds.), *Proc. ODP, Sci. Results,* 189: College Station, TX (Ocean Drilling Program), 1–42. doi:10.2973/odp.proc.sr.189.104.2003

Snyder, S.W., Waters, V.J., and Moore, T.L., 1989. Benthic foraminifera and paleocology of Miocene Pungo River Formation sediments in Onslow Bay, North Carolina continental shelf. *In* Snyder, S.W. (Ed.), *Micropaleontology of Miocene Sediments in the Shallow Subsurface of Onslow Bay, North Carolina Continental Shelf.* Spec. Publ.—Cushman. Found. Foraminiferal Res., 25:43–96.

Stephenson, A., 1980. Gyromagnetism and the remanence acquired by a rotating rock in an alternating field. *Nature (London, U. K.),* 284(5751):48–49. doi:10.1038/284048a0

Stow, D.A.V., Howell, D.G., and Nelson, C.H., 1984. Sedimentary, tectonic, and sea-level controls on submarine fan and slope-apron turbidite systems. *Geo-Mar. Lett.,* 3(2–4):57–64. doi:10.1007/BF02462448

Sugarman, P.J., Miller, K.G., Owens, J.P., and Feigenson, M.D., 1993. Strontium-isotope and sequence stratigraphy of the Miocene Kirkwood Formation, southern New Jersey. *Geol. Soc. Am. Bull.,* 105(4):423–436. doi:10.1130/0016-7606(1993)105<0423:SIASSO>2.3.CO;2

Traverse, A., 2007. *Topics in Geobiology,* Vol. 28: *Paleopalynolgy* (2nd ed.): New York (Springer).

van Morkhoven, F.P.C.M., Berggren, W.A., and Edwards, A.S., 1986. *Cenozoic Cosmopolitan Deep-Water Benthic Foraminifera.* Bull. Cent. Rech. Explor.—Prod. Elf-Aquitaine, 11.

Van Simaeys, S., De Man, E., Vandenberghe, N., Brinkhuis, H., and Steurbaut, E., 2004. Stratigraphic and paleoenvironmental analysis of the Rupelian–Chattian transition in the type region: evidence from dinoflagellate cysts, foraminifera and calcareous nannofossils. *Palaeogeogr., Palaeoclimatol., Palaeoecol.,* 208(1–2):31–58. doi:10.1016/j.palaeo.2004.02.029

Van Simaeys, S., Munsterman, D., and Brinkhuis, H., 2005. Oligocene dinoflagellate cyst biostratigraphy of the southern North Sea Basin. *Rev. Palaeobot. Palynol.,* 134(1–2):105–128. doi:10.1016/j.revpalbo.2004.12.003

Villa, G., Fioroni, C., Pea, L., Bohaty, S., and Persico, D., 2008. Middle Eocene–late Oligocene climate variability: calcareous nannofossil response at Kerguelen Plateau, Site 748. *Mar. Micropaleontol.,* 69(2):173–192. doi:10.1016/j.marmicro.2008.07.006

Vogt, C., 1997. Regional and temporal variations of mineral assemblages in Arctic Ocean sediments as climatic indicator during glacial/interglacial changes [Ph.D. thesis]. Alfred Wegener Institute, Bremerhaven.

Vogt, C., 2009. Data report: semiquantitative determination of detrital input to ACEX sites based on bulk sample X-ray diffraction data. *In* Backman, J., Moran, K., McInroy, D.B., Mayer, L.A., and the Expedition 302 Scientists, *Proc. IODP,* 302: Edinburgh (Integrated Ocean Drilling Program Management International, Inc.). doi:10.2204/iodp.proc.302.203.2009

Vogt, C., Knies, J., Spielhagen, R.F., and Stein, R., 2001. Detailed mineralogical evidence for two nearly identical glacial/deglacial cycles and Atlantic water advection to the Arctic Ocean during the last 90,000 years. *Global Planet. Change,* 31(1–4):23–44. doi:10.1016/S0921-8181(01)00111-4

Von Herzen, R., and Maxwell, A.E., 1959. The measurement of thermal conductivity of deep-sea sediments by a needle-probe method. *J. Geophys. Res.,* 64(10):1557–1563. doi:10.1029/JZ064i010p01557

Walker, R.G., and James, N.P., 1992. *Facies Models: Response to Sea Level Change:* St. Johns, Newfoundland (Geol. Assoc. Can.).

Walker, R.G., and Plint, A.G., 1992. Wave- and storm-dominated shallow marine systems. *In* Walker, R.W., and James, N.P. (Eds.), *Facies Models: Response to Sea Level Change:* St. Johns, Newfoundland (Geol. Assoc. Can.), 219–238.

Wentworth, C.K., 1922. A scale of grade and class terms for clastic sediments. *J. Geol.,* 30(5):377–392. doi:10.1086/622910

White, J.M., and Ager, T.A., 1994. Palynology, paleoclimatology and correlation of middle Miocene beds from Porcupine River (Locality 90-1), Alaska. *Quat. Int.,* 22–23:43–77. doi:10.1016/1040-6182(94)90006-X

Wilgus, C.K., Hastings,B.S., Ross, C.A., Posamentier, H., Van Wagoner, J., and Kendall, C.G.St.C. (Eds.), 1988. *Sea-Level Changes: An Integrated Approach.* Spec. Publ.—Soc. Econ. Paleontol. Min., 42.

Williams, G.L., and Manum, S.B., 1999. Oligocene–early Miocene dinocyst stratigraphy of Hole 985A (Norwegian Sea). *In* Raymo, M.E., Jansen, E., Blum, P., and Herbert, T.D. (Eds.), 1999. *Proc. ODP, Sci. Results,* 162: College Station, TX (Ocean Drilling Program), 99–109. doi:10.2973/odp.proc.sr.162.030.1999

Figure F1. Schematic of recovery and naming conventions used by IODP and during Expedition 313.
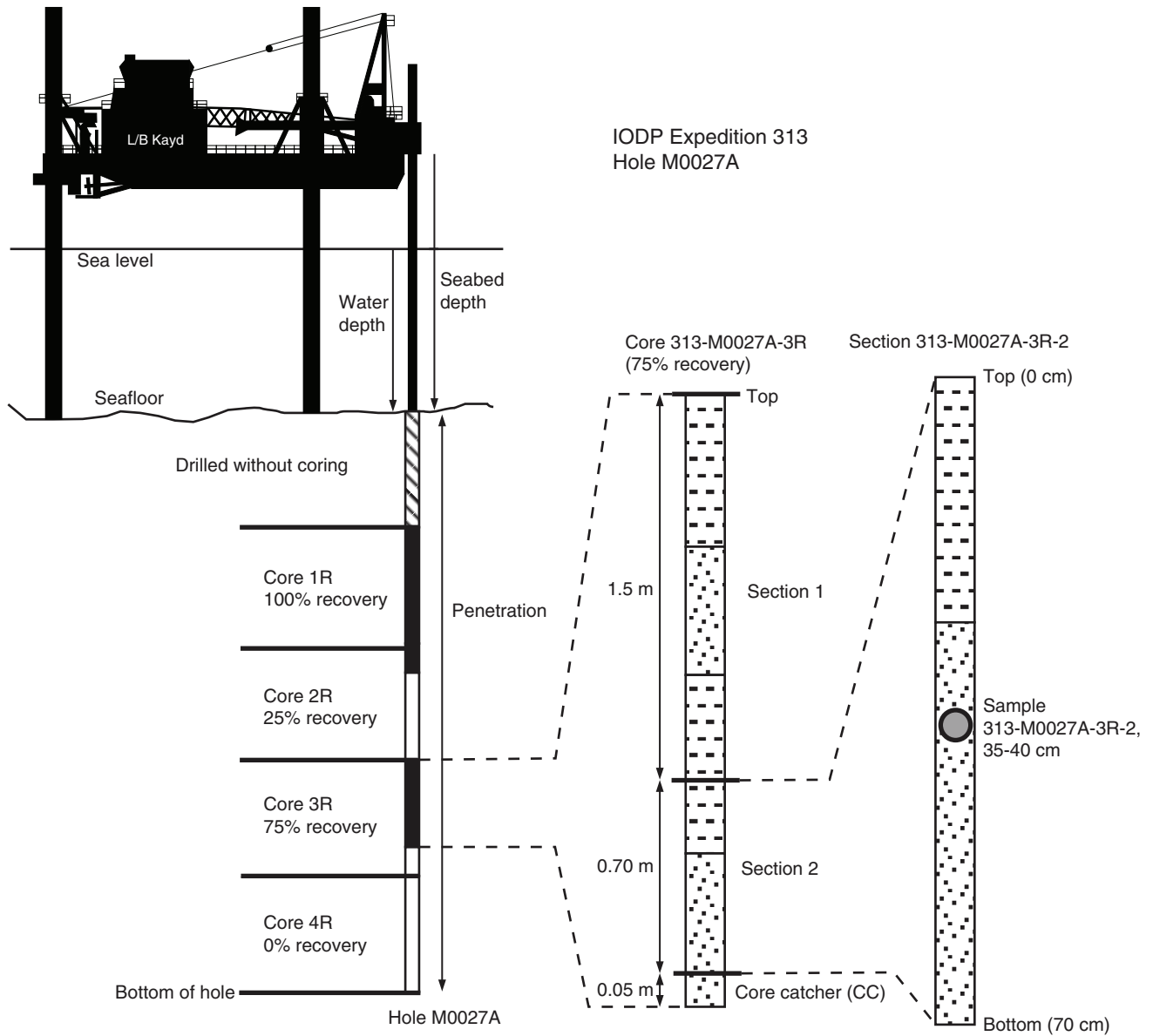
Figure F2. Photograph of the *L/B Kayd,* drilling platform for Expedition 313. The DOSECC-provided drill rig was situated on the bow of the *L/B Kayd* (left side of photograph).

Figure F3. Photograph of the DOSECC-provided Atlas Copco CS4002 mining rig, taken from the *L/B Kayd*'s transfer basket during Expedition 313.

Figure F4. Key to symbols used to represent lithology, contacts, sedimentary structures, trace fossils, diagenetic components, and drilling disturbance in the Expedition 313 VCDs.

Lithology

Sand(stone)

Silty sand(stone)

Clayey sand(stone)

Muddy sand(stone)

Shelly sand(stone)

Gravelly sand(stone)

Conglomerate

Sandy gravel

Muddy gravel

Silt(stone)

Sandy silt(stone)

Clayey silt(stone)

Sandy mud(stone)

Clay(stone)

Silty clay(stone)

Sandy clay(stone)

Glauconite sand(stone)

Glauconite clay(stone)

Glauconitic mud(stone)

Physical structures

Very thinly bedded, foliated, or banded (1–3 cm)

Thinly bedded, foliated or banded (3–10 cm)

Medium bedded, foliated, or banded (10–30 cm)

Very thickly bedded, foliated, or banded (>100 cm)

Interbedding/alternate bedding

Cross bedding/cross lamination

Parallel bedding

Nonparallel bedding

Horizontal bedding

Low angle/oblique bedding

Parallel lamination

Nonparallel lamination

Horizontal lamination

Interlamination

Fining upward

Coarsening upward

Climbing ripple

Asymmetrical/current ripple

Convolute

Flame structure

High angle

Hummocky

Lenticular

Mottles

Nodular

Normal graded

Structureless

Lithologic accessories

Black organic fragments

Gl Glauconite, glauconitic

Mc Micaceous

Nodule/concretion, general

Opaque heavy minerals/dark grains

Pebbles/granules

Py Pyrite

Q Quartz

Sand laminae

Shell fragments (1–3)

Silt lamina

Undefined burrow

Wd Wood fragments

Fossils

Bivalves

Chondrites

Diatoms

Echinoid fragments

Foraminifers, benthic

Foraminifers, larger benthic

Foraminifers, planktonic

Macrophytes, roots

Wd Macrophytes, wood

Mollusks, gastropods

Mollusks, scaphopods

Ophiomorpha

Ostracodes

Planolites

Shell fragments

Shells

Skeletal debris

Taenidium

Teichichnus

Terebellina

Thalassinoides

Unidentified burrows

Zoophycos

Disturbance type

Biscuit

Brecciated

Disturbed

Flow-in

Fractured

Slurry

Soupy

Disturbance intensity

Slight

Moderate

Severe/extreme

Variable or not given

Bioturbation intensity

0	Not determined
1	Barren or no bioturbation
2	
3	
4	
5/x	Abundant bioturbation or homogenous

Figure F5. Ternary diagram to illustrate classification of sediment texture used during Expedition 313 (modified from Shepard, 1954). Symbols in Shepard diagram are the same as in Figure F4. Classification can be adapted to include modifiers (e.g., glauconite) and different grain sizes (e.g., gravel). Sediment with components of clay, silt, and sand (i.e., the center of the triangle) are either muddy sand or sandy mud.
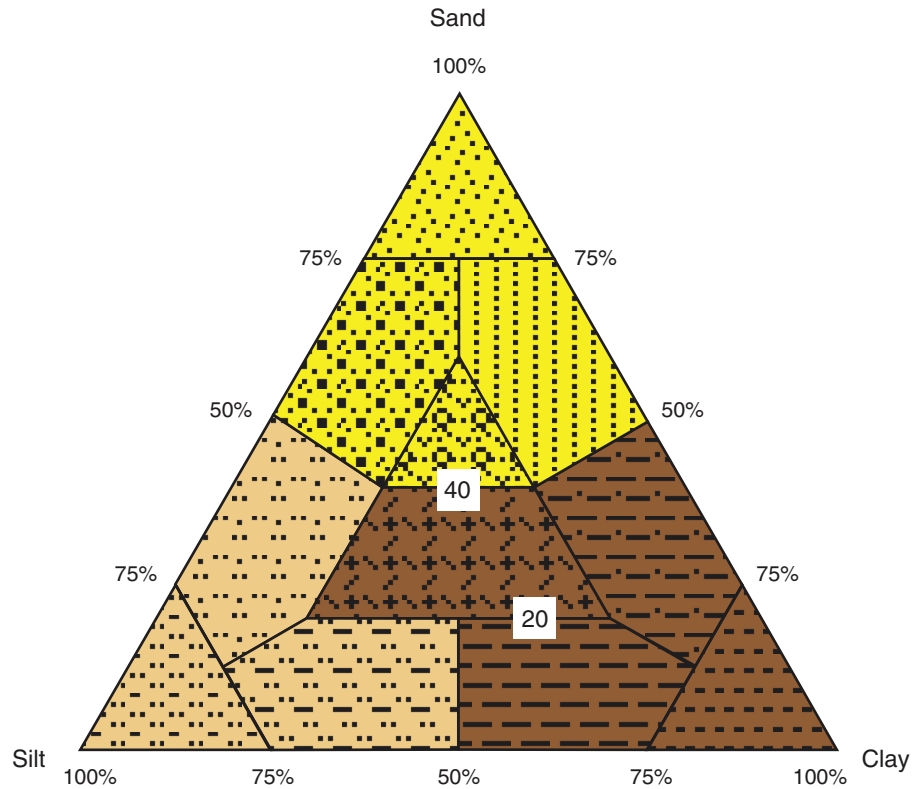
Figure F6. A. Diagram of X-ray CT scan procedure used during Expedition 313. Compilation X-ray CT data for a 1.5 m long core section requires three 50 cm scans starting from the bottom. Between scans 2 and 3, core has to be moved. **B.** Diagram of procedure for orthogonal longitudinal 2-D scans made through core axis used during Expedition 313. Note that for longitudinal scans made in a horizontal plane, artifacts occur because of interference with the underlying table.

A

B
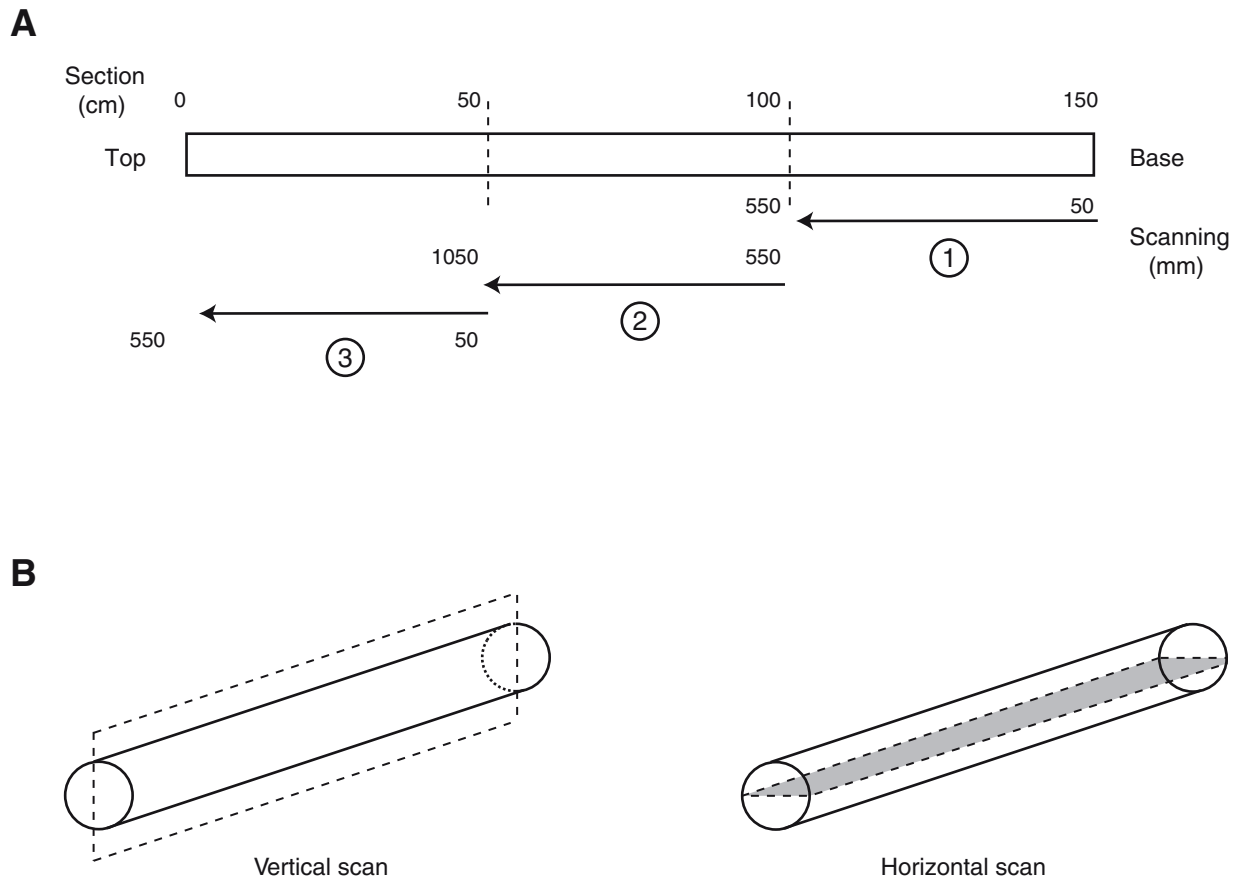
Figure F7. A. X-ray CT image of a 1 mm transverse slice in sedimentary core made during Expedition 313. Different mineral components in sand can be identified, and quantitative estimation of total sediment density is also possible. **B.** 3-D image block (AMIRA software).
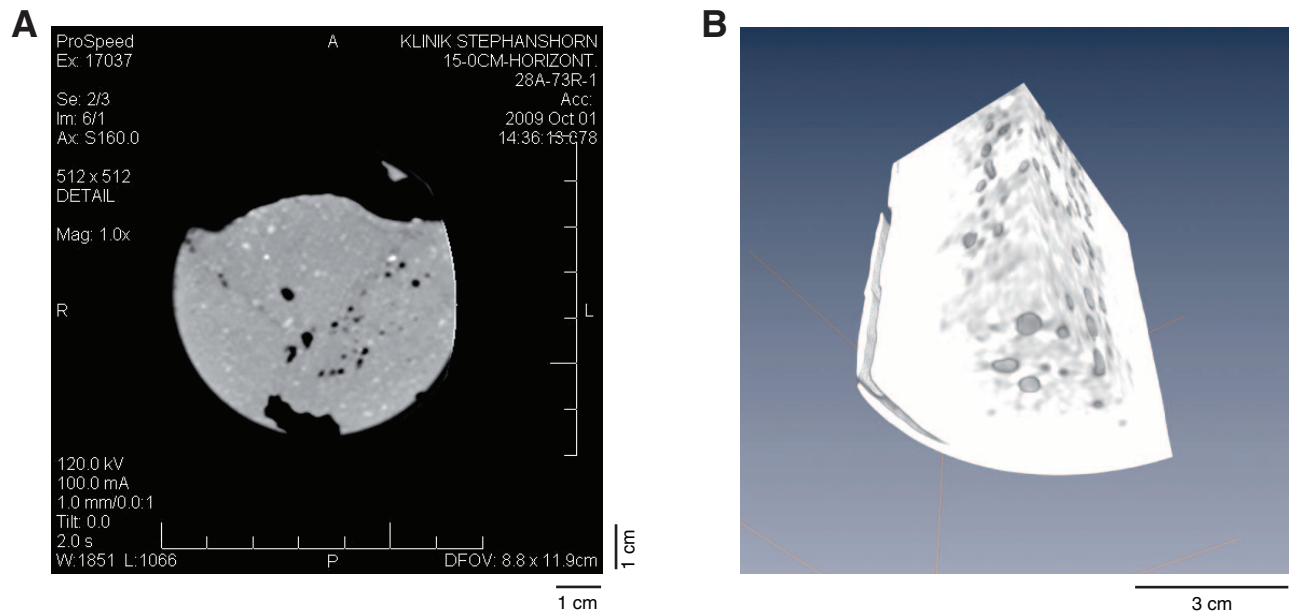
Figure F8. Diagram of different scales of clinoform and clinothem and the nomenclature of key physiographic provinces and points used during Expedition 313. Clinoform scales vary, merging to form "compound clinoforms" depending on the interplay of sediment supply and local sea level change. (Adapted from Helland-Hansen and Hampson, 2009.) **A.** Depositional dip profile of three scales of clinoform. **B.** Intermediate scale, intrashelf clinoforms. This scale was the focus of Expedition 313. **C.** Overview of clinoform and clinothem provinces.
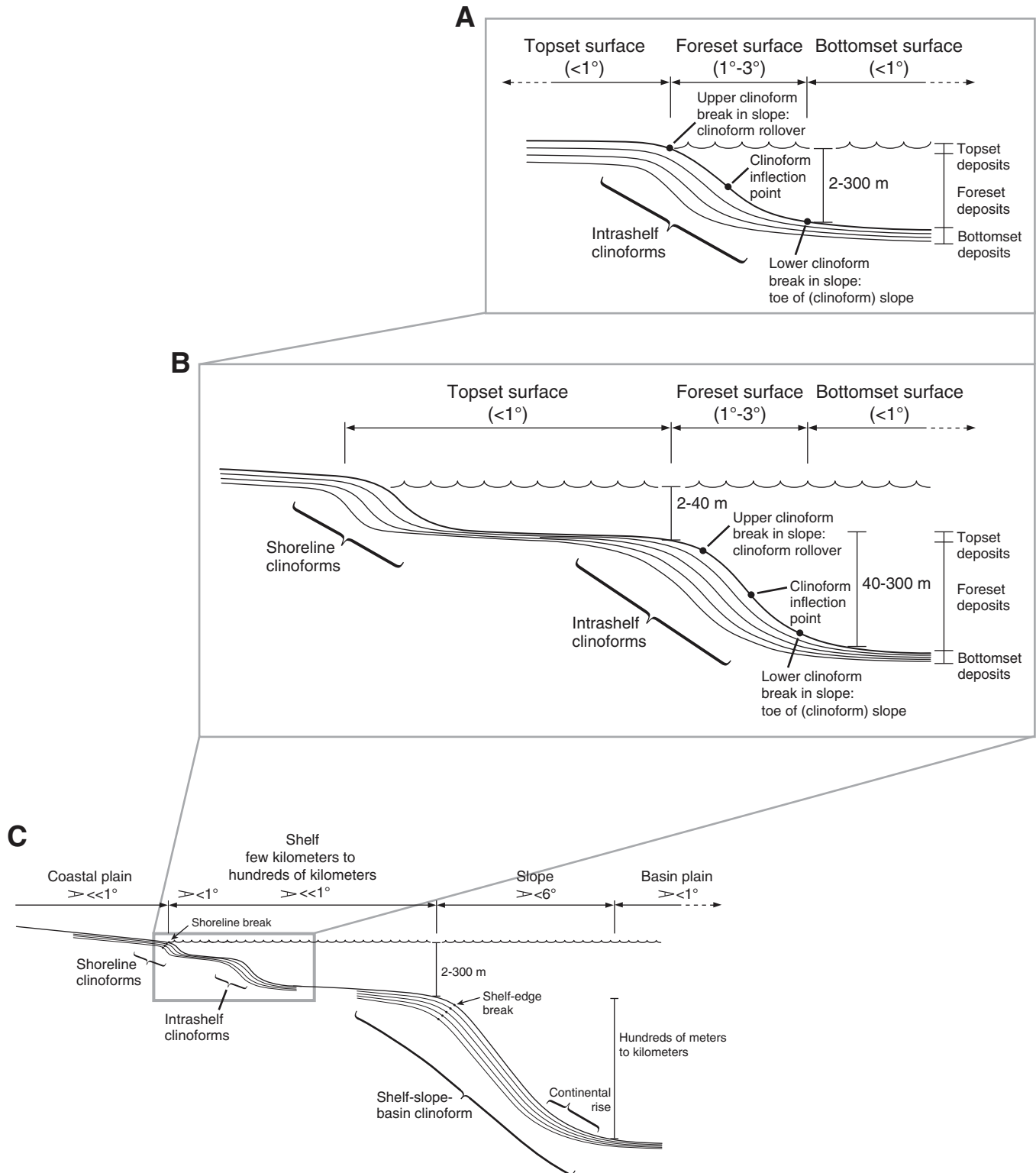
Figure F9. Diagram of terminology for depth zones along a shoreface–offshore transect in a wave-dominated linear clastic sedimentary setting used during Expedition 313. Shoreface, shoreface–offshore transition, and offshore are terms used in this report; terms listed as 1 to 5 represent complementary or alternative schemes (1) based on biofacies or (2–5) drawn from the sedimentology literature. 1 = depth-related biofacies (Van Morkhoven et al., 1986); 2 = Walker and Plint (1992), Howell and Flint (2003); 3 = Browning et al. (2006); 4 = Ando (1990); 5 = Einsele (2000). HCS = hummocky cross stratification, vf-f = very fine–fine. Water depths are indicative and vary between locations (e.g., because of local wave climate and extreme events).
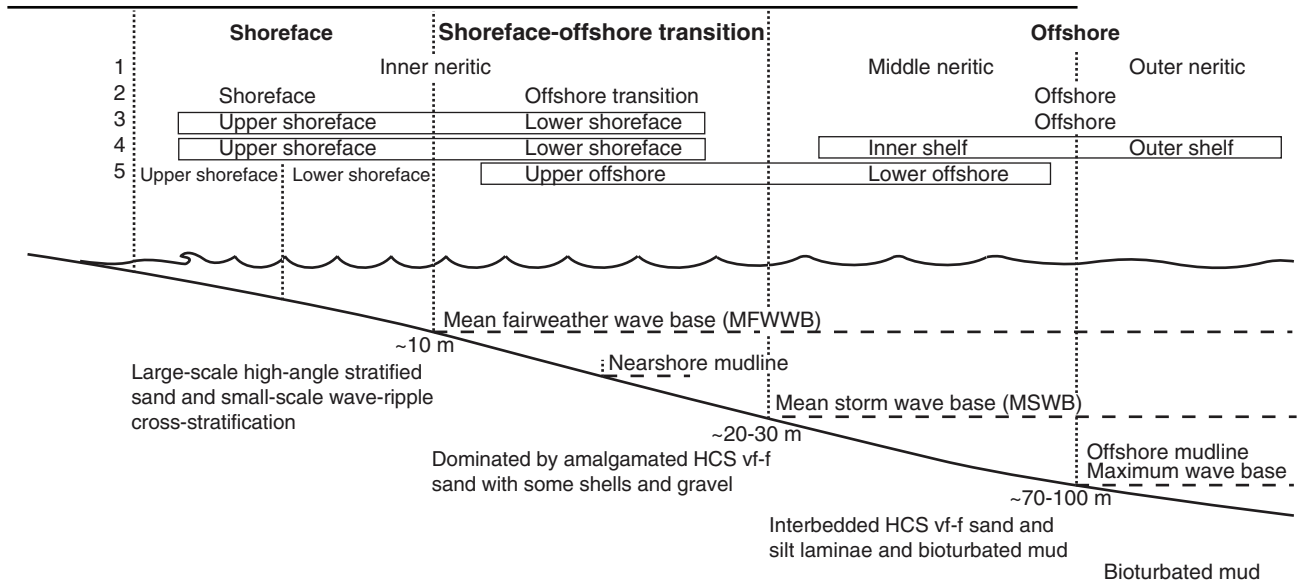
Figure F10. Diagram of main environments of deposition interpreted from facies descriptions used during Expedition 313. Diagram does not indicate along-shoreline variation at a point in time. Diagram shows more storm/wave–dominated coastal systems to the left and more river-dominated coastal systems to the right. Arrows indicate dominant direction and relative magnitude of sediment transport. MFWWB = mean fair-weather wave base, SWWB = storm wave wave base.
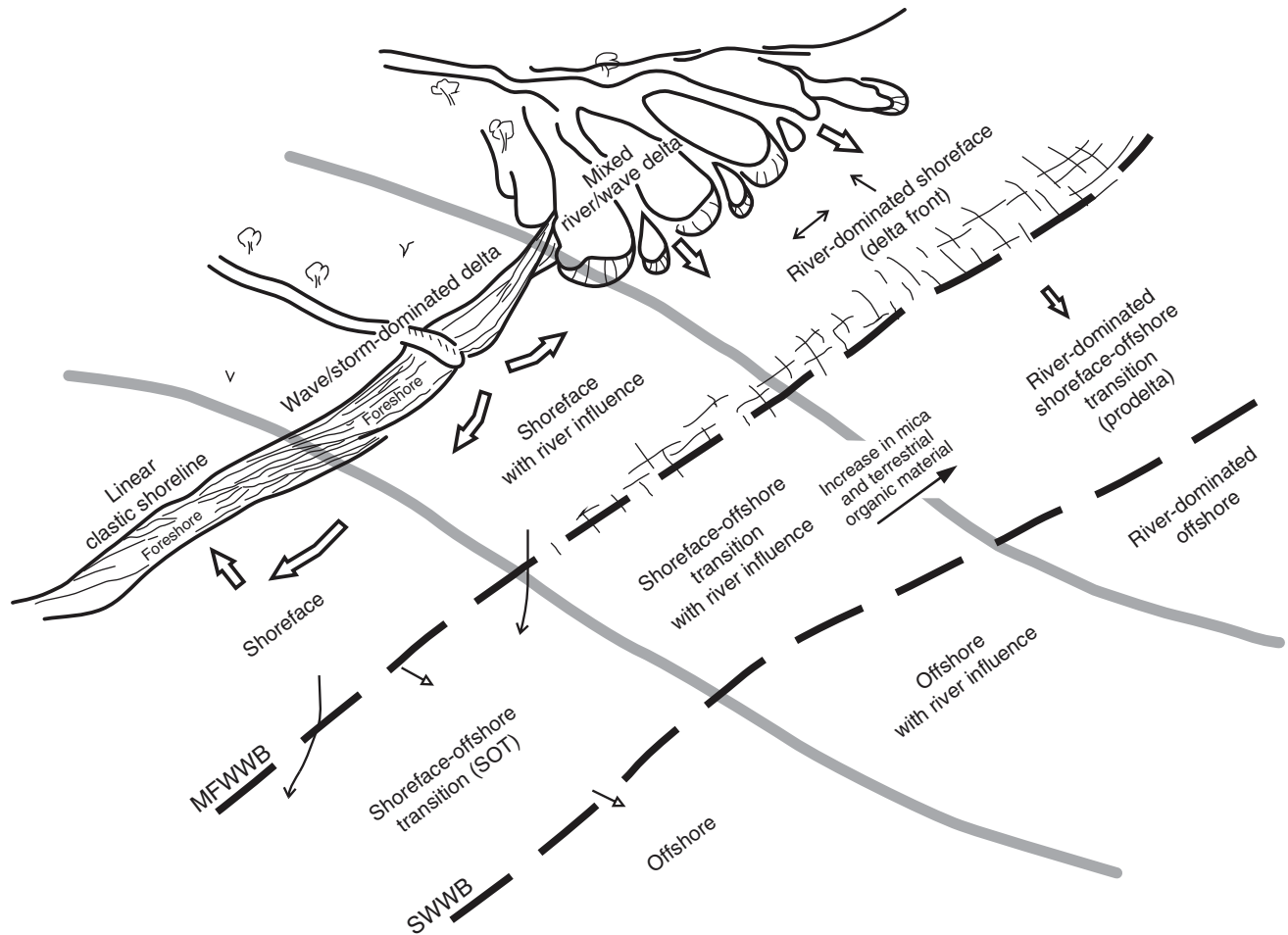
Figure F11. Diagram of preliminary conceptual model used during Expedition 313 to account for the regular occurrence of coarse sand and gravels that are commonly poorly sorted, stratified, and glauconite rich. Multiple channels and/or regressive shorefaces at the rollover erode into and entrain older topset deposits. These sediments are remobilized down the clinoform slope via debris flows and turbidity currents to form apron or coalesced fans at the toe of slope. NJ = New Jersey.
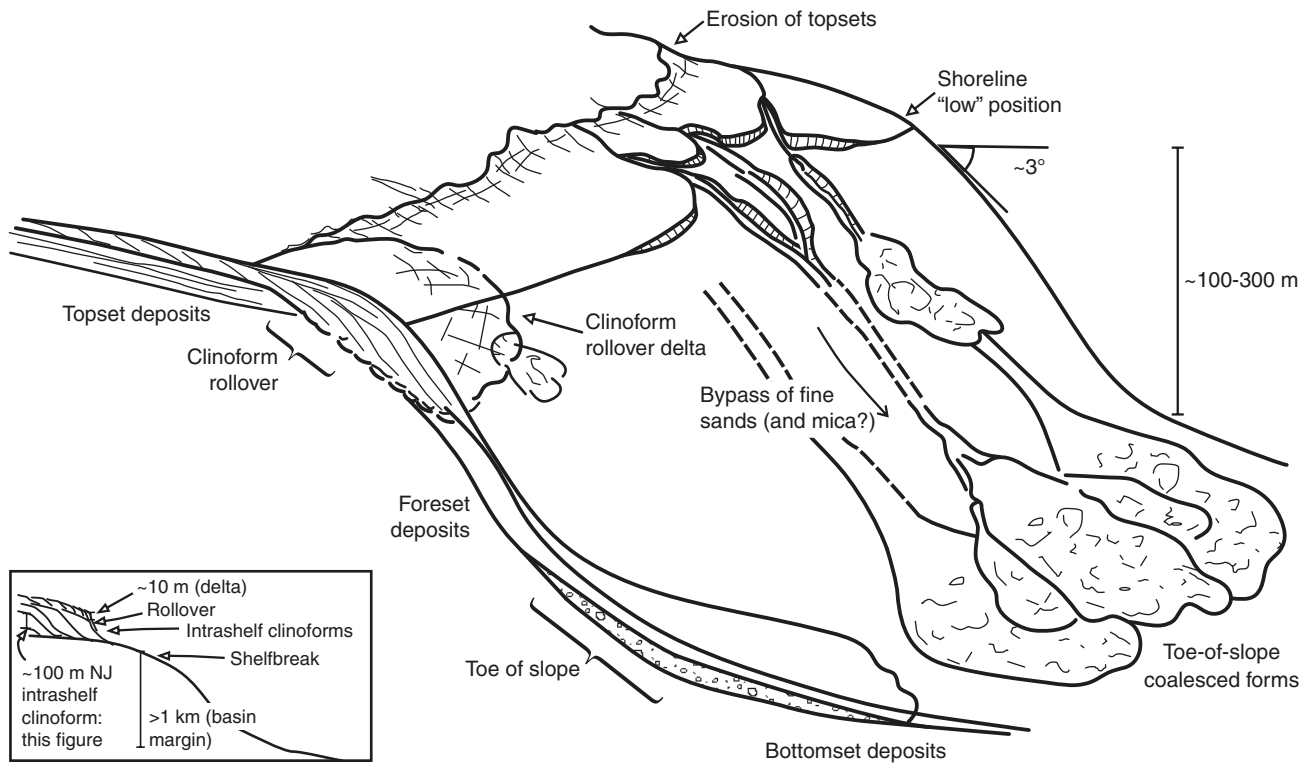
Figure F12. Correlation of geomagnetic polarity timescale (Cande and Kent, 1995), biostratigraphic zonations, and biohorizons used during Expedition 313. Bold text = planktonic foraminifers, plain text = calcareous nannofossils, underlined text = dinocysts. T = top, B = base, Tc = top common, X = abundance crossover. **A.** 10–20 Ma. (**Continued on next page.**)
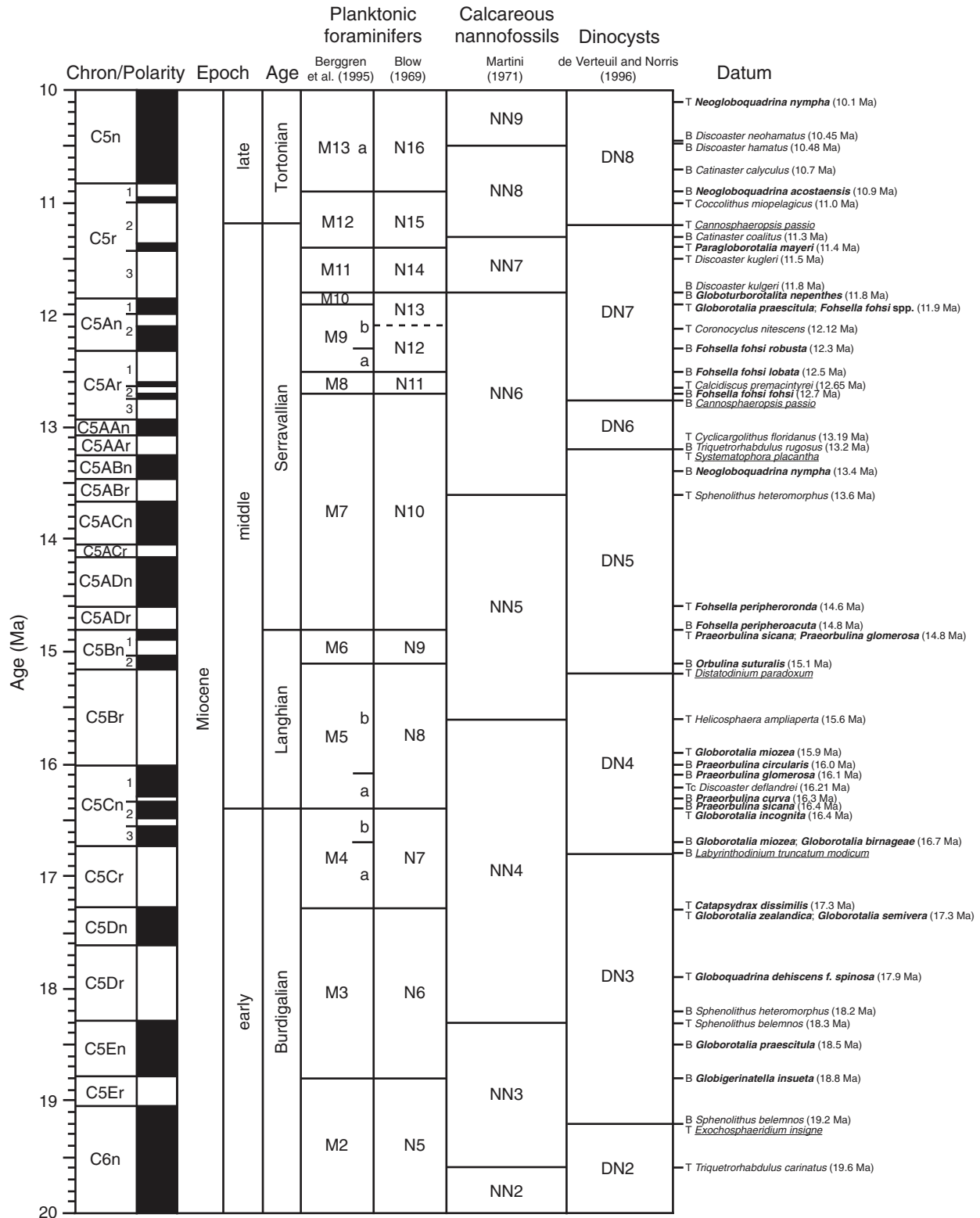
Figure F12 (continued). B. 20–36 Ma. Note that Berggren and Pearson (2005) and Berggren and Miller (1988) were used for the entire Paleogene (23.8–36 Ma), not only for Zones O6 and P22.
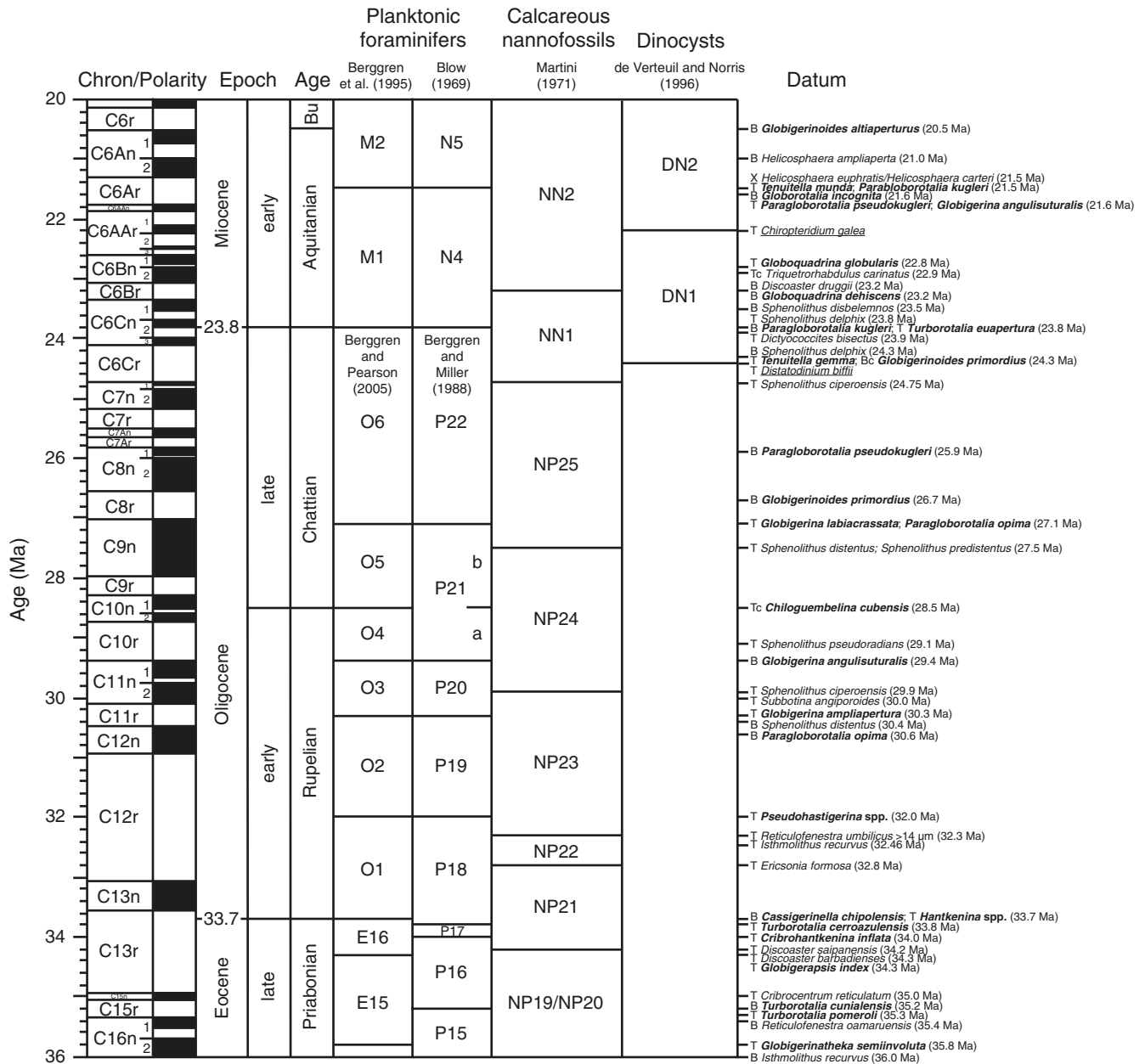
Figure F13. Plots showing reproducibility of MSCL data as assessed by repeat logging a selection of core sections from each site while offshore conducted during Expedition 313. QA/QC = quality assurance/quality control. **A.** Density. **B.** *P*-wave velocity. (**Continued on next page.**)
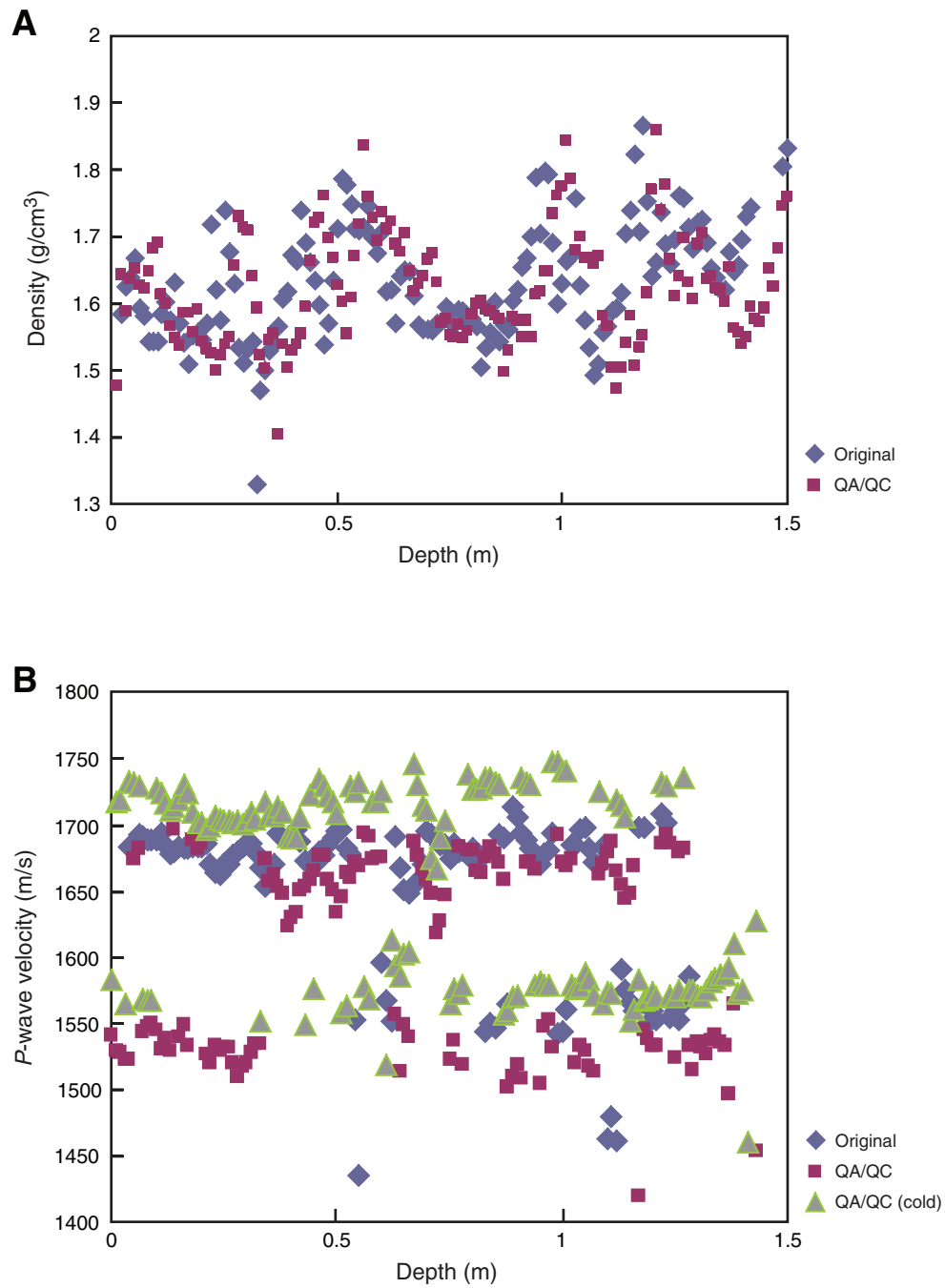
Figure F13 (continued). C. Resistivity. D. Magnetic susceptibility.
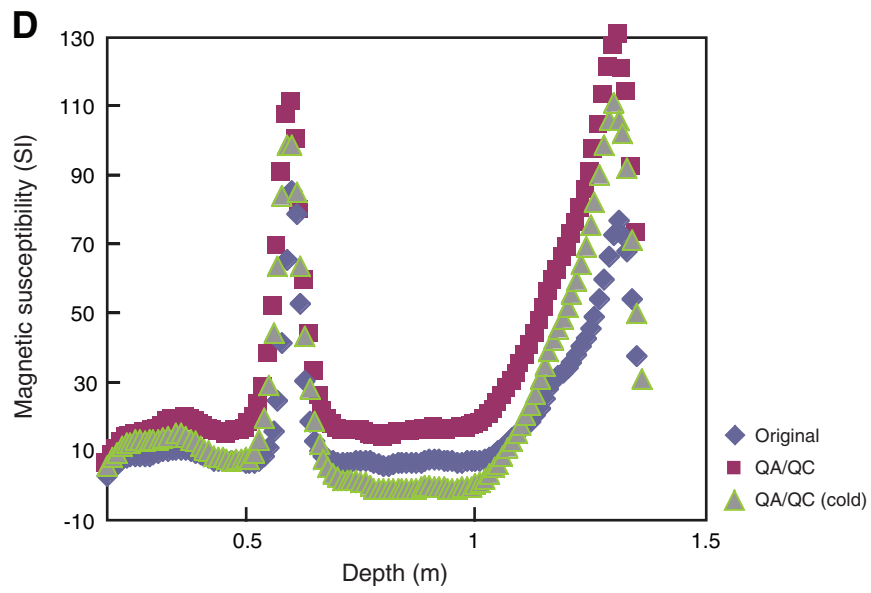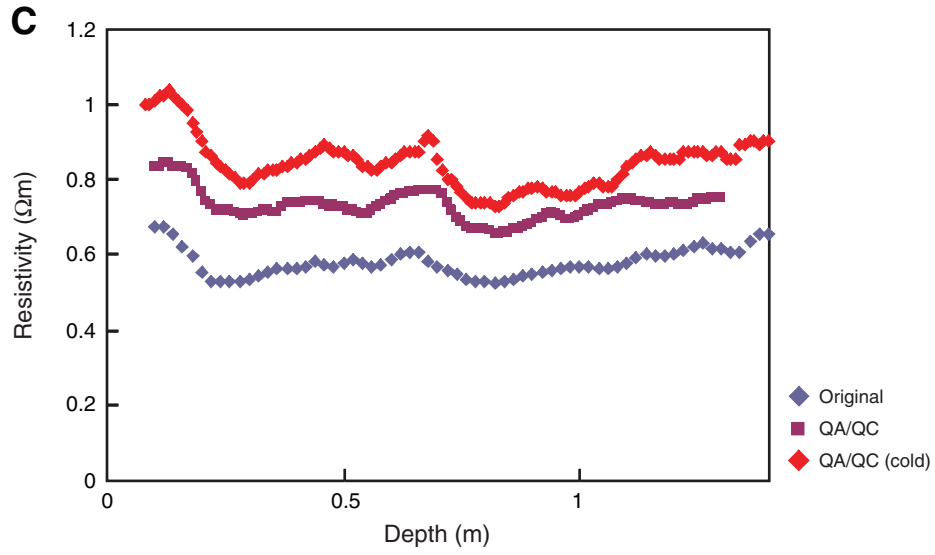
Figure F14. Diagram of coil axes orientation (one for axial and two for transverse moment measurement) of cryogenic SQUID magnetometer at the University of Bremen used during Expedition 313. Orientation of a cube from working-half core lies on the *x*–*z* axes plane.
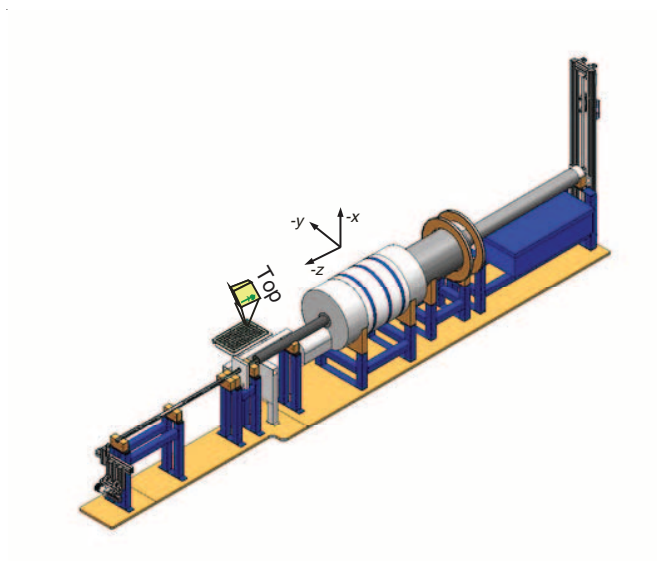
Figure F15. Simplified diagram showing depth setup during logging operations for Expedition 313. WRF = wireline log depth below rig floor.
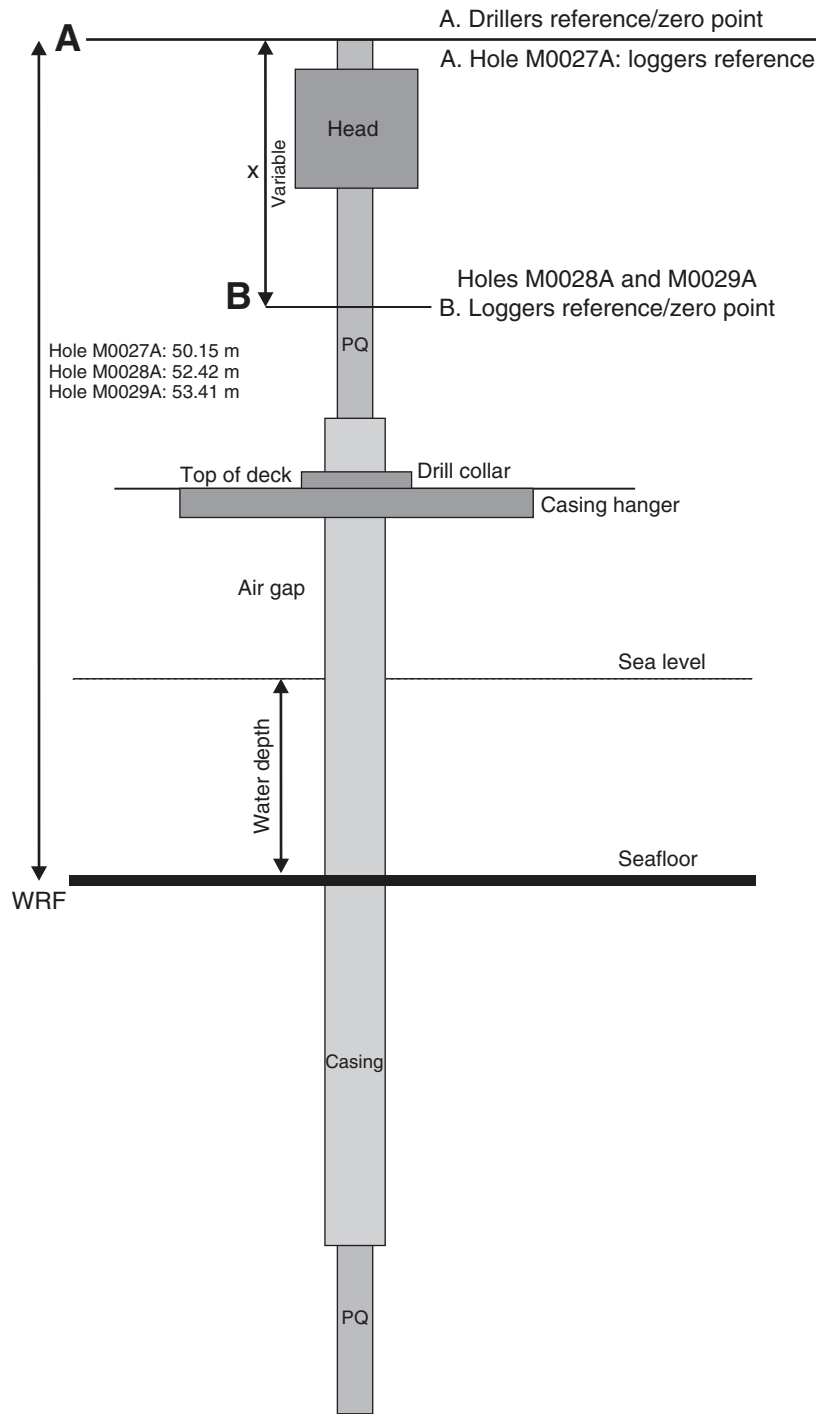
Figure F16. Simplified configuration of vertical seismic profiling measurements used during Expedition 313.
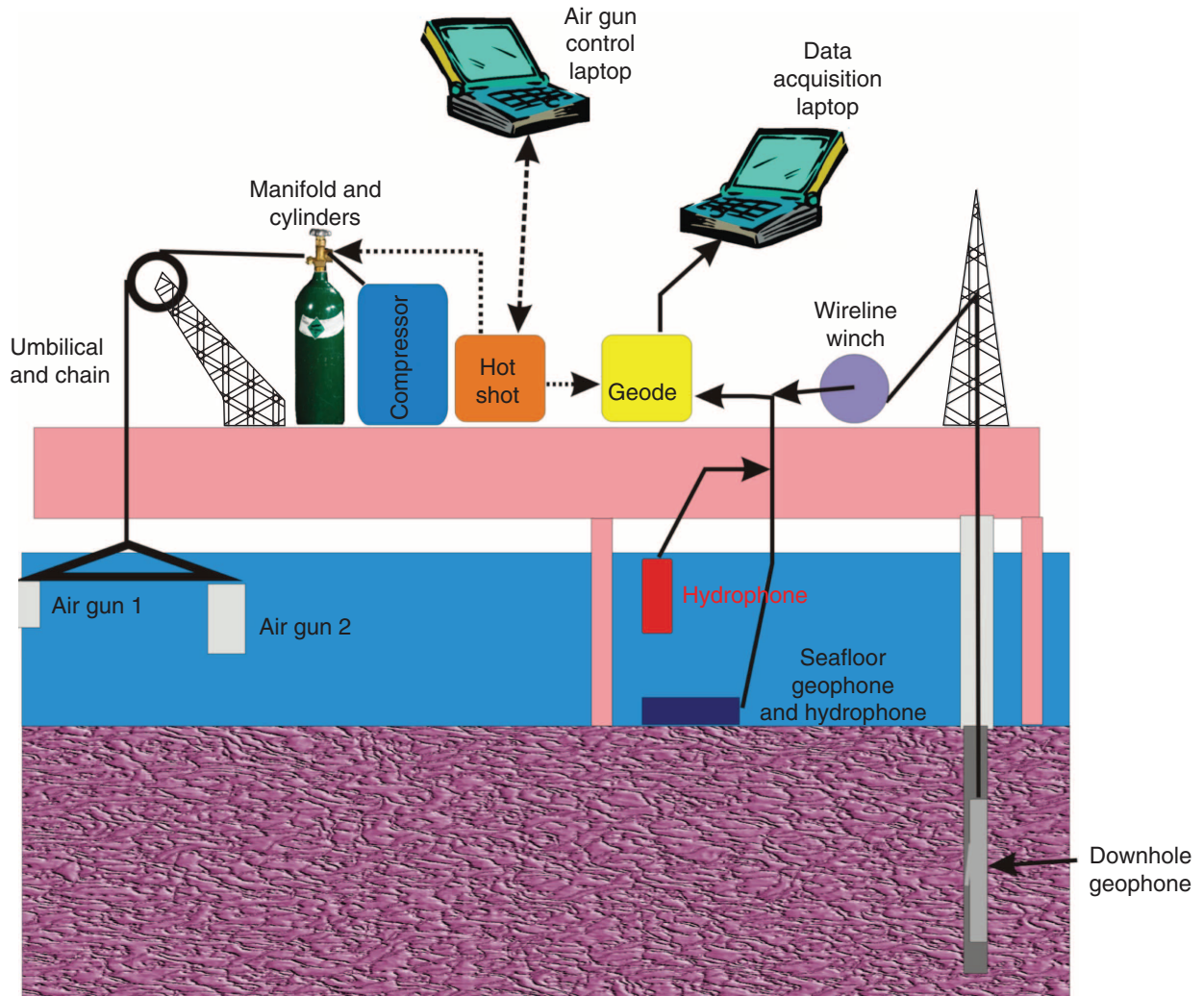
Figure F17. Simplified technical schemes of slimline logging tools used during Expedition 313. ILD = induction electrical conductivity of greater investigation depth, ILM = induction electrical conductivity of medium investigation depth.
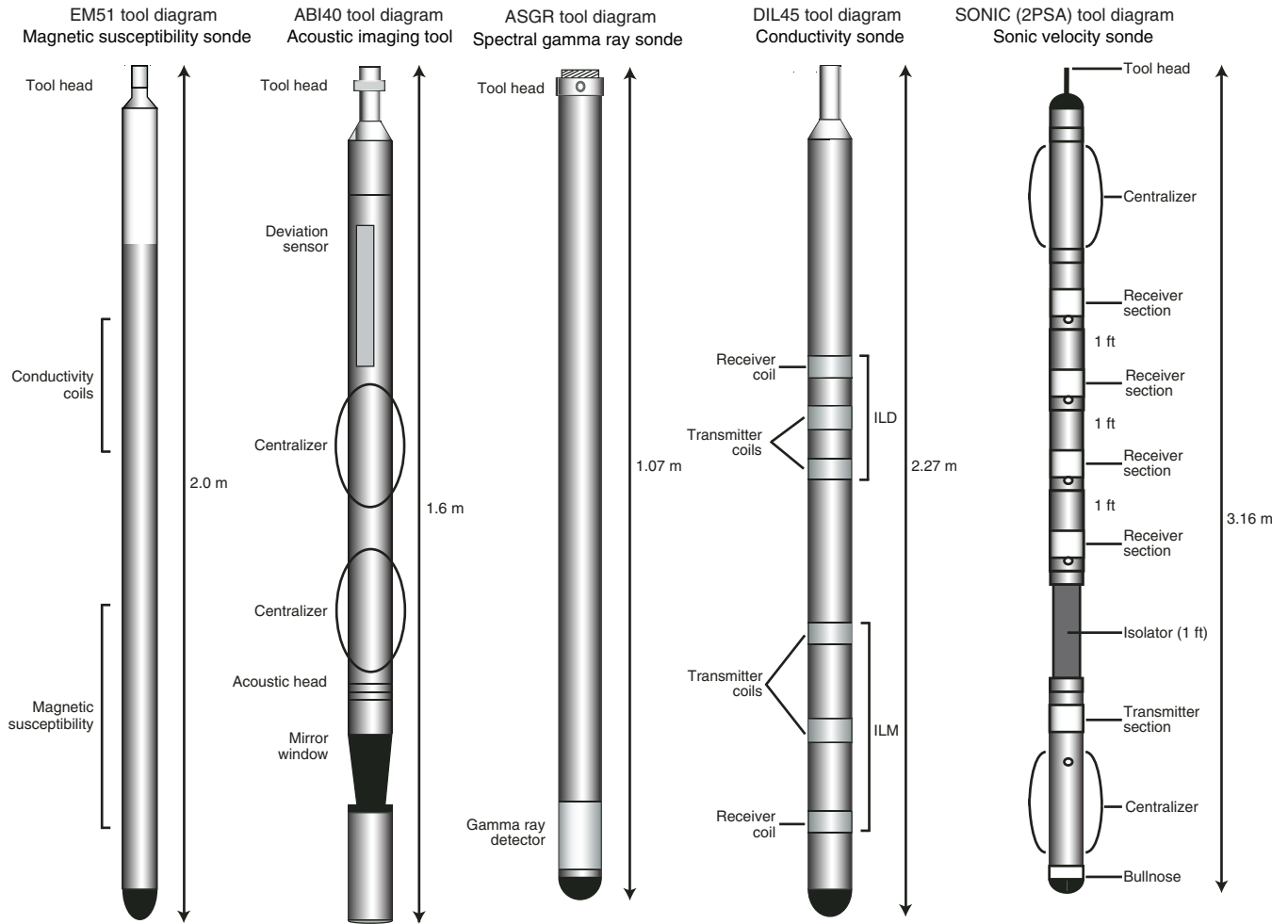
Figure F18. Plots of two-way traveltime (ms) vs. depth (mbsf) derived by different methods and applied at Expedition 313 holes. Vertical seismic profile (VSP) check shot values (red) were measured in each hole (see "Downhole measurements"), but for reasons discussed in text, the alternate method of time-depth relationships derived from MCS stacking velocities was used to estimate the burial depths of seismic reflections. The time-depth relationship applied to all conversions in this volume (see "Stacking Velocity, OSP") is shown in black circles. A small refinement, shown in green circles (see "Stacking Velocity, post-OSP"), is believed to be more reliable. **A.** Hole M0027A. **B.** Hole M0028A. **C.** Hole M0029A.

Table T1. Calcareous nannofossil datum events, Expedition 313. (**See table notes.**) (**Continued on next page.**)

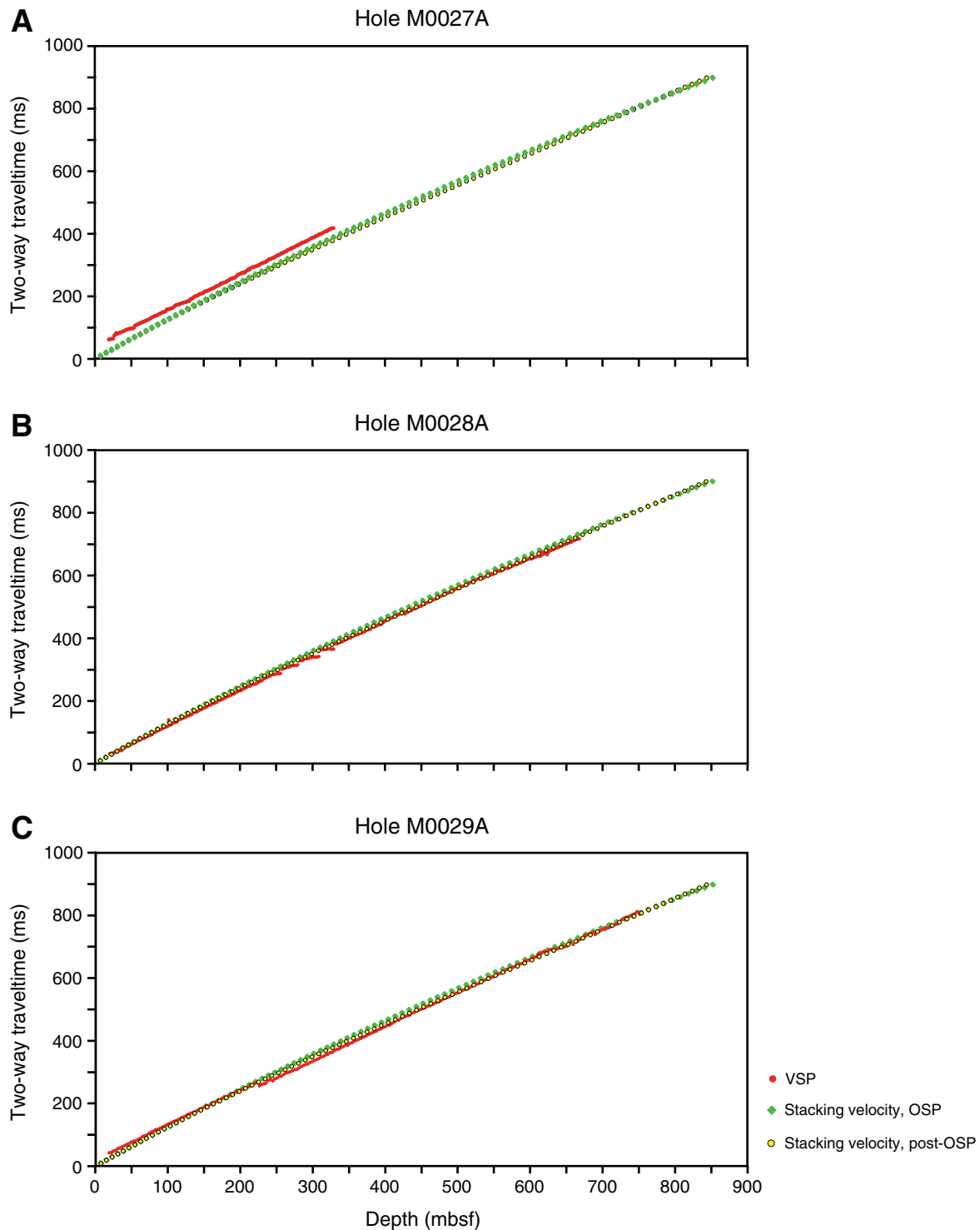| Epoch	Zone (Martini, 1971)	Calcareous nannofossil event	Age (Ma)	Reference
Pleistocene	NN21	T *Helicosphaera inversa*	0.16	Sato et al., 1999
		B *Emiliania huxleyi*	0.25	Sato et al., 1999
	NN20	**T *Pseudoemiliania lacunosa***	0.41	Sato et al., 1999
	NN19	T *Reticulofenestra asanoi*	0.85	Sato et al., 1999
		B *Reticulofenestra asanoi*	1.16	Sato et al., 1999
		T *Gephyrocapsa* (>5.5 µm)	1.21	Sato et al., 1999
		T *Helicosphaera sellii*	1.27	Sato et al., 1999
		B *Gephyrocapsa* (>5.5 µm)	1.45	Sato et al., 1999
		B *Gephyrocapsa oceanica* (>4 µm)	1.65	Sato et al., 1999
		B *Gephyrocapsa caribbeanica* (>4 µm)	1.73	Sato et al., 1999
		T *Discoaster brouweri*	1.97	Sato et al., 1999
Pliocene	NN18	**T *Discoaster pentaradiatus***	2.38	Sato et al., 1999
	NN17	**T *Discoaster surculus***	2.54	Sato et al., 1999
	NN16	T *Discoaster tamalis*	2.74	Sato et al., 1999
		T *Sphenolithus* spp.	3.65	Raffi and Flores, 1995
		T *Reticulofenestra pseudoumbilicus*	3.85	Sato et al., 1999
	NN14/NN15	Bc *Discoaster asymmetricus*	4.13	Raffi et al., 2006
	NN13	T *Amaurolithus* spp.	4.56	Shackleton et al., 1995
		T *Ceratolithus acutus*	5.05	Backman and Raffi, 1997
		X *Ceratolithus acutus/Ceratolithus rugosus*	5.07	Backman and Raffi, 1997
		B *Ceratolithus rugosus*	5.09	Backman and Raffi, 1997
	NN12	T *Triquetrorhabdulus rugosus*	5.23	Backman and Raffi, 1997
		B *Ceratolithus acutus*	5.37	Backman and Raffi, 1997
		B *Ceratolithus atlanticus*	5.40	Backman and Raffi, 1997
		T *Discoaster quinqueramus*	5.60	Berggren et al., 1995
Miocene	NN10/NN11	T *Amaurolithus amplificus*	5.90	Berggren et al., 1995
		B *Amaurolithus amplificus*	6.60	Berggren et al., 1995
		B *Amaurolithus* spp.	7.20	Berggren et al., 1995
		B *Discoaster berggrenii*	8.60	Berggren et al., 1995
		T *Discoaster bollii*	9.10	Berggren et al., 1995
		T *Discoaster hamatus*	9.40	Berggren et al., 1995
	NN9	T *Catinaster calyculus*	9.64	Backman and Raffi, 1997
		T *Catinaster coalitus*	9.70	Backman and Raffi, 1997
		B *Discoaster neohamatus*	10.45	Backman and Raffi, 1997
		B *Discoaster hamatus*	10.48	Backman and Raffi, 1997
	NN8	**B *Catinaster calyculus***	10.70	Berggren et al., 1995
		B *Catinaster coalitus*	11.30	Berggren et al., 1995
	NN7	T *Coccolithus miopelagicus*	11.00	Berggren et al., 1995
		T *Discoaster kugleri*	11.50	Berggren et al., 1995
		B *Discoaster kugleri*	11.80	Berggren et al., 1995
	NN6	T *Coronocyclus nitescens*	12.12	Raffi and Flores, 1995
		T *Calcidiscus premacintyrei*	12.65	Raffi and Flores, 1995
		T *Cyclicargolithus floridanus*	13.19	Raffi and Flores, 1995
		B *Triquetrorhabdulus rugosus*	13.20	Berggren et al., 1995
		T *Sphenolithus heteromorphus*	13.60	Berggren et al., 1995
	NN5	**T *Helicosphaera ampliaperta***	15.60	Berggren et al., 1995
	NN4	Tc *Discoaster deflandrei*	16.21	Raffi and Flores, 1995
		B *Sphenolithus heteromorphus*	18.20	Berggren et al., 1995
		T *Sphenolithus belemnos*	18.30	Berggren et al., 1995
	NN3	B *Sphenolithus belemnos*	19.20	Berggren et al., 1995
		T *Triquetrorhabdulus carinatus*	19.60	*
	NN2	B *Helicosphaera ampliaperta*	21.00	Lourens et al., 2004[†]
		X *Helicosphaera euphratis/Heliocosphaera carteri*	21.50	Lourens et al., 2004[†]
		Tc *Triquetrorhabdulus carinatus*	22.90	[†]
	NN1	**B *Discoaster druggii***	23.20	Berggren et al., 1995
		B *Sphenolithus disbelemnos*	23.50	Shackleton et al., 1999
		T *Sphenolithus delphix*	23.80	Berggren et al., 1995
		T *Dictyococcites bisectus*	23.90	Berggren et al., 1995
		B *Sphenolithus delphix*	24.30	Berggren et al., 1995
		T *Sphenolithus ciperoensis*	24.75	Berggren et al., 1995
Oligocene	NP25	**T *Sphenolithus distentus***	27.50	Berggren et al., 1995
	NP24	T *Sphenolithus predistentus*	27.50	Berggren et al., 1995
		T *Spenolithus pseudoradians*	29.10	Berggren et al., 1995
		B *Sphenolithus ciperoensis*	29.90	Berggren et al., 1995
	NP23	B *Sphenolithus distentus*	30.40	Olafsson and Villa, 1992
		T *Reticulofenestra umbilicus* (>14 µm)	32.30	Berggren et al., 1995

Table T1 (continued).

Epoch	Zone (Martini, 1971)	Calcareous nannofossil event	Age (Ma)	Reference
Oligocene	NP22	T *Isthmolithus recurvus*	32.46	Villa et al., 2008
		T *Ericsonia formosa*	32.80	Berggren et al., 1995
Eocene	NP21	**T *Discoaster saipanensis***	34.20	Berggren et al., 1995
	NP19/NP20	T *Discoaster barbadiensis*	34.30	Berggren et al., 1995
		T *Cribrocentrum reticulatum*	35.00	Berggren et al., 1995
		B *Reticulofenestra oamaruensis*	35.40	Berggren et al., 1995
		B *Isthmolithus recurvus*	36.00	Berggren et al., 1995

Notes: * = age estimate derived through calibration to magnetostratigraphy at ODP Site 1218. † = age converted to Berggren et al. (1995) time-scale. T = top, B = base, Bc = base common, X = abundance crossover, Tc = top common. Bold text = biostratigraphic marker for the base of each zone.

Table T2. Planktonic foraminifer datum events for 10–35 Ma, Expedition 313. (**See table notes.**)

Epoch	Zone	Planktonic foraminifer event	Age (Ma)	Reference
Miocene	M13/N16	T *Neogloboquadrina nympha*	10.1	Berggren et al., 1995
	M13/N16	**B *Neogloboquadrina acostaensis***	10.9	Berggren et al., 1995
	M12/N15	**T *Paragloborotalia mayeri***	11.4	Berggren et al., 1995
	M11/N14	**B *Globoturborotalita nepenthes***	11.8	Berggren et al., 1995
	M10/N13	T *Globorotalia praescitula*	11.9	Berggren et al., 1995
	M10/N13	**T *Fohsella fohsi* spp.**	11.9	Berggren et al., 1995
	M9b	**B *Fohsella fohsi robusta***	12.3	Berggren et al., 1995
	M9a/N12	**B *Fohsella fohsi lobata***	12.5	Berggren et al., 1995
	M8/N11	**B *Fohsella fohsi fohsi***	12.7	Berggren et al., 1995
	M7/N10	B *Neogloboquadrina nympha*	13.4	Berggren et al., 1995
	M7/N10	T *Fohsella peripheroronda*	13.8	Shackleton et al., 1999
	M7/N10	T *Globorotalia archeomenardii*	13.9	Shackleton et al., 1999
	M7/N10	B *Globorotalia praemenardii*	14.2	Shackleton et al., 1999
	M7/N10	**B *Fohsella peripheroacuta***	14.8	Berggren et al., 1995
	M6/N9	T *Praeorbulina sicana*	14.8	Berggren et al., 1995
	M6/N9	T *Praeorbulina glomerosa*	14.8	Berggren et al., 1995
	M6/N9	**B *Orbulina suturalis***	15.1	Berggren et al., 1995
	M5b	T *Globorotalia miozea*	15.9	Berggren et al., 1995
	M5b	B *Praeorbulina circularis*	16.0	Berggren et al., 1995
	M5b	**B *Praeorbulina glomerosa***	16.1	Berggren et al., 1995
	M5a/N8	B *Praeorbulina curva*	16.3	Berggren et al., 1995
	M5a/N8	**B *Praeorbulina sicana***	16.4	Berggren et al., 1995
	M4b	T *Globorotalia incognita*	16.4	Berggren et al., 1995
	M4b	B *Globorotalia miozea*	16.7	Berggren et al., 1995
	M4b	**B *Globorotalia birnageae***	16.7	Berggren et al., 1995
	M4a/N7	**T *Catapsydrax dissimilis***	17.3	Berggren et al., 1995
	M3/N6	T *Globorotalia zealandica*	17.3	Berggren et al., 1995
	M3/N6	T *Globorotalia semivera*	17.3	Berggren et al., 1995
	M3/N6	T *Globoquadrina dehiscens f. spinosa*	17.9	Berggren et al., 1995
	M3/N6	B *Globorotalia praescitula*	18.5	Berggren et al., 1995
	M3/N6	**B *Globigerinatella insueta***	18.8	Berggren et al., 1995
	M2/N5	B *Globigerinoides altiaperturus*	20.5	Berggren et al., 1995
	M2/N5	T *Tenuitella munda*	21.5	Berggren et al., 1995
	M2/N5	**T *Paragloborotalia kugleri***	21.5	Berggren et al., 1995
	M1b	B *Globorotalia incognita*	21.6	Berggren et al., 1995
	M1b	T *Paragloborotalia pseudokugleri*	21.6	Berggren et al., 1995
	M1b	T *Globigerina angulisuturalis*	21.6	Berggren et al., 1995
	M1b	T *Globoquadrina globularis*	22.8	Berggren et al., 1995
	M1b	**B *Globoquadrina dehiscens***	23.2	Berggren et al., 1995
	M1a/N4	**B *Paragloborotalia kugleri***	23.8	Berggren et al., 1995
Oligocene	O6/P22	T *Turborotalia euapertura*	23.8	Berggren et al., 1995
	O6/P22	T *Tenuitella gemma*	24.3	Berggren et al., 1995
	O6/P22	Bc *Globigerinoides primordius*	24.3	Berggren et al., 1995
	O6/P22	B *Paragloborotalia pseudokugleri*	25.9	Berggren et al., 1995
	O6/P22	B *Globigerinoides primordius*	26.7	Berggren et al., 1995
	O6/P22	T *Globigerina labiacrassata*	27.1	Berggren et al., 1995
	O6/P22	**T *Paragloborotalia opima***	27.1	Berggren et al., 1995
	O5/P21b	**Tc *Chiloguembelina cubensis***	28.5	Berggren et al., 1995
	O4/P21a	**B *Globigerina angulisuturalis***	29.4	Berggren et al., 1995
	O3/P20	T *Subbotina angiporoides*	30.0	Berggren et al., 1995
	O3/P20	**T *Globigerina ampliapertura***	30.3	Berggren et al., 1995
	O2/P19	B *Paragloborotalia opima*	30.6	Berggren et al., 1995
	O2/P19	**T *Pseudohastigerina* spp.**	32.0	Berggren et al., 1995
	O1 / P18	B *Cassigerinella chipolensis*	33.7	Berggren et al., 1995
	O1 / P18	**T *Hantkenina* spp.**	33.7	Berggren et al., 1995
Eocene	E16 / P17	**T *Turborotalia cerroazulensis***	33.8	Berggren et al., 1995
	E16 / P17	**T *Cribrohantkenina inflata***	34.0	Berggren et al., 1995
	P16	**T *Globigerapsis index***	34.3	Berggren et al., 1995
	P16	**B *Turborotalia cunialensis***	35.2	Berggren et al., 1995
	E15 / P15	T *Turborotalia pomeroli*	35.3	Berggren et al., 1995
	E15 / P15	**T *Globigerinatheka semiinvoluta***	35.8	Berggren et al., 1995

Notes: T = top, B = base, Bc = base common, Tc = top common. Bold text = biostratigraphic marker for the base of each zone. Planktonic foraminifer M zones from Berggren et al. (1995), E and O zones from Berggren and Pearson (2005), N zones from Blow (1969), and P zones from Berggren and Miller (1988).

Table T3. Multisensor core logger sensor summary, Expedition 313. (**See table notes.**)

Sensor	Calibration pieces used		Acceptable departure from full calibration values	Sampling interval (cm)	Spatial resolution (cm)
	Full calibration	Calibration check			
Gamma density	Stepped Al/H$_2$O (6, 5, 4, 3, 2, and 0 cm Al)	Distilled water	±100 cps	1	1
P-wave velocity	Distilled water	Distilled water	±1 µs	1	1
Noncontact resistivity	Saline fluids (35, 17.5, 8.75, 3.5, 1.75, and 0.35 g/L)	3.5 g/L saline fluid	±10 mV	1	~2–3 cm
Magnetic susceptibility	Impregnated resin	Impregnated resin	±5 SI	1	~2–3 cm 80 cm loop ~3–5 cm 120 cm loop

Notes: Sampling interval of 2 cm was selected per certain intervals. Spatial resolution given is that of the machine in the set-up used, not necessarily the maximum achievable resolution.

Table T4. Reproducibility of MSCL data, Holes M0027A, M0028A, and M0029A. (**See table note.**)

Hole	Number of cores in analysis	Mean percent difference between original value and repeated value			
		Gamma density	*P*-wave velocity	Electrical resistivity	Magnetic susceptibility
M0027A	6	±1.7	±16	±19	±14
M0028A	7	±2.4	±9.6	±39	±23
M0029A	7	±3.7	±10	±15	±116[*]

Note: [*] = value includes cores with different loops and cores measured cold and thus is not accurate reflection of deviation during normal operation.

Table T5. Summary of quality assurance/quality control (QA/QC) on moisture and density data, Expedition 313.

QA/QC sample	Mean percent difference from original value to repeated value or from Sample 1 to Sample 2			
	Wet bulk density	Dry bulk density	Grain density	Porosity
Same sample, different day	2.27	4.91	–0.57	–8.09
Different sample, same day	4.08	7.50	2.26	–6.33

Table T6. Summary of slimline probes, Expedition 313.

Acronym	Slimline tool	Manufacturer	Recording device	Software	Downhole measurement spacing interval (m)
ASGR	Spectral natural gamma probe	ANTARES Datensysteme GmbH	ALT A-BOX	ALTLogger	0.1
DIL45	Induction resistivity probe	Advanced Logging Technologies Ltd.	ALT A-BOX	ALTLogger	0.05
EM51	Magnetic susceptibility probe	Geovista Intelligent Borehole Logging Systems	ALT A-BOX	ALTLogger	0.05
ABI40	Acoustic borehole televiewer	Advanced Logging Technologies Ltd.	ALT A-BOX	ALTLogger	0.002–0.004
2PSA	Full waveform sonic probe	Mount Sopris Instrument Company, Inc.	MSI MGX II	MSLog	0.1

Table T7. Summary of intervals and tools logged, Holes M0027A, M0028A, and M0029A. (**See table notes.**)

Slimline tools	Logged intervals (m WSF)		
	Hole M0027A	Hole M0028A	Hole M0029A
ASGRcgs	0.00–603.37	0.00–670.20	0.00–757.31
ASGR	188.13–337.43	—	322.21–348.02
	409.96–620.76	—	—
DIL45	193.23–343.08	395.30–648.50	340.07–723.87
	418.76–623.56	—	—
EM51	192.93–623.83	425.40–657.00	403.66–729.27
ABI40	194.25–328.14	396.03–429.16	483.20–656.53
	419.94–575.29	426.30–637.97	—
2PSA	191.97–327.27	—	404.56–491.05
	417.67–621.67	—	482.51–719.93

Notes: — = tool not used. See Table **T6** for descriptions of slimline tools.

Table T8. Summary calendar of vertical seismic profile measurements, Holes M0027A, M0028A, and M0029A. (**See table notes.**)

Hole	Date (2009)	Depth (m WSF)		Spacing (m)	Open hole survey (m WSF)	Through-pipe survey (m WSF)
		Start	End			
M0027A	21 May	328.72	0.45	0.91	204–329	0–204
M0028A	16 Jun	667.94	395.45	1.83	—	PQ: 0–404
						HQ: 0–668
	17 Jun	656.36	402.15	1.83	425–656	PQ: 0–404
						HQ: 0–425
	18 Jun	431.53	20.05	1.83	404–432	PQ: 0–404
M0029A	11 Jul	753.42	207.83	3.05	—	0–753
	14 Jul	226.12	12.76	3.05	—	0–226

Notes: — = tool not used. PQ = PQ diameter borehole, HQ = HQ diameter borehole.

Table T9. Vertical seismic profile sensors recorded and corresponding channel, Holes M0027A, M0028A, and M0029A. (**See table notes.**)

	Channel							
Hole	1	5	6	7	8	9	10	12
M0027A	Downhole geo V	Seafloor geo H1	Seafloor geo V	Seafloor geo H2	Seafloor hydro	Floating hydro	20 in^3 air gun	40 in^3 air gun
M0028A	Downhole geo V	Seafloor geo H1	Seafloor geo V	Seafloor geo H2	Seafloor hydro	Floating hydro	—	—
M0029A	Downhole geo V	Seafloor geo H1	Seafloor geo V	Seafloor geo H2	Seafloor hydro	—	Floating hydro	—

Notes: Geo = geophone, hydro = hydrophone. — = sensors not used.

Table T10. Evolution of seismic reflector nomenclature, Expedition 313. (**See table notes.**)

EPR/Rutgers Seismic Workshop, 1990 (unpublished)	Offshore seismics (Greenlee et al., 1992)	Offshore Leg 150 (Mountain et al., 1994)	Onshore Leg 150X (Miller et al., 1997)	Offshore seismics (Monteverde et al., 2008)	Onshore equivalents to offshore (Monteverde, 2008)	Sampled during Expedition 313
Tuscan	Tuscan	m1				m1*
Orange		m1.5				
Yellow-2	Yellow-2	m2	Kw-Ch			m2*
Blue	Blue	m3	Kw3			
Pink-2/Red-2	Pink-2/Red-2	m4				m4*
						m4.1[†]
						m4.2[†]
						m4.3[†]
						m4.4[†]
						m4.5[†]
Green	Green	m5	Kw2b	Green: m5	Kw2c	m5
Ochre		m5.2	Kw2a	Orange: m5.2	Kw2b	m5.2
				Red: m5.3	Kw2a	m5.3
						m5.32
						m5.33
						m5.34
Sand		m5.4	Kw1b	Yellow: m5.4	Kw2a	m5.4
				Pink: m5.45	Kw1c	m5.45
				Light blue: m5.47	Kw1b	m5.47
				Green: m5.5	Kw1b	m5.5
True blue		m5.6	Kw1a	Dark blue: 5.6	Kw1a3	m5.6
				Red: m5.7	Kw1a2	m5.7
				Brown: m5.8	Kw1a1	m5.8
Pink-3		m6	Kw0	Purple: m6	Kw0	m6
						o.5
Green-2		o1				o1
Yellow-3		e1				
Red-3		e2				

Notes: * = reflectors sampled and dated elsewhere, traced to Expedition 313 holes with difficulty, but sampled only in spot-cored intervals. † = reflectors sampled and dated during Expedition 313 for the first time but not yet rigorously mapped across the available seismic grid to determine the type of stratigraphic surface based on geometry. Columns labeled by the reference that either generated the reflector name or carried it forward from previous work are arranged from earliest naming on left to the most recent Expedition 313 designations on the right. The stratigraphically oldest reflectors are at the bottom; youngest are at the top.

Table T11. Sr isotope values and ages for all samples analyzed prior to the OSP, Expedition 313. (**See table notes.**) (**Continued on next page.**)

Core, section, interval (cm)	Sample depth (m)	Laboratory number	Sr value	Internal (machine) precision	Age (Ma)	McArthur et al. (2001) Sr ratio	Age
313-M0027A-							
1H-1, 144–150	1.44	1838	0.709115	0.000004	1.4	0.709120	1.3
6H-1, 145–150	12.99	1836	0.709159	0.000006	0.5	0.709164	0.4
6H-1, 145–150	12.99	1932	0.709185	0.000005	−0.1	0.709190	NA
9H-CC, 0–5	19.54	1929	0.709144	0.000006	0.8	0.709149	0.8
15H-CC	28.04	1812	0.709125	0.000005	1.2	0.709130	1.1
15H-CC	28.04	1920	0.709113	0.000006	1.5	0.709118	1.3
70X-CC, 0–3	209.41	1841	0.708819	0.000006	13.7	0.708824	12.6
73X-CC, 0–3	213.15	1991	0.708821	0.000005	13.6	0.708826	12.5
81R-1, 103–108	229.44	1809	0.708750	0.000008	16.0	0.708755	15.1
81R-1, 103–108	229.44	1931	0.708763	0.000004	15.8	0.708768	15.3
89R-CC, 0–2	255.90	1842	0.708727	0.000006	16.3	0.708732	15.8
91R-CC, 9–10	262.04	1845	0.708685	0.000006	17.0	0.708690	16.5
91R-CC, 9–10	262.04	1988	0.708452	0.000005	20.4	0.708457	19.7
95R-1, 139–143	272.50	1843	0.708665	0.000005	17.2	0.708670	16.9
101R-3, 34–38	292.75	1844	0.708625	0.000006	17.8	0.708630	17.5
105R-CC, 0–11	305.04	1982	0.708588	0.000006	18.4	0.708593	18.0
105R-CC, 0–11	305.04	2025	0.708640	0.000005	17.6	0.708645	17.3
149R-CC, 11–13	426.71	1897	0.708447	0.000008	20.4	0.708452	19.8
151R-1, 155–160	431.26	1808	0.708413	0.000004	20.9	0.708418	20.4
151R-1, 155–160	431.26	1987	0.708416	0.000007	20.9	0.708421	20.3
154R-2, 72–77	441.08	2053	0.708441	0.000015	20.5	0.708446	19.9
161R-CC, 8–10	463.61	1895	0.708401	0.000006	21.1	0.708406	20.6
168R-1, base	482.54	1813	0.708398	0.000005	21.2	0.708403	20.6
168R-1, base	482.54	1927	0.708412	0.000006	20.9	0.708417	20.4
183R-CC, 6–8	518.50	1983	0.708187	0.000006	25.3	0.708192	24.2
192R-2, 147–148	542.48	1850	0.708054	0.000006	28.2	0.708059	28.1
195R-2, 9–11	550.25	1848	0.708031	0.000007	28.8	0.708036	28.6
200R-3, 13–15	560.94	1847	0.708014	0.000006	29.3	0.708019	29.0
201R-CC, 13–14	564.21	1985	0.708023	0.000006	29.0	0.708028	28.8
202R-CC, 13–15	567.38	1851	0.708073	0.000005	27.7	0.708078	27.5
203R-CC, 3–5	570.23	1986	0.708030	0.000006	28.8	0.708035	28.6
205R-CC, 0–3	576.16	1849	0.708053	0.000006	28.2	0.708058	28.1
206R-3, 9–11	579.20	1928	0.708027	0.000004	28.9	0.708032	28.7
208R-2, 139–141	585.10	1896	0.708026	0.000006	28.9	0.708031	28.7
210R-CC, 0–3	591.32	1893	0.708011	0.000004	29.3	0.708016	29.1
211R-3, 0–2	594.36	1811	0.707974	0.000007	30.3	0.707979	30.1
219R-3, 24–28	619.00	1846	0.708011	0.000004	29.3	0.708016	29.1
223R-3, 18–20	628.09	1894	0.707816	0.000005	Old	0.707821	33.7
313-M0028A-							
10R-3, 0–29	250.73	1995	0.708810	0.000005	14.0	0.708815	13.0
11R-CC, 0–12	254.18	2031	0.708002	0.000007	29.6	0.708007	29.3
16R-2, 110–115	265.58	2023	0.708767	0.000006	15.8	0.708772	15.2
27R-1, 145–150	291.62	1996	0.708785	0.000009	15.5	0.708790	14.8
29R-CC, 14–16	299.72	2017	0.708746	0.000005	16.1	0.708751	15.5
34R-CC, 0–2	311.43	2022	0.708802	0.000005	14.3	0.708807	13.4
38R-CC, 0–2	323.92	2015	0.708699	0.000006	16.7	0.708704	16.3
45R-1, 145–150	323.67	1998	0.708725	0.000004	16.4	0.708730	15.8
54R-CC, 11–14	352.95	1995	0.708706	0.000004	16.6	0.708711	16.1
66R-CC, 0–2	389.34	2024	0.709130	0.000014	1.1	0.709135	1.1
70R-CC, 9–11	397.89	2021	0.710403	0.000008	−26.2	0.710408	NA
82R-1, 149–154	425.12	1993	0.708661	0.000005	17.3	0.708666	16.9
94R-CC, 0–2	464.10	2020	0.708610	0.000006	18.0	0.708615	17.7
100R-CC, 6–8	482.53	1997	0.708559	0.000011	18.8	0.708564	18.3
102R-CC, 0–2	487.68	2013	0.708596	0.000004	18.3	0.708601	17.9
107R-CC, 0–3	503.79	2014	0.708574	0.000004	18.6	0.708579	18.1
170R-CC, 6–8	668.63	2016	0.708427	0.000004	20.7	0.708432	20.1
313-M0029A-							
53R-CC, 11–14	292.28	1918	0.708805	0.000004	14.2	0.708810	13.2
56R-CC, 15–17	295.49	1913	0.708814	0.000005	13.8	0.708819	12.8
64R-CC, 0–2	322.20	1916	0.708829	0.000006	12.4	0.708834	12.1
67R-CC, 0–2	331.84	1914	0.708857	0.000011	11.6	0.708862	10.8
68R-1, 145–150	333.41	1948	0.708838	0.000006	12.2	0.708843	11.6
74R-2, 84–86	352.60	1915	0.708778	0.000006	15.6	0.708783	15.0
78R-CC, 0–3	362.50	1908	0.708828	0.000005	13.3	0.708833	12.2

Table T11 (continued).

Core, section, interval (cm)	Sample depth (m)	Laboratory number	Sr value	Internal (machine) precision	Age (Ma)	McArthur et al. (2001)	
						Sr ratio	Age
78R-1, 148–153	360.89	1917	0.708831	0.000006	12.4	0.708836	12.0
81R-CC, 0–2	371.83	2026	0.708794	0.000004	14.6	0.708799	14.4
81R-CC, 0–2	371.83	1909	0.708801	0.000007	14.3	0.708806	13.5
82R-CC, 13–15	374.31	1910	0.708783	0.000006	15.5	0.708788	14.8
94R-2, 149–151	411.20	1905	0.708794	0.000006	14.6	0.708799	14.4
100R-CC, 32–24	429.83	2030	0.708721	0.000007	16.4	0.708726	15.9
102R-3, 13–15	435.74	1906	0.708754	0.000006	15.9	0.708759	15.4
104R-CC, 0–4	439.85	1907	0.708753	0.000004	16.0	0.708758	15.4
108R-CC, 0–5	451.25	1923	0.708787	0.000005	15.5	0.708792	14.7
109R-CC, 0–3	453.74	1919	0.708798	0.000006	14.4	0.708803	13.8
110R-CC, 0–2	455.99	1947	0.708789	0.000004	15.4	0.708794	14.6
111R-CC, 14–17	460.50	1938	0.708824	0.000006	13.5	0.708829	12.4
112R-CC, 0–2	463.27	1924	0.708771	0.000006	15.7	0.708776	15.1
114R-CC, 0–5	469.14	1946	0.708748	0.000005	16.0	0.708753	15.5
120R-CC, 13–15	484.42	1935	0.708791	0.000007	14.7	0.708796	14.6
122R-CC, 0–2	490.52	1936	0.708785	0.000004	15.5	0.708790	14.8
130R-CC, 0–2	514.88	1904	0.708771	0.000007	15.7	0.708776	15.1
132R-CC, 0–4	521.19	1901	0.708761	0.000005	15.8	0.708766	15.3
135R-CC, 0–2	528.20	1937	0.708738	0.000005	16.2	0.708743	15.6
135R-CC, 0–2	528.20	1902	0.708757	0.000004	15.9	0.708762	15.4
137R-CC, 14–16	533.70	1903	0.708745	0.000006	16.1	0.708750	15.5
141R-CC, 0–5	545.39	1934	0.708743	0.000006	16.1	0.708748	15.6
141R-CC, 0–5	545.39	1899	0.708745	0.000005	16.1	0.708750	15.5
143R-CC, 8–10	551.55	1921	0.708729	0.000006	16.3	0.708734	15.8
146R-CC, 7–9	557.73	1933	0.708703	0.000006	16.7	0.708708	16.2
148R-CC, 0–4	563.86	1920	0.708744	0.000006	16.1	0.708749	15.5
150R-2, 149–151	569.80	1900	0.708733	0.000008	16.2	0.708738	15.7
152R-CC, 0–2	576.02	1922	0.708745	0.000006	16.1	0.708750	15.5
156R-CC, 0–3	588.20	1945	0.708706	0.000004	16.6	0.708711	16.1
167R-2, 151–153	621.67	1944	0.708688	0.000006	16.9	0.708693	16.4
189R-CC, 16–18	675.22	1979	0.708350	0.000014	21.9	0.708355	21.5
195R-CC, 10–12	695.29	2027	0.707986	0.000008	30.0	0.707991	29.7
195R-CC, 10–12	695.29	1978	0.708596	0.000004	18.3	0.708601	17.9
214R-1, 51–53	747.27	2028	0.708406	0.000005	21.0	0.708411	20.5
217R-1, 0–4	752.86	2029	0.708386	0.000005	21.3	0.708391	20.9

Notes: Sr value = Sr isotope value relative to NBS 987 value of 0.710241. Age = ages derived using regressions outlined in text. Also given for comparison are Sr values corrected to McArthur et al. (2001) and ages derived from that study's "lookup tables;" these were not plotted in the age-depth plots.